AD NUMBER: AD0052416
CLASSIFICATION CHANGES
TO: Unclassified
FROM: Confidential
LIMITATION CHANGES
TO: Approved for public release; distribution is unlimited.
FROM: Distribution authorized to US Government Agencies and their Contractors; Administrative/Operational Use; 14 May 1954. Other requests shall be referred to Air Force Flight Dynamics Laboratory, Wright-Patterson AFB, OH, 45433.
AUTHORITY
C to U per ASTIA Tab No. U59-15 dtd 1 Aug 1959; ST-A per AFFDL ltr dtd 2 May 1979

Copy No. 2 of 21 copies

NORTHROP AIRCRAFT, INC.

HAWTHORNE, CALIFORNIA

CONTRACT AF33(616)-205

E. O. No. R-458-433c SR-1g

LAMINAR BOUNDARY LAYER CONTROL INVESTIGATIONS

Report to:
Wright Air Development Center
For period ending 14 May 1954

NOTICE: THIS DOCUMENT CONTAINS INFORMATION AFFECTING THE NATIONAL DEFENSE OF THE UNITED STATES WITHIN THE MEANING OF THE ESPIONAGE LAWS, TITLE 18, U.S.C., SECTIONS 793 and 794. THE TRANSMISSION OR THE REVELATION OF ITS CONTENTS IN ANY MANNER TO AN UNAUTHORIZED PERSON IS PROHIBITED BY LAW.

Copy No. 2 of 21 copies

REPORT NO. NAI-54-331

PROGRESS REPORT
CONTRACT AF33(616)-205

E. O. No. R-458-433c SR-1g

LAMINAR BOUNDARY LAYER CONTROL INVESTIGATION

REPORT TO:

WRIGHT AIR DEVELOPMENT CENTER

FOR PERIOD ENDING 14 MAY 1954

PREPARED BY:

BOUNDARY LAYER RESEARCH PROJECTS OFFICE

TABLE OF CONTENTS

APPENDICES (cont'd.):

NORTHROP AIRCRAFT, INC.

PROGRESS REPORT - LAMINAR BOUNDARY LAYER CONTROL INVESTIGATION

CONTRACT AF33(616)-205

I. BRIEF OF CONTRACT

A. Financial

Estimated Contract Value through Change Order No. 3	$1,671,250.00
Expenditure through 9 May 1954	1,179,429.26
Unexpended Balance	$ 491,820.74

B. Basic Contract Purpose

To supply the necessary personnel, services, and facilities to investigate laminar boundary layer control on wings and bodies through suction and to develop methods for the design and construction of a laminar boundary layer control airplane.

II. FACILITIES AND EQUIPMENT

There has been no change in the facility and equipment situation during the period covered by this report.

III. ORGANIZATION AND PERSONNEL

A. Organization

There have been no organizational changes during this period.

B. Personnel

The staff now engaged full time on this contract consists of the following:

Engineering	
Supervision	2
Clerical and Secretarial	3
Direct Charging	37
	42
Shop	
Supervision	1
Direct Charging	18
Clerical	1
	20
Flight Test Department	
Direct Charging	10

IV. TECHNICAL PROGRESS

A. Theoretical Investigations of the Laminar Boundary Layer on a Swept Suction Wing

1. Numerical Integration of Boundary Layer Equations

Work was continued on the integrations aimed at the determination of the realm in which the optimum pressure and suction distribution for a wing of 10° taper and 35° sweepback should be sought.

2. Calculation of Boundary Layer Stability

a. The investigation continued for a calculation method based on replacing the Orr-Sommerfeld differential system by an integral system, particularly the adaptation of this method to a simple preliminary evaluation of the stability of any profile. Various numerical checks were successfully carried out, indicating, so far, that the simplified evaluation itself should be sufficiently reliable for most purposes. Preparation of a report describing the method has begun.

b. Calculations have been made on the neutral stability curve of crossflow profile A-2 located near the wing trailing edge and utilizing suction. Preliminary results indicate a critical Reynolds number about 70 percent to 80 percent larger than the one computed for the stagnation point profile.

The procedure (for various crossflow profiles) for the fast computing machine is nearly ready for trial. A preliminary report on the method is enclosed as BLC-43.

A profile with more suction than the profile mentioned above is being prepared for calculation.

B. Basic Laminar Suction and Transition Investigations

1. Suction Experiments with 80 Slots in Two-Inch Tube

a. During previous suction experiments, a turbulent wedge at the end of the tube was found at high Reynolds numbers and

moderately strong pressure rises (30 percent to approximately 70 percent of the reference dynamic pressure at the edge of the boundary layer ahead of the suction region). This turbulent wedge originated from a partly clogged slot (grease in slot from O-ring). After cleansing the suction tube, completely laminar flow was observed through the test tube up to $20 \cdot 10^6$ length Reynolds numbers and pressure rises to 30 percent to 45 percent of the reference dynamic pressure rise. With a stronger pressure rise a small turbulent wedge still existed. Suction experiments (wall surface and suction chamber static pressures and suction quantities) have been started. It is planned to measure, in addition to the above, boundary layer profiles along the tube. The state of the boundary layer will be observed by means of the stethoscope and hot wire.

The following parameters will be varied:

length Reynolds number;

pressure rise and suction quantity;

suction distribution;

length of the straight two-inch tube ahead of the suction region (20 ft, 26 ft, 29 ft, 32 ft).

b. It is intended to discover what causes the beginning of the small turbulent wedge at the end of the suction tube for pressure rises beyond 45 percent. A check of the suction tube showed that two rings toward the end of the test section are not quite concentric, thus causing locally a stepped-down slot which can be very

sensitive to flow disturbances. Furthermore, it is suspected that the pressure rise across the slot in the relatively small diameter tube is considerably stronger than on a suction wing -- this might cause local amplification of disturbances in the vicinity of the slots. In order to verify this supposition, suction experiments have been conducted with the first chamber with ten slots with various amounts of vertical displacement between the slot inlet and the rear edge of the slot. No significant differences have yet been found. These experiments are being continued.

2. Transition Experiments with Two-Inch Tube

With the use of a sonic throat arrangement in a two-inch i.d. 75-ft long straight tube, transition length Reynolds numbers $\frac{\bar{U}x}{\nu}$ of $40 \cdot 10^6$ were observed.

The disadvantage of an experimental setup with a sonic throat is the high power which becomes serious for larger diameter tubes and two-dimensional channels. In order to obtain information on the feasibility of drive systems without sonic throats, preliminary transition experiments were conducted with the same two-inch tube and a big settling chamber between the centrifugal compressors and the test tube. With a 50-ft long 2-inch tube, continuously laminar flow was achieved in this manner up to $27 \cdot 10^6$. At higher Reynolds numbers (up to $50 \cdot 10^6$) intermittently laminar and turbulent flow was observed. These experiments indicate that it is quite feasible to obtain high Reynolds numbers with

laminar flow without using a sonic throat. Further experiments in this direction are planned.

3. Basic Suction Experiments in Eight-Inch I.D. Tube at Moderately High Speeds

No further work has been accomplished during the past month because of higher priority work.

4. Basic Suction Experiments in Eight-Inch I.D. Tube At Low Speeds

The various parts of the experimental setup are being assembled. The first experiments are expected beginning June, 1954. It is intended first to study suction through holes and to gain more information regarding the boundary layer crossflow in this suction case. The flow direction will be observed by means of fine tufts of (black widow) spider web. The magnitude of the flow velocity will be obtained in a conventional manner with total pressure tubes. Together with the observation of the flow by means of smoke, it is expected to gain a better understanding of the rather complex flow phenomena with suction through holes.

5. Basic Laminar Suction Experiments with Suction Through Large Number of Rows of Holes

Most parts of the experimental setup have been completed. The suction holes have to be drilled. Since rows of

closely spaced holes have been quite promising, it is intended to concentrate on suction through 80 rows of closely spaced holes. In order to verify whether or not steps in the surface across each row of holes are required, a suction experiment is being prepared in the two-inch tube with the first chamber and ten slots, with zero step across each slot (flush surface). The parts of this modified first section have been completed. The holes will be drilled according to the results with this modified section.

C. Basic Laminar Suction Experiments of the Flow in a Channel with a Swept Test Section

During this period further progress in the design of the experimental equipment was made. Attention was directed to the aerodynamic and structural problems in building the suction slots into the tunnel wall, as well as to the requirements for the suction chambers, metering stations, etc. These requirements in turn defined the geometrical specifications of the instruments and their holders. The planning of the tunnel development still calls for finishing the instruments as early as possible in order to allow time for calibrations before the experiment itself is begun.

Completed also was a final study of the propulsion requirements for the experimental setup, resulting in several alternatives. The choice between them depends upon availability, price, and advanced planning for the laboratory.

D. Bodies of Revolution

1. Fabrication of the 144-inch ellipsoid with suction slots is in progress. The inside castings are finished; about 40 percent of the outside rings has been rough machined.

2. Further preliminary studies have been conducted with the purpose in mind of maintaining laminar flow around the wing root juncture.

E. Aerodynamic Investigation of Suction Ducting Systems

1. Experiments have been conducted to determine the pressure recovery obtainable from booster jets added to a suction duct. The results show that the pressure distribution in the duct can be altered appreciably by the use of booster jets. A quantitative evaluation of the effect of the jets has not been completed.

A report of experiments to determine the pressure distribution and boundary layer characteristics in a suction duct with nominally zero-deceleration inlet (velocity at exit of turning vanes equal to local duct velocity) is being prepared. Some of the preliminary results of these experiments were summarized in a previous progress report.

Further attempts are being made to analyze the results of the duct experiments in order to provide a rational basis for the design of other ducts.

2. Basic Experiments Concerning the Influence of Internal Flow Passages on the Velocity Distribution along a Slot (applicable to suction through large number of fine slots)

Calibration of the test model has been completed and experiments were begun to determine the effect of the distance between a slot and a row of holes below the slot.

The first experiments were conducted with a row of holes spaced 0.50 inch on centers and 0.120 inch in diameter. The 0.010-inch wide slot was centered over the row of holes, and static pressure readings were taken at various distances along the span of the slot inlet. A small sonic nozzle was used to maintain constant total airflow, and a calibrated laminar flow tube measured the airflow quantity.

First analysis of the data indicates that with the rather large and widely spaced holes in the test configuration, the downstream edge of the slot can be as close to the holes as 0.040 inch before spanwise suction variations larger than two to three per cent are observed. With a hole spacing of 0.25 inch, considerably smaller spanwise variations result.

Additional experiments are now underway to determine the influence of the following:

a) The slot Reynolds number

b) The spacing of the holes in the row

c) Offsetting the row of holes from the centerline of the slot.

F. F-94 Flight Laminar Suction Investigations on a Glove Section

After completion of the initial fitting of the glove section, the airplane was moved from the Boundary Layer Building to Hangar 13. There the nose was reinstalled and the installation of the flight test boom, the photo recorders, and the instrumentation were completed. Fabrication of the fairings between the glove and the F-94 wing is in process.

Final assembly of the glove section and installation of the instrumentation are progressing. The rake for the drag measurements has been completed; the suction box is being reassembled. The tube connections and the housing for the compressor are being fabricated, and the compressor package itself is scheduled to be delivered by AirResearch by the end of May.

A jig and two male templates have been built for polishing the surface of the glove. The waviness of the templates is of the order of 0.0005 for the ratio of maximum amplitude over half wave length. Further improvement of the templates seems to be unnecessary, since the final polishing will be made after installation of the glove on the airplane.

A brief check of the half pitot tubes in the 2-inch tube setup showed a very pronounced difference in the pressure reading at laminar and turbulent flow. The step in the surface due to the protrusion of the element did not affect the status of the boundary layer behind the half pitot.

G. Structural Investigations

1. Full Scale Wing Segment (Wing Test Panel)

Waviness measurements of the Northrop N-69 and F-89 wings showed them to be as smooth as the Douglas X-3 and Bell X-1 wings and even more smooth than the Douglas D-558 Phase II wing. This seems to indicate that no great superiority of current skin-forming techniques among companies (so far as smoothness is concerned) was evident. In fact, variations in smoothness between different chordwise sections of the same wing were sometimes as great as variations in smoothness between airplanes of different companies. Plots of the data discussed above are included in this report on pages 15 to 20.

As a possible approach to improving the basic smoothness of the skin, some experiments were performed with the technique of "draping" the skin over the spars without the aid of preforming. A report on these experiments is presented herein as BLC-42.

A method was worked out for carrying shear forward to the 80 per cent chord line without the use of chordwise ribs, thus allowing the ducts in this area to remain unimpeded for optimum air flow.

A study of the loads induced in a continuous hinge aileron by wing bending was made and the results submitted with this progress report as BLC-39.

The use of a foamed-in-place plastic to stabilize thin skins in the aileron appears desirable, with the possible exception of its volumetric change due to low pressures at altitude. A short investigation of this was made and will be presented as a test report. (See Item 22 under Structural Component Test, below.)

2. Complete Airplane - Configuration III

The stability analysis of the swept strut braced wing was completed and is presented herein as BLC-44.

3. Structural Component Tests

Changes in the status of tests since the April 14, 1954 report are listed below:

Item	Description	Remarks
7	Aluminum Overlay Slotted Structure Tests	Report BLC-41 enclosed.
19	Aileron Test	Test completed. Report pending.
22	Stafoam Pressurization Test	Test completed. Report pending.

4. Flight Test Panel - F-94

Several holding fixtures are now being fabricated to

provide for polishing of the glove prior to installation on the F-94 wing and for methods of checking the contours of the glove section after installation and throughout the flight test program.

H. Design Studies

1. Further study of the gust requirements of the proposed USAF specification, MIL-S-5700, indicates that for unrestricted flight at 35,000 ft the positive limit load factor for the 11.5 aspect ratio, 30° swept wing version of the hypothetical laminar suction airplane would have to be increased to 3.50 g (was +3.00 g maneuver). The 3.50 g load factor would exceed gust requirements at all other altitueds. Because of the extreme flexibility of the wings of this high aspect ratio airplane, a realistic determination of gust load factor would require a dynamic gust analysis of the airplane. The significant conclusion of this reconsideration of gust load factor is that the higher altitude (lower wing loading) versions of the laminar boundary layer airplane will be designed by gust requirements unless flight speed at 35,000 ft will be accordingly restricted. Gust alleviators might be desirable.

2. The report of the photoreflective stress analysis of the initial swept wing strut system has been received from the Presan Corporation. This report data and that of other forthcoming Presan reports are being evaluated and will be compiled in a Boundary Layer report.

3. Transonic Model Investigation for Wright Field 10-Ft Tunnel

a. Detail design work on the Wright Field 10-Ft Tunnel Model is in process.

b. Area distribution studies are progressing satisfactorily. The present philosophy is to optimize the configuration for Mach numbers close to 1.0.

c. A hali-span wood, plaster, and clay mockup of the tunnel model is being constructed to facilitate filleting and contouring the body and nacelles.

FORM 20-11A
(R. 6-51)

ENGINEER: CLEM	**CONFIDENTIAL** NORTHROP AIRCRAFT INC.	PAGE: 15
CHECKER:		REPORT NO.: NAI-54-331
DATE: APRIL 8, 1954	X-1	MODEL:

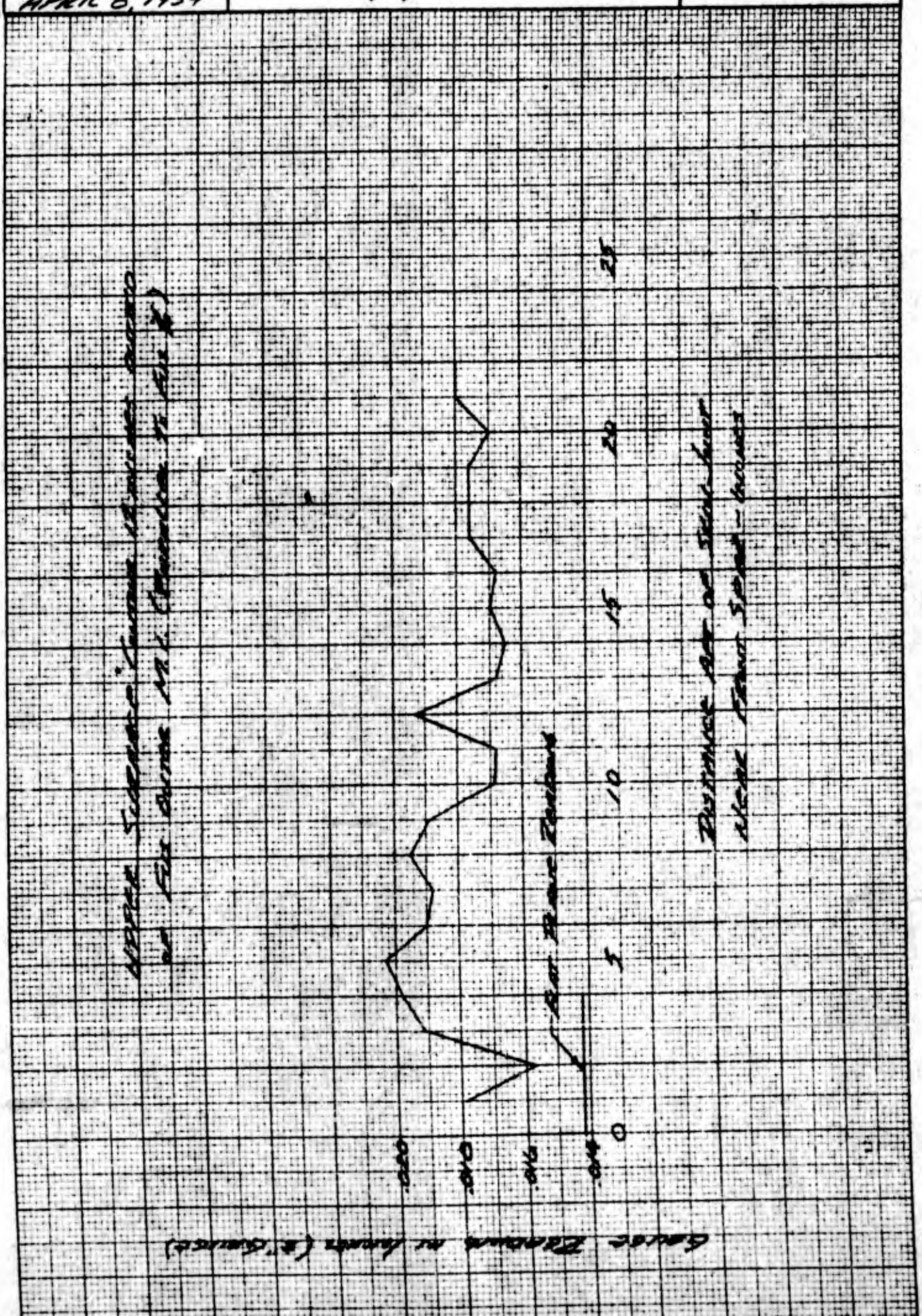

Form 30-118 (R. 6-51)

ENGINEER: CLEM	NORTHROP AIRCRAFT INC.	PAGE: 16
CHECKER:		REPORT NO.: NAI-54-331
DATE: APRIL 7, 1954	X-3 WING	MODEL:

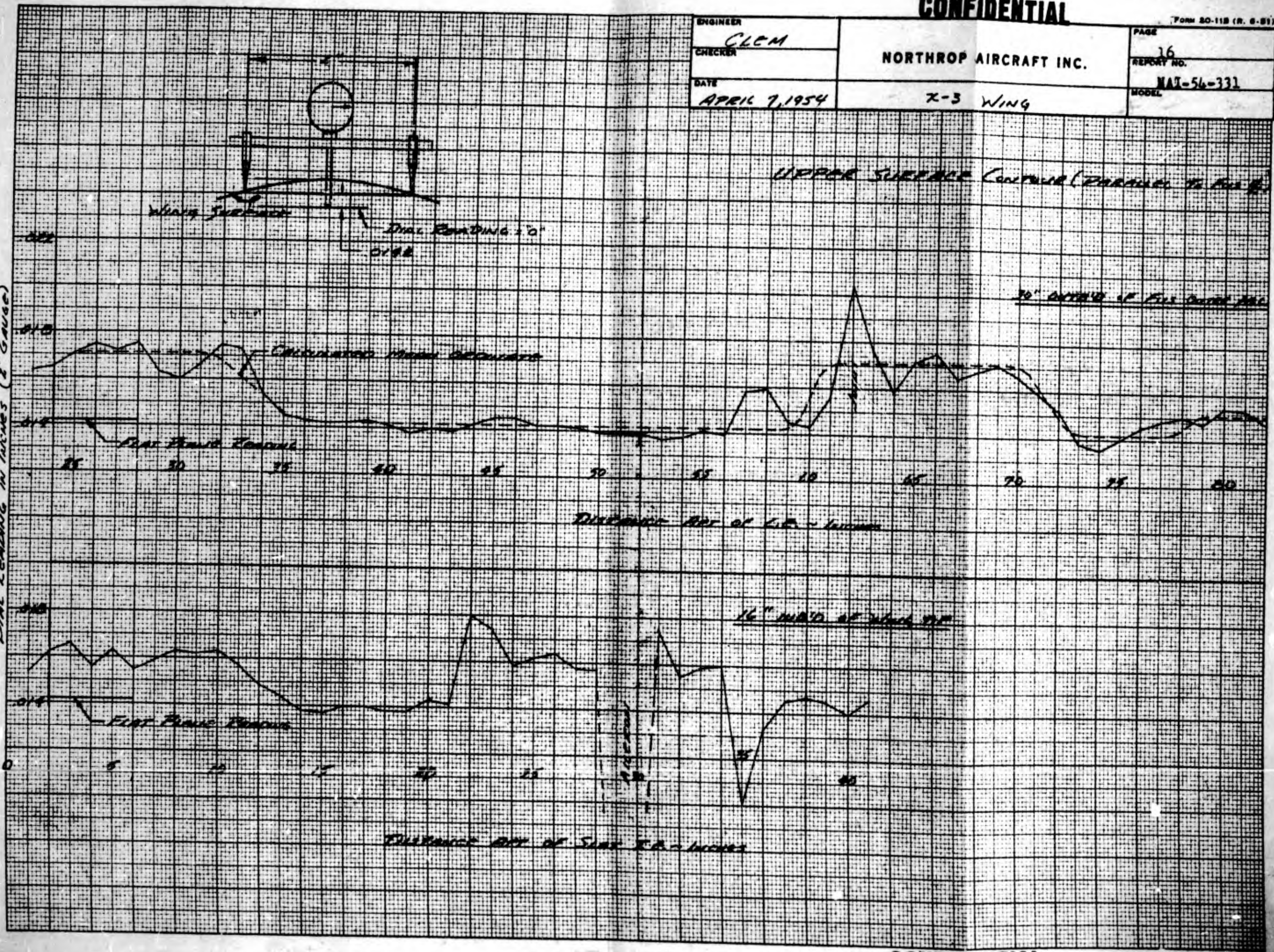

Form 20-118 (R. 6-51)

ENGINEER		PAGE
Clem	NORTHROP AIRCRAFT INC.	17
CHECKER		REPORT NO. NAI-54-331
DATE April 23, 1954	X-3 Wing	MODEL

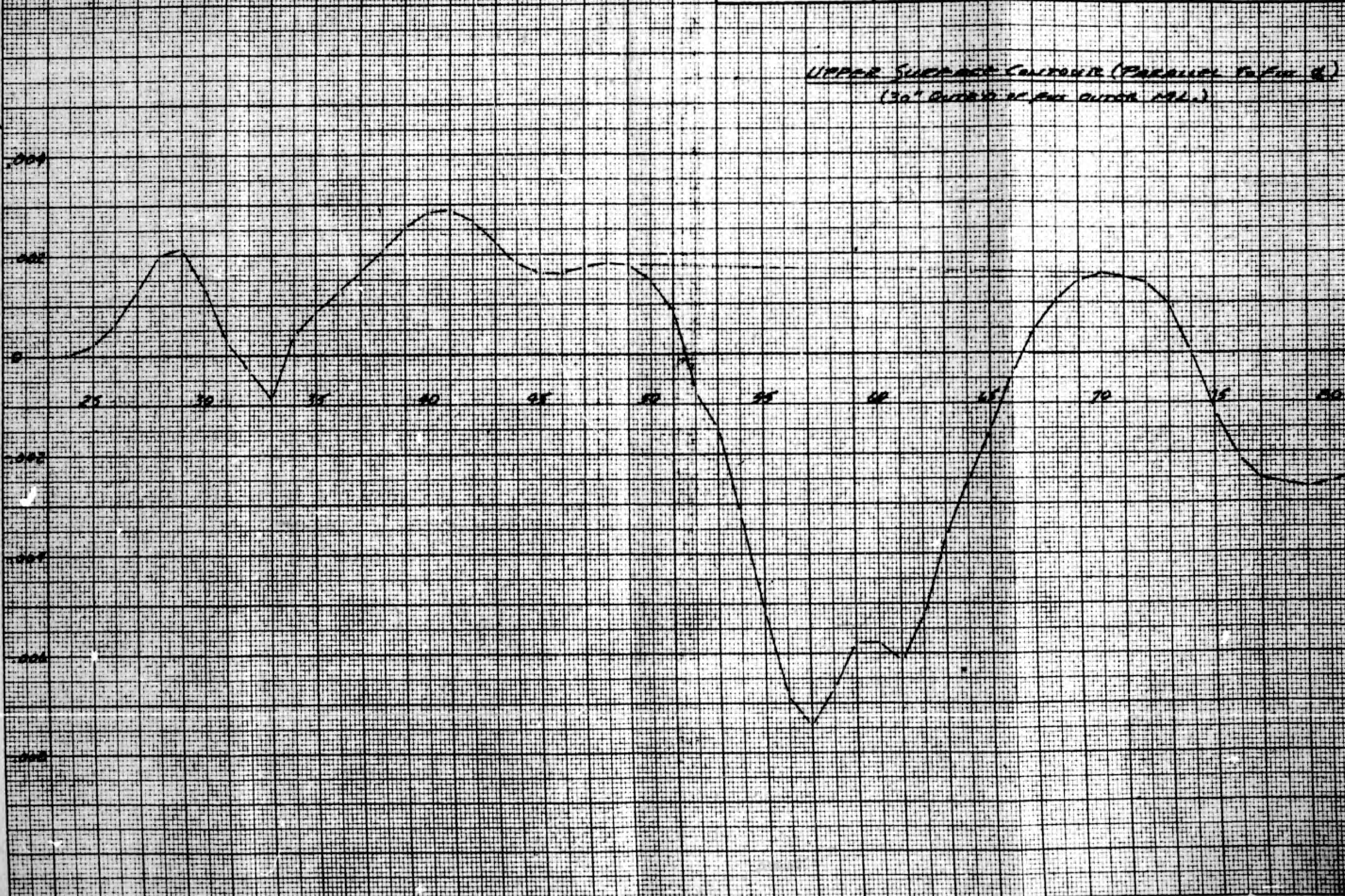

FORM 30-119 (R. 6-51)

ENGINEER: CLEM	NORTHROP AIRCRAFT INC.	PAGE: 18
CHECKER:		REPORT NO.: NAI-54-331
DATE: APRIL 27, 1954	N-69 WING	MODEL:

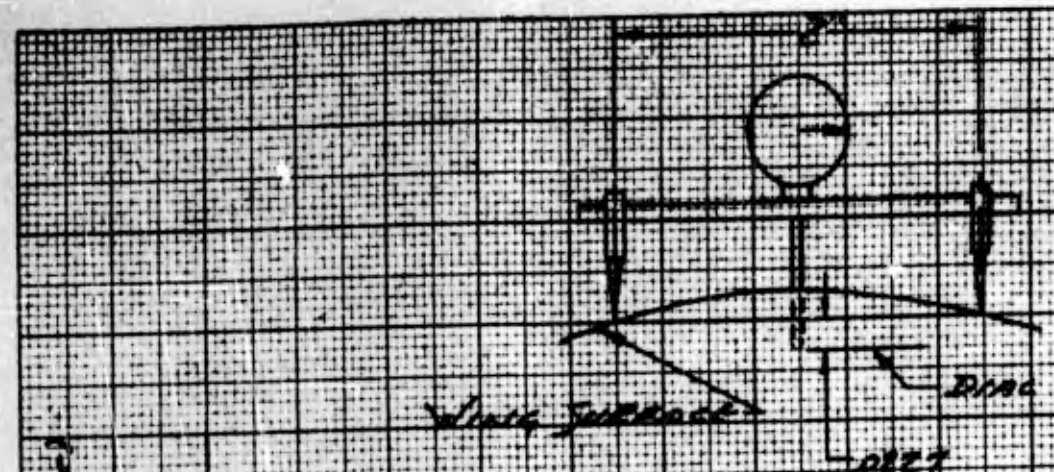

UPPER SURFACE CONTOUR (29 inches outbd of inbd)

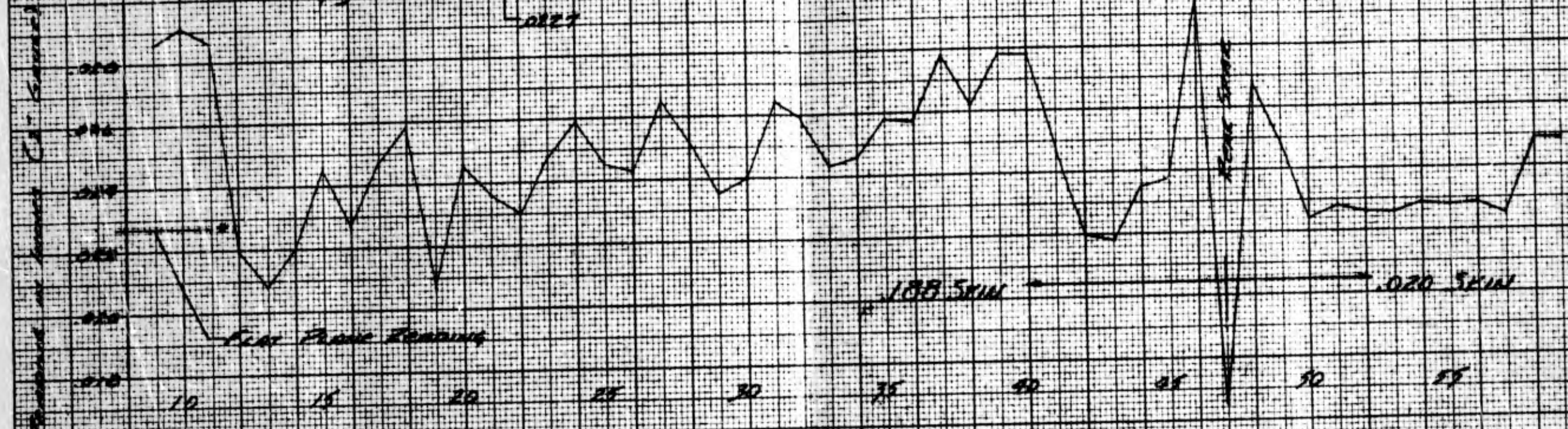

UPPER SURFACE CONTOUR (50 inches outbd of wing joint)

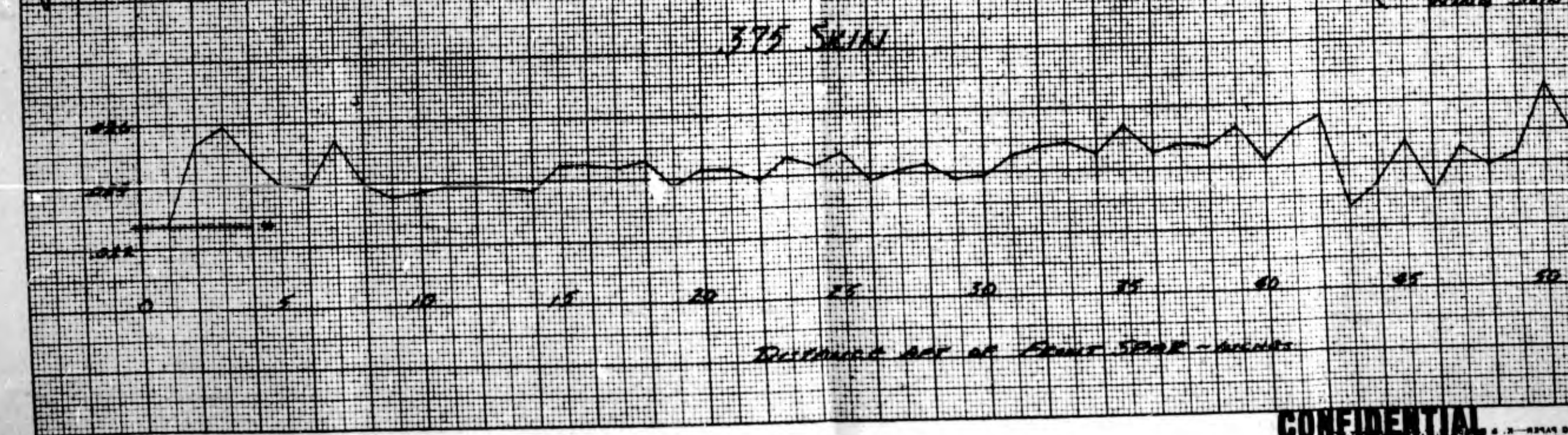

FORM 20-118 (R. 6-51)

ENGINEER: CLEM	NORTHROP AIRCRAFT INC.	PAGE: 19
CHECKER:		REPORT NO.: NAI-54-331
DATE: APRIL 27, 1954	F-89D WING	MODEL:

UPPER SURFACE CONTOUR AT ANGLE OF FLAT PLATE

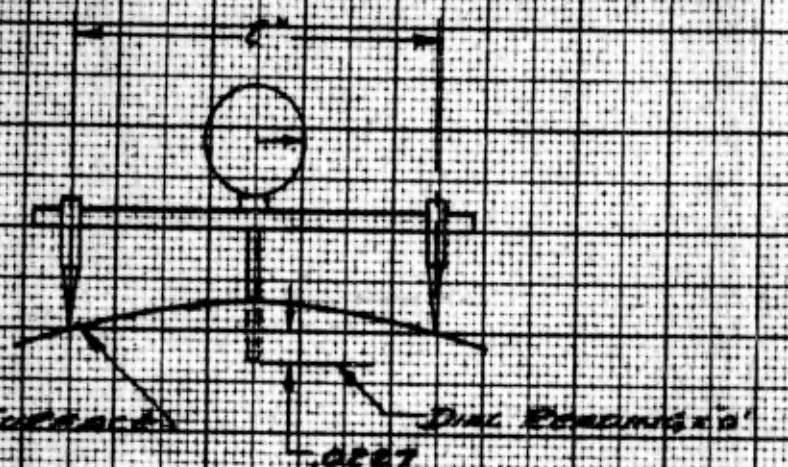

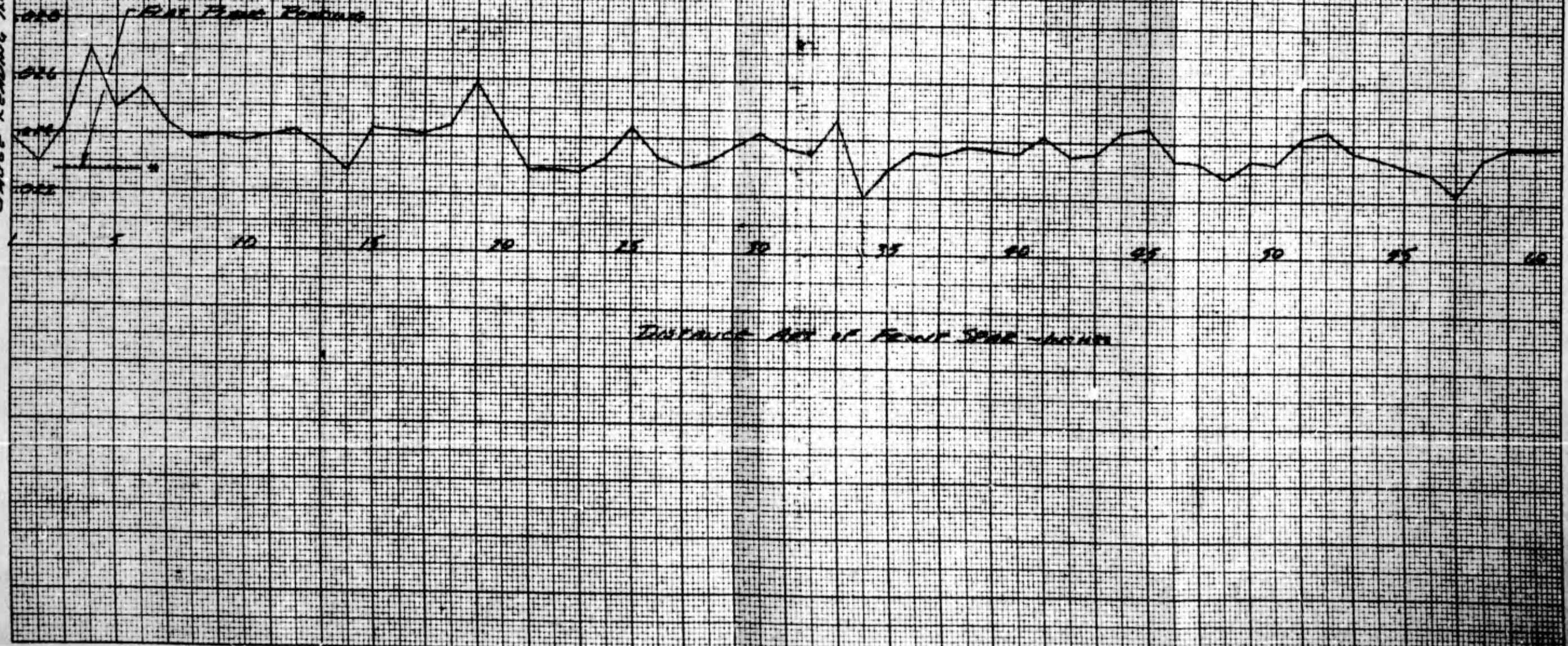

Form 20-11B (R. 8-51)

ENGINEER: CLEM	NORTHROP AIRCRAFT INC.	PAGE: 20
CHECKER:		REPORT NO.: NAI-54-331
DATE: APRIL 7, 1954	550 ~ PHASE 2	MODEL:

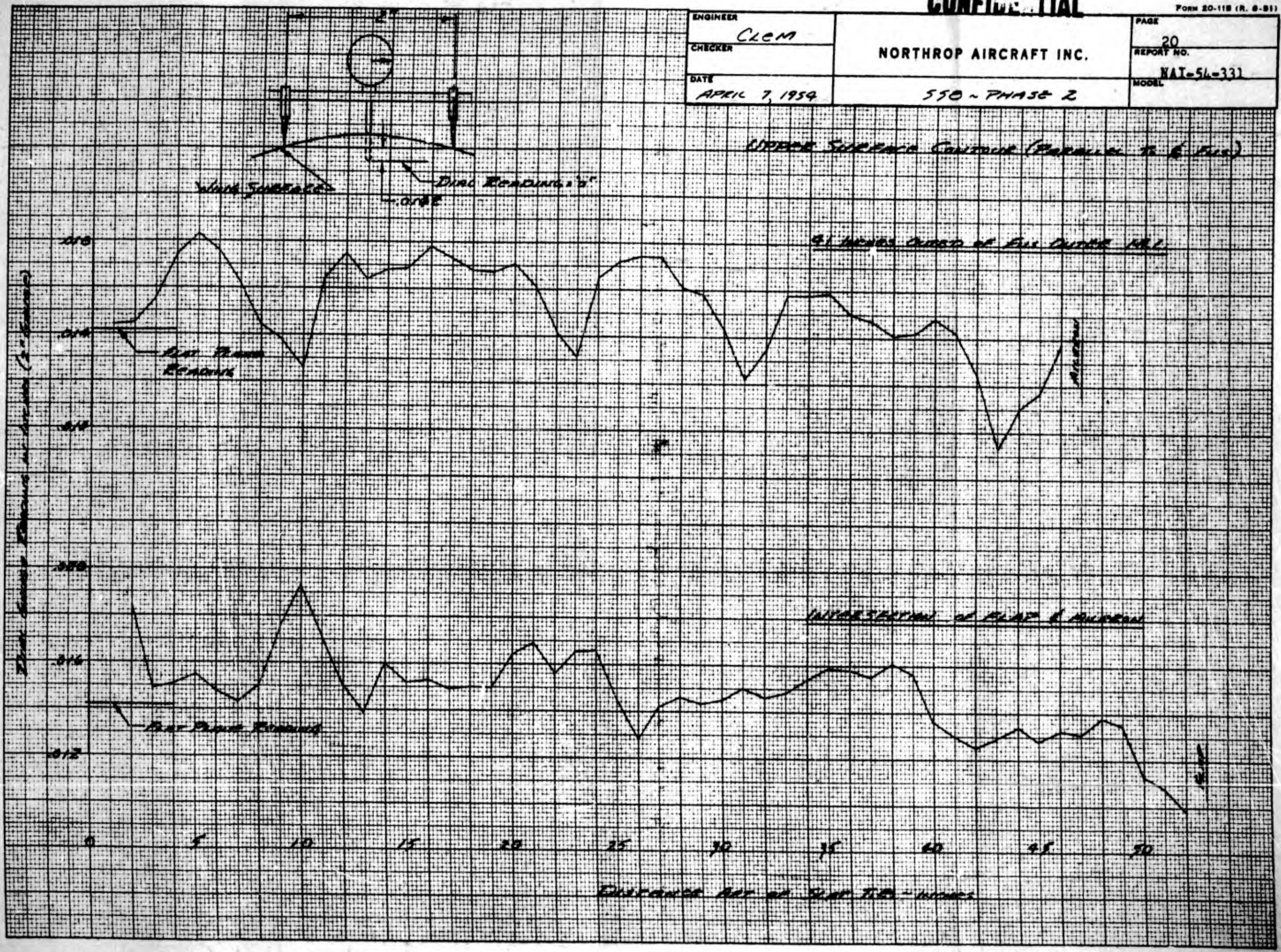

NORTHROP AIRCRAFT, INC.

HAWTHORNE, CALIFORNIA

REPORT NO. BLC-43

AN EXACT SOLUTION OF THE ORR-SOMMERFELD STABILITY EQUATION FOR LOW REYNOLDS NUMBERS

May 1954

PREPARED BY

W. Byron Brown
W. Byron Brown

Philip H. Sayre
Philip H. Sayre

APPROVED BY

W. Pfenninger
W. Pfenninger

TABLE OF CONTENTS

ILLUSTRATIONS

NOTATION

C	integration constant
c	critical velocity (non dimensional)
e	Napierian base
i	$\sqrt{-1}$
k	integration constant
ℓ	left side of equation (12)
r	right side of equation (12)
t	time
u	velocity component parallel to streamline
U_m	reference velocity $\dfrac{u_1 w_1}{\sqrt{u_1^2 + w_1^2}}$
u_1	potential flow velocity component wing leading edge
w_1	potential flow velocity component wing leading edge
w	velocity component streamline (non-dimensional)
x	distance from stagnation point parallel to wall
y	distance from wall

NOTATION (cont'd.)

X	real part of $\ell - r$
Y	imaginary part of $\ell - r$
y*	non-dimensional wall distance
R	Reynolds number $\frac{U_m x}{\nu}$
Re	$\sqrt{R}$
α	wave number of disturbance, always real
β	root of characteristic equation
δ	boundary layer thickness
δ^*	boundary layer thickness (non-dimensional)
ν	kinematic viscosity
$\bar{a}$	fundamental solution of equation (1)
ϕ	amplitude factor of the stream function
ψ	stream function of the periodic disturbance

Superscript

'	indicates differentiation with respect to y*

NOTATION (cont'd.)

Subscripts

c_r	critical
r	real part
i	imaginary part

I. INTRODUCTION

Experiments on boundary layer transition on a sweptback wing (Ref. 1), have shown that transition occurs further forward than it does with straight wings. The same reference attributes this phenomenon to the three-dimensional character of the flow in the boundary layer of a yawed wing.

This three-dimensional flow is expressible by two velocity profiles, one drawn parallel to the potential streamline just outside the boundary layer and the other, normal to this potential streamline, as shown in Figure 1.

As far as stability is concerned, Ref. 2 shows that the transverse component (normal to the potential streamline), can be regarded as a two-dimensional flow and the usual stability theory applied. Because the transverse velocity profile contains a point of inflection, its critical Reynolds number is usually a magnitude or two less than the critical Reynolds number for the parallel profile, that is, the transverse flow becomes unstable at much lower Reynolds numbers than the parallel flow. The transition point is thus determined by the shape of the transverse velocity profile.

The beginning of instability can then be calculated by solving the Orr-Sommerfeld stability equation for the transverse velocity profile at any desired point on the sweptback wing.

The purpose of this report is (1) to develop a method of solving the Orr-Sommerfeld equation adapted to the transverse velocity profiles of interest here and (2) to apply this method to a transverse profile near the stagnation point of a sweptback wing.

II. SOLUTION OF THE ORR-SOMMERFELD EQUATION

The usual stability theory is based on the solution of the Orr-Sommerfeld equation which is given in Ref. 3 (in our dimensionless notation) as

$$(w-c)(\phi''-\alpha^2\phi) - w''\phi = \frac{-i}{\alpha \cdot Re}(\phi''''-2\alpha^2\phi''+\alpha^4\phi) \qquad (1$$

All velocities are referred to a reference velocity U_m and all lengths to a reference length $xR^{-1/2}$. Symbols are defined in the Notation. The periodic disturbance ϕ is expressed in terms of a stream-function ψ by the relation

$$\psi = \phi(y^*)e^{i\alpha(x-ct)} \qquad (2$$

The primes refer to differentiation with respect to the non-dimensional distance from the wall y^*. The symbols are defined in the Notation.

Because the disturbance must vanish at the wall and in the freestream at an infinite distance from the wall, the boundary conditions are

$$\text{When } y^* = 0 \qquad \phi = \phi' = 0 \qquad \text{and}$$
$$\text{when } y^* \longrightarrow \infty \qquad \phi = \phi' \longrightarrow 0 \qquad (3)$$

A. General Solution of the Equation

Because equation (1) is linear and the coefficients are continuous $0 \leq y^* < \infty$ it is possible (Ref. 4) to express its solution in the form

$$\phi = k_1\bar{\phi}_1 + k_2\bar{\phi}_2 + k_3\bar{\phi}_3 + k_4\bar{\phi}_4 \qquad (4)$$

where the four $\bar{\phi}$'s form a fundamental system of solutions and are linearly

independent. The k's are constants of integration. The $\bar{a}$'s are defined as follows (Ref. 4).

$$\begin{array}{llll}
\bar{a}_1(o) = 1+i & \bar{a}_1'(o) = 0 & = \bar{a}_1'' & = \bar{a}_1''' \\
\bar{a}_2(o) = 0 & \bar{a}_2'(o) = 1+i & \bar{a}_2''(o) = \bar{a}_2'''(o) & = 0 \\
\bar{a}_3(o) = 0 & \bar{a}_3'(o) = 0 & \bar{a}_3''(o) = 1+i & \bar{a}_3'''(o) = 0 \\
\bar{a}_4(o) = 0 & \bar{a}_4'(o) = 0 & \bar{a}_4''(o) = 0 & \bar{a}_4'''(o) = 1+i
\end{array} \tag{5}$$

The complex value used for $\bar{a}_1(o)$, $\bar{a}_2'(o)$, etc., can be any complex constant. The only requirement is that the Wronskian should not vanish, i.e.,

$$\begin{vmatrix}
\bar{a}_1(o) & \bar{a}_1'(o) & \bar{a}_1''(o) & \bar{a}_1'''(o) \\
\bar{a}_2(o) & \bar{a}_2'(o) & \bar{a}_2''(o) & \bar{a}_2'''(o) \\
\bar{a}_3(o) & \bar{a}_3'(o) & \bar{a}_3''(o) & \bar{a}_3'''(o) \\
\bar{a}_4(o) & \bar{a}_4'(o) & \bar{a}_4''(o) & \bar{a}_4'''(o)
\end{vmatrix} \neq 0$$

It is easily seen that the $\bar{a}$'s chosen satisfy this condition.

B. Application of the Boundary Conditions at the Wall

Insertion of the boundary conditions at the wall (3) into equation (4) yields the two equations

$$0 = k_1(1 + i) \qquad \text{and}$$

$$0 = k_2(1 + i)$$

so that $k_1 = k_2 = 0$ and the complete solution can be expressed in the simple form

$$\phi = k_3\bar{a}_3 + k_4\bar{a}_4 \tag{6}$$

C. Application of the Boundary Conditions at Infinity

The usual method of handling this situation is to modify these conditions to others that can be applied at a finite distance δ from the wall. Suppose then that δ is the distance where w and w'' equal their free-stream values to four decimal places. (Let δ^* be the dimensionless value.) In this particular profile $w = w'' = 0$. For the Blasius profile $w = 1$ and $w'' = 0$.

Beyond this point ($y^* = o^*$) equation (1) becomes a linear equation with constant coefficients and the solution can therefore be written

$$\phi = C_1e^{-\alpha y^*} + C_2e^{\alpha y^*} + C_3e^{-\beta y^*} + C_4e^{\beta y^*} \tag{7}$$

where

$$\beta = \frac{\alpha}{\sqrt{2}}\sqrt{\sqrt{1 + \frac{c^2R^2}{\alpha^2}} + 1} \quad -i\frac{\alpha}{\sqrt{2}}\sqrt{\sqrt{1 + \frac{c^2R^2}{\alpha^2}} - 1} \tag{8}$$

In order that ϕ and ϕ' may vanish as $y^* \longrightarrow \infty$ C_2 and C_4 must both vanish. Two solutions remain,

$$C_1e^{-\alpha y^*} \qquad \text{and} \qquad C_3e^{-\beta y^*}$$

Either of these solutions will satisfy the differential equation and also the conditions $\phi \simeq \phi' \longrightarrow 0$ as $y^* \longrightarrow \infty$

Because $\alpha <$ (the real part of β), the solution $C_1 e^{-\alpha y^*}$ is somewhat less restrictive than the other, i.e., ϕ and ϕ' approach 0 more gradually. It has therefore been customary to use $\phi = C_1 e^{-\alpha y^*}$ (9) as the proper solution when $y^* > \delta^*$ to satisfy the outer boundary conditions.

D. Conditions at the Junction of the Boundary Layer and the Free-stream

It has been shown that when $y^* \leq \delta^*$

$$\phi = k_3 \bar{a} + k_4 \bar{a}_4 \qquad \text{and} \tag{6}$$

when $y^* \geq \delta^*$

$$\phi = C_1 e^{-\alpha y^*} \tag{9}$$

At the point $y^* = \delta^*$, both (6) and (9) must be satisfied in order to fit the two curves together. The slopes and curvatures should agree also so as to make a smooth junction. Thus

$$\begin{aligned} k_3 \bar{a}_{32} + k_4 \bar{a}_{42} - C_1 e^{-\alpha \delta^*} &= 0 \\ k_3 \bar{a}'_{32} + k_4 \bar{a}'_{42} + \alpha C_1 e^{-\alpha \delta^*} &= 0 \\ k_3 \bar{a}''_{32} + k_4 \bar{a}''_{42} - \alpha^2 C_1 e^{-\alpha \delta^*} &= 0 \end{aligned} \tag{10}$$

where the second subscript 2 denotes values at the position $y^* = \delta^*$.

It is obvious that (10) can only be satisfied if the constants are not zero when

$$\begin{vmatrix} \bar{a}_{32} & \bar{a}_{42} & -1 \\ \bar{a}'_{32} & \bar{a}'_{42} & \alpha \\ \bar{a}''_{32} & \bar{a}''_{42} & -\alpha^2 \end{vmatrix} = 0 \tag{11}$$

or when

$$\frac{\bar{a}'_{32} + \alpha\bar{a}_{32}}{\bar{a}''_{32} - \alpha^2\bar{a}_{32}} = \frac{\bar{a}'_{42} + \alpha\bar{a}_{42}}{\bar{a}''_{42} - \alpha^2\bar{a}_{42}} \tag{12}$$

Equating the real and imaginary parts of (12) yields two relations between c, α and R, the parameters in equation (1).

Elimination of c will then yield a relation between α and R. This relation when plotted gives the desired stability curve.

III. NUMERICAL SOLUTION OF THE DETERMINANT

Of the quantities occurring in equation (1), w, y^*, α, R are always real. c is complex in general so that $c = c_r + ic_i$. ϕ is also complex so that $\phi = \phi_r + i\phi_i$. This is true also for the fundamental solutions $\bar{a}_3$ and $\bar{a}_4$.

Insertion of this value of c in equation (2) yields

$$\psi = \phi\, e^{c_i \alpha t}\, e^{i\alpha(x - c_r t)} \tag{13}$$

Inspection of this equation shows that when $c_i < 0$ the disturbance will decay with time while, if $c_i > 0$, the disturbance will increase with time. If $c_i = 0$, the magnitude of the disturbance will be independent of the time and will depend only on y, since ϕ is a function of y only.

For the present, c_i will be taken zero, giving an α, R relation that is called the neutral stability curve. This will give the largest unstable

region possible. The problem is to calculate points on the neutral stability curve.

A. Real Equations to Be Solved

Substitution of $\phi = \phi_r + i\phi_i$ in equation (1) and separation of the real and imaginary parts yields the two real equations

$$\left.\begin{aligned} \phi_r'''' &= 2\alpha^2\phi_r'' - \alpha^4\phi_r - \alpha R\left[(w-c)(\phi_i'' - \alpha^2\phi_r) - w''\phi_i\right] \\ \phi_i'''' &= 2\alpha^2\phi_i'' - \alpha^4\phi_i + \alpha R\left[(w-c)(\phi_r'' - \alpha^2\phi_r) - w''\phi_r\right] \end{aligned}\right\} \quad (14)$$

B. Calculation of $\bar{\phi}_{32}$, $\bar{\phi}_{42}$ and their Derivatives

The wall values of $\bar{\phi}_3$ and $\bar{\phi}_4$ and their derivatives are known from their definitions. Thus

$$\bar{\phi}_3 = 0 \qquad \bar{\phi}_3' = 0 \qquad \bar{\phi}_3'' = 1 + i \qquad \bar{\phi}_3''' = 0$$

$$\bar{\phi}_4 = 0 \qquad \bar{\phi}_4' = 0 \qquad \bar{\phi}_4'' = 0 \qquad \bar{\phi}_4''' = 1 + i$$

To avoid large numbers, it is sometimes helpful to use $.1(1+i)$ or $.01(1+i)$ for wall values instead of $1 + i$.

When values of the parameters R, c and α have been chosen, $\bar{\phi}_3$ can be solved by a numerical step-by-step method on the I.B.M. card punch machine (see Appendix A) and $\bar{\phi}_{32}, \bar{\phi}_{32}', \bar{\phi}_{32}''$ found. Similarly $\bar{\phi}_{42}$ and its derivatives are found. In equation (12) let l be the lefthand side and r the righthand one. Then each calculation in the machine furnishes a value of l or r. Let

$$l - r = X + iY \quad (15)$$

where X and Y are real quantities. The problem is to find values for α, c and R that will cause $X = Y = 0$.

C. Procedure for Locating the Zeros

To find corresponding values of α, c and R, first a value of $R > R_c$ was selected. In the case of the stagnation point curve, suppose it is $R = 200$. Then select a value of $c > c_r$. An approximate value of c_{cr} is the value of c corresponding to the point where $w'' = 0$. In the curve of Fig. 1 c_{cr} is .1564. Let c be .16. Successive values of α, say $\alpha = .20$ .25 .30 .35 were chosen. For each set of values of R, c, α, values of X and Y were computed for $y^* = o^*$ by method of Appendix A. Both X and Y are plotted in Fig. 2. Intersections with the horizontal axis give the α values when X and Y are zero. Other values of c and α gave other zeros for X and Y. Fig. 3 shows the curves $X = 0$ and $Y = 0$ plotted in the c, α plane. The intersection gives the required values of α and c.

The process was repeated for other values of R until the stability curve α vs R was traced.

IV. SOLUTION FOR TRANSVERSE VELOCITY PROFILE AT THE STAGNATION POINT

The transverse velocity profile shown in Fig. 1 is tabulated in full in Table 1. The tabulation is based on equations (7) and (8) of Ref. 6. These values of w and w'' are substituted in equation (14).

The calculation of corresponding values of α and R was carried out as described for $R = 300$, 200, on both the upper and lower branches of the neutral stability curve. In order to check the value of R_{cr}, calculations will be made with $c = .1564$ wherein α and R were varied to get $X = Y = 0$.

Preliminary results for the neutral curve are shown in Figure 4 where the wave number α is plotted against Reynolds number in the usual manner. Because R is $\frac{U_m x}{\nu}$ and the reference length in the Orr-Sommerfeld equation is

$$\frac{x}{\sqrt{\frac{U_m x}{\nu}}},$$

the Reynolds number in the Orr-Sommerfeld equation is

$$\frac{\frac{U_m x}{\nu}}{\sqrt{\frac{U_m x}{\nu}}} = \sqrt{R} = Re$$

V. COMPARISON WITH EXPERIMENT

In Reference 1 a criterion χ for the onset of instability is defined and measured on a number of sweptback wings. The criterion χ is obtained by multiplying the peak velocity of the profile by the width of the profile δ and dividing by the kinematic viscosity ν.

Substitution of these values from profile (b) of Figure 1 yields

$$\chi = \frac{.24\, U_m\, 3.6x}{\nu\sqrt{\frac{U_m x}{\nu}}} = .864\, Re$$

Because Re_{cr} in Figure 4 is about 140, χ will become about 121 which is not far from the experimental value of 125 given in Reference 1.

A formula for the characteristic wave length of the disturbance, supported by experiment, is given in Reference 7.

It is

$$\frac{2\pi}{\alpha\delta} = 3.06 \qquad \text{so that}$$

$$\alpha = \frac{2\pi}{3.06\delta} = \frac{2}{3.06 \times 3.6} = .57$$

again in agreement with Figure 4.

VI. CONCLUSIONS

A new method for the exact numerical solution of the Orr-Sommerfeld stability equation has been developed.

When applied to the cross flow profile near the stagnation point of a sweptback wing, good agreement was found between calculated and observed values of the critical Reynolds number and the characteristic wave number of the disturbance there.

REFERENCES

1 Owen, P.R. and Randall, D.G.: Boundary Layer Transition on a Sweptback Wing, R.A.E. Tech. Memo No. Aero 277 (ARC 15,022), May 1952. (Confidential)

2 Stuart, J.T.: An Interim Note on the Stability of the Boundary Layer on a Swept Wing, ARC 14,991, June 1952. (Confidential)

3 Goldstein, S.: Modern Developments in Fluid Dynamics, Vol. I, p. 198, Oxford Uni. Press, 1938 (reprinted in 1952).

4 Agnew, R.P.: Differential Equations, pp. 325, 326, McGraw-Hill, New York, 1942.

5 Lin, C.C.: On the Stability of Two-Dimensional Parallel Flows, Quart. Appl. Math., Vol. III, 1945/46, pp. 117-142.

6 Raetz, G.S.: Method of Calculating the Incompressible Laminar Boundary Layer on Infinitely-Long Swept Suction Wings, Adaptable to Small-Capacity Automatic Digital Computers, Northrop Aircraft, Inc., Report No. BLC-11, September 1953. (Confidential)

7 Owen, P.R. and Randall, D.G.: Boundary Layer on a Sweptback Wing: A Further Investigation, R.A.E. Tech. Memo No. Aero 330, February 1953. (Confidential)

TABLE 1

y*	w	w''
0	0	-1.0000
.1	.0613	-.9894
.2	.1126	-.9595
.3	.1543	-.9132
.4	.1869	-.8533
.5	.2111	-.7823
.6	.2273	-.7030
.7	.2366	-.6182
.8	.2397	-.5403
.9	.2375	-.4422
1.0	.2309	-.3558
1.1	.2208	-.2731
1.2	.2079	-.1959
1.3	.1930	-.1257
1.4	.1769	-.0636
1.5	.1601	-.0104
1.6	.1432	+.0341
1.7	.1266	.0696
1.8	.1107	.0964
1.9	.0957	.1150
2.0	.0819	.1266
2.1	.0695	.1322
2.2	.0584	.1330
2.3	.0484	.1289
2.4	.0396	.1214
2.5	.0327	.1121
2.6	.0260	.1015
2.7	.0208	.0903
2.8	.0164	.0790
2.9	.0129	.0680
3.0	.0100	.0577
3.1	.0077	.0483
3.2	.0058	.0397
3.3	.0043	.0316
3.4	.0032	.0245
3.5	.0023	.0193
3.6	.0017	.0152
3.7	.0012	.0117
3.8	.0009	.0089
3.9	.0006	.0067
4.0	.0004	.0050
4.1	.0003	.0037
4.2	.0002	.0028
4.3	.0001	.0022
4.4	.0000	.0017
4.5	.0000	.0012
4.6	.0000	.0007
4.7	.0000	.0003
4.8	.0000	.0001
4.9	.0000	.0000
5.0	.0000	.0000

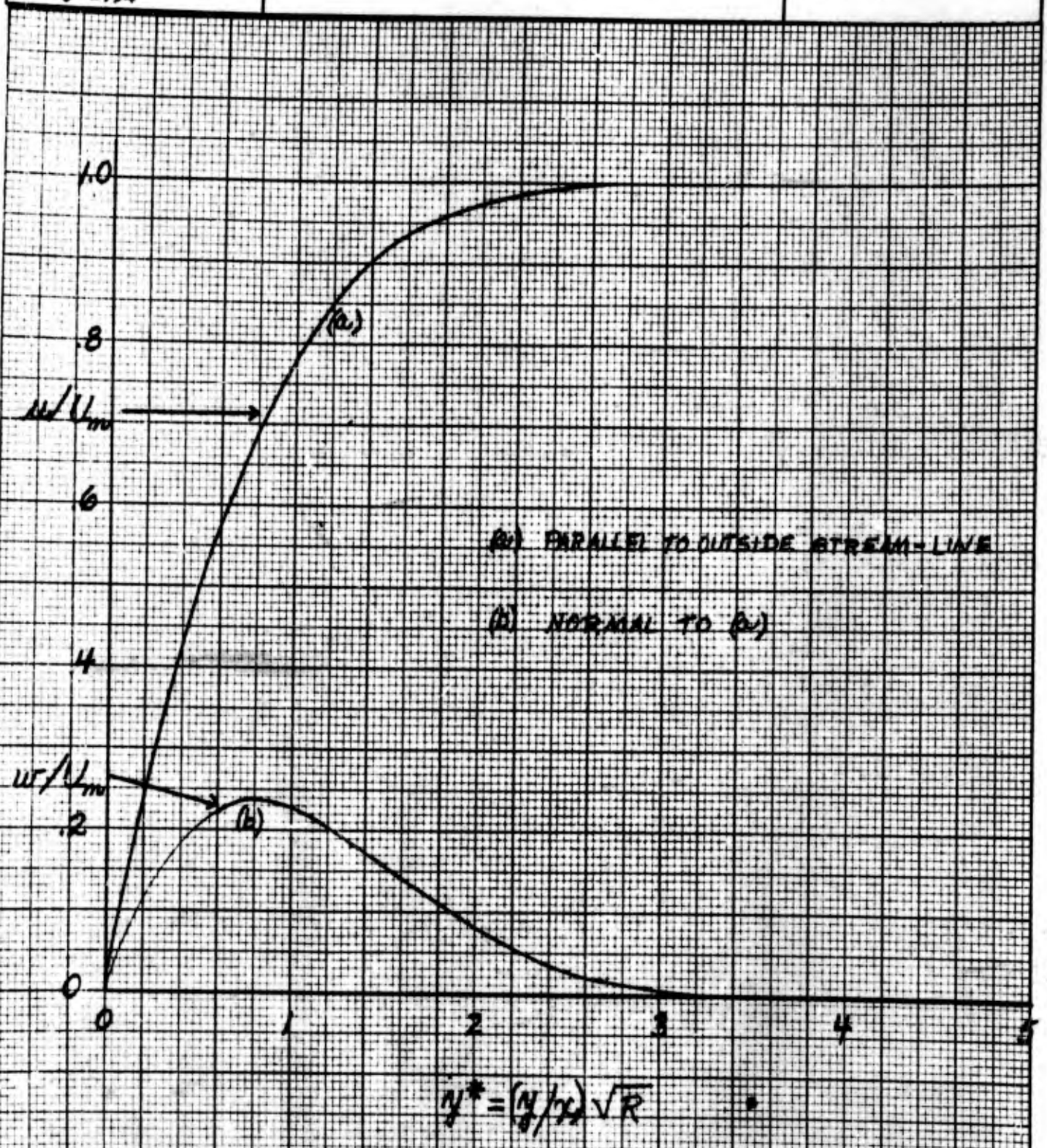

FIG. 1 - VELOCITY COMPONENTS IN THE BOUNDARY LAYER AT THE STAGNATION POINT OF A SWEPTBACK WING

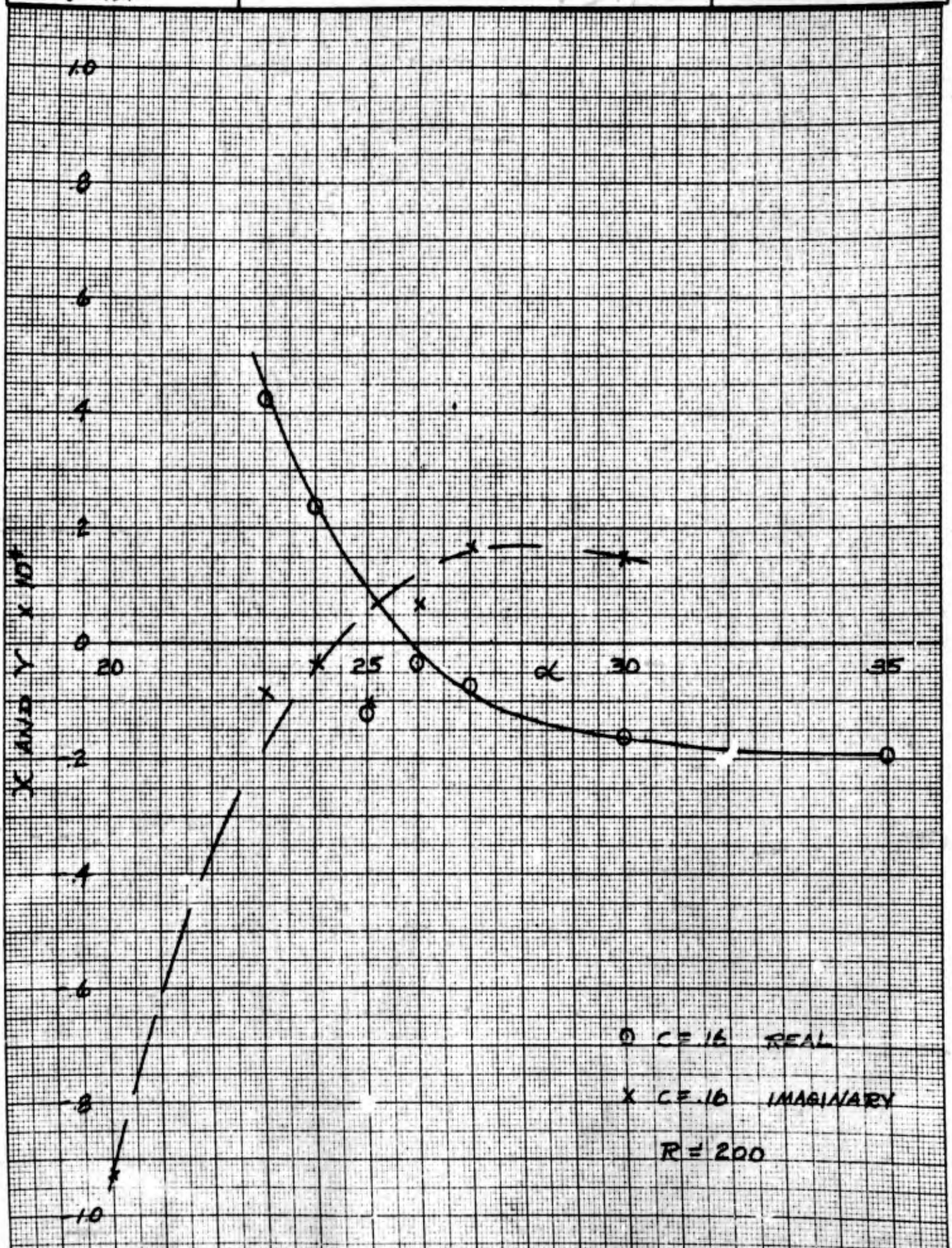

FIG.2. - REAL AND IMAGINARY ZEROS OF $\ell - k$, THE SECULAR EQUATION

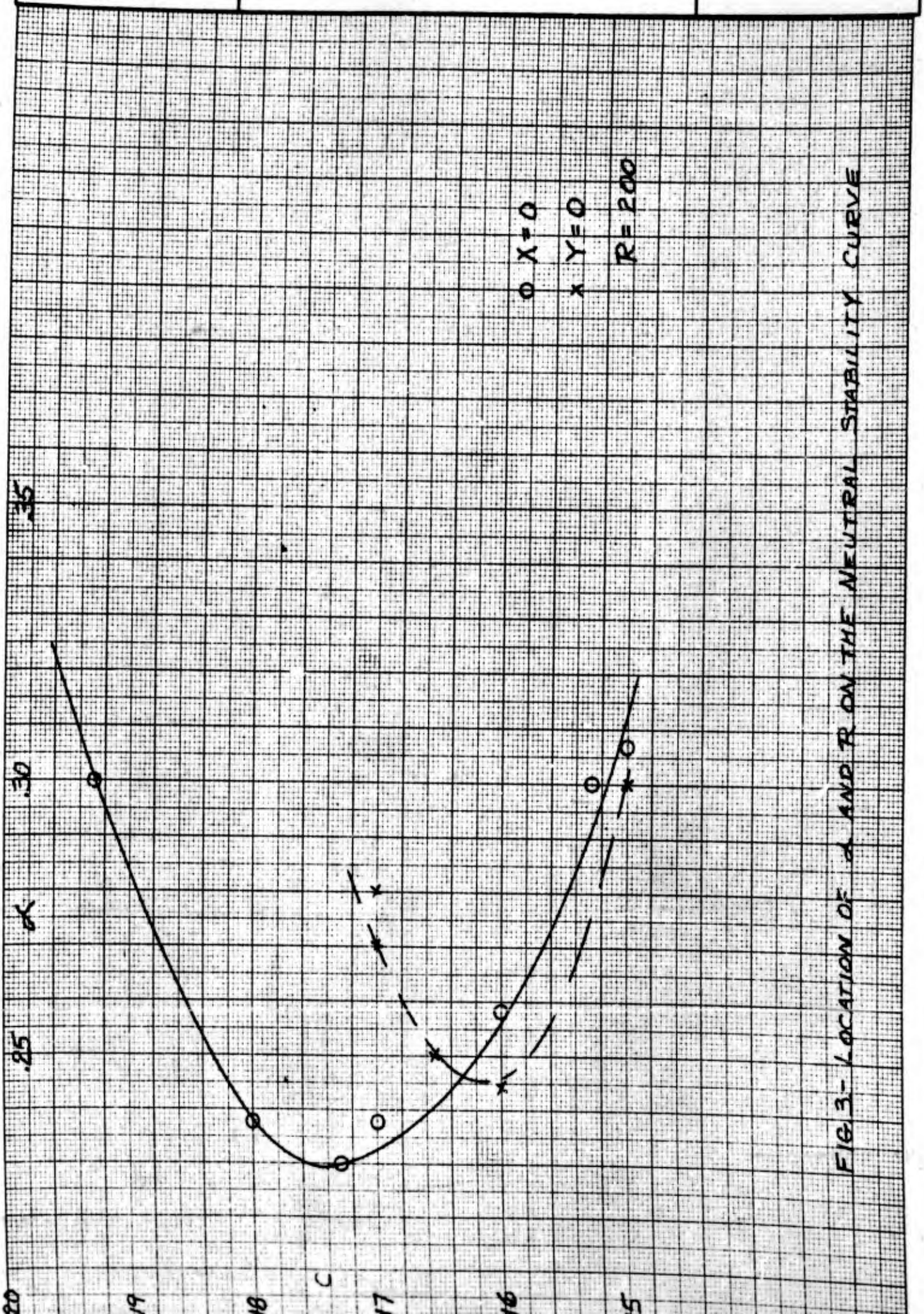

FIG 3- LOCATION OF c_l AND R ON THE NEUTRAL STABILITY CURVE

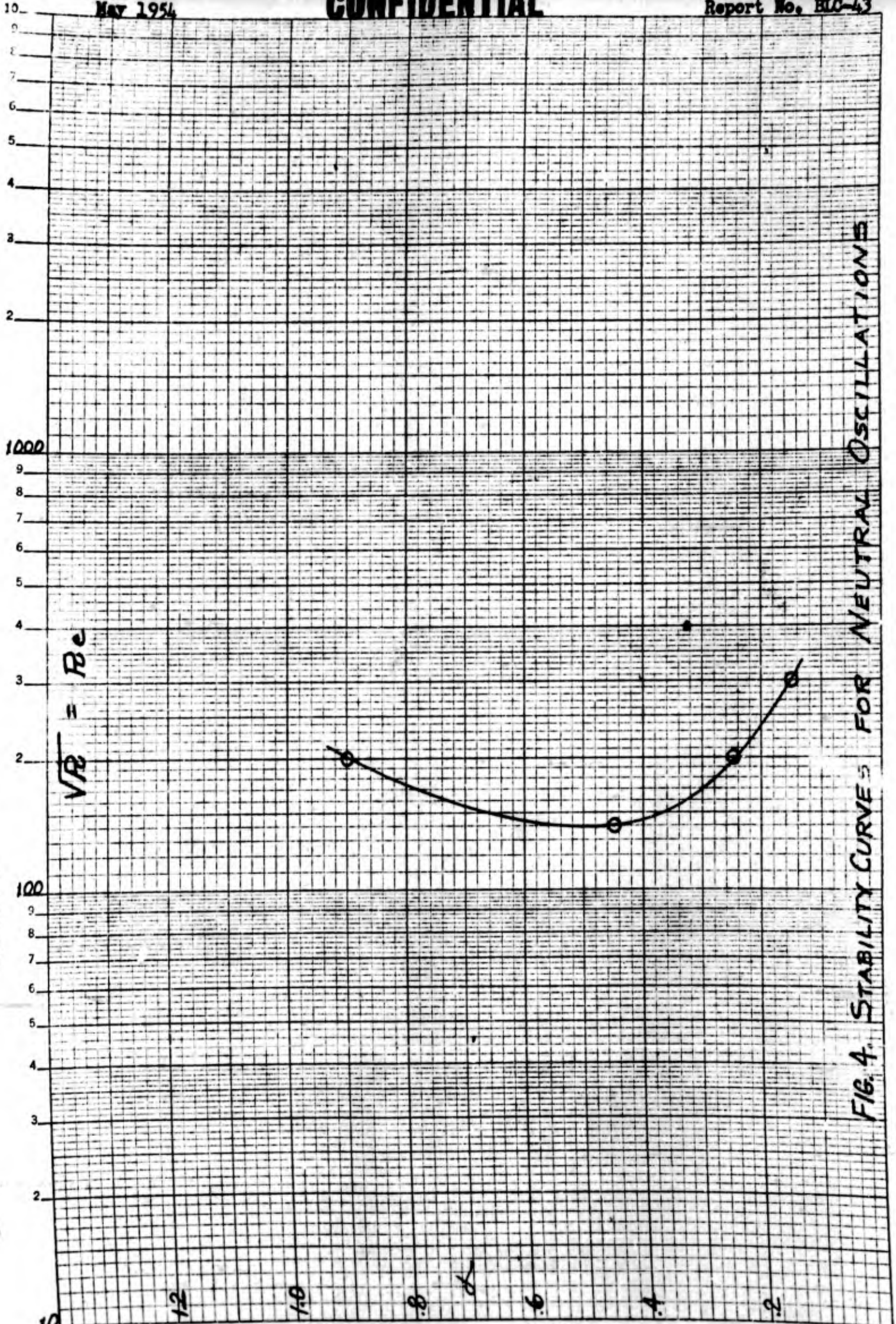

FIG. 4. STABILITY CURVES FOR NEUTRAL OSCILLATIONS

APPENDIX A

NUMERICAL SOLUTION OF EQUATIONS 14

The function $w(y^*)$ and $w''(y^*)$ are tabulated at equal intervals as in Table 1. $y_n = nh (h = 0.1)$ $\quad n = 0, 1, 2 \text{ —— } 50$ $\quad w_n = w(y_n)$

A Milne predictor-corrector method based on formulas in equidistant ordinates is used.

I. Predictor Cycle (for ϕ read ϕ_r or ϕ_i)

B4) $$\overline{\phi''_{n+1}} = \phi''_{n-3} + \phi''_{n-2} + \phi''_n + \frac{h^2}{4}(5\phi''''_{n-2} + 2\phi''''_{n-1} + 5\phi''''_n)$$

B5) $$\overline{\phi'_{n+1}} = \phi'_{n-1} + \frac{h}{3}(\phi''_{n-1} + 4\phi''_n + \overline{\phi''_{n+1}})$$

B6) $$\overline{\phi_{n+1}} = \phi_{n-1} + \frac{h}{3}(\phi'_{n-1} + 4\phi'_n + \phi'_{n+1})$$

$$\overline{\phi''''_{r_{n+1}}} = f_r(\overline{\phi''_{r_{n+1}}}, \overline{\phi_{r_{n+1}}}, \overline{\phi''_{i_{n+1}}}, \overline{\phi_{i_{n+1}}}, w_{n+1}, w''_{n+1})$$

14

$$\phi''''_{i_{n+1}} = f_i(\overline{\phi''_{r_{n+1}}}, \overline{\phi_{r_{n+1}}}, \overline{\phi''_{i_{n+1}}}, \overline{\phi_{i_{n+1}}}, w_{n+1}, w''_{n+1})$$

II. Corrector Cycle ((n+1) replaced by n)

B7) $\phi_n'' = -\phi_{n-2}'' + 2\phi_{n-1}'' + \frac{h^2}{12}(\phi_{n-2}'''' + 10\phi_{n-1}'''' + \overline{\phi_n''''})$

B8) $\phi_n' = \phi_{n-2}' + \frac{h}{3}(\phi_{n-2}'' + 4\phi_{n-1}'' + \phi_n'')$

B9) $\phi_n = \phi_{n-2} + \frac{h}{3}(\phi_{n-2}' + 4\phi_{n-1}' + \phi_n')$

14) $\phi_n'''' = f(\phi_n'' , \phi_n ; x_n , w_n'')$

Starting the Solution

Formula B4) requires function values at four preceeding values of y. The first application of B4, B5, B6, occurs, therefore, at $n = 3$, and values of ϕ'', ϕ' and ϕ must be obtained at y_0, y_1, y_2, y_3.

I. Predictor Cycle:

B10) $\overline{\phi_{n+1}'''} = \phi_n''' + h\phi_n''''$

B11) $\overline{\phi_{n+1}''} = \phi_n'' + h\phi_n''' + \frac{h^2}{2}\phi_n''''$

$n = 0, 1, 2$

B12) $\phi_{n+1}' = \phi_n' + h\phi_n'' + \frac{h^2}{2}\phi_n''' + \frac{h^3}{6}\phi_n''''$

B13) $\phi_{n+1} = \phi_n + h\phi_n' + \frac{h^2}{2}\phi_n'' + \frac{h^3}{6}\phi_n''' + \frac{h^4}{24}\phi_n''''$

14) $\overline{\phi_{n+1}''''} = f(\overline{\phi_{n+1}''} , \phi_{n+1} ; w_{n+1} , w_{n+1}'')$

II. Corrector Cycle:

B14) $$\phi'''_{n+1} = \phi'''_n + \frac{h}{2}(\phi''''_n + \overline{\phi''''_{n+1}})$$

B15) $$\phi''_{n+1} = \phi''_n + \frac{h}{2}(\phi'''_n + \phi'''_{n+1}) + \frac{h^2}{2}\left(\frac{\phi''''_n - \overline{\phi''''_{n+1}}}{6}\right)$$

14 $$\phi''''_{n+1} = f(\phi''_{n+1}, \phi_{n+1}; w_{n+1}, w''_{n+1})$$

ENGINEER SAYRE	NORTHROP AIRCRAFT, INC.	PAGE 29
CHECKER		REPORT NO. BLC-43
DATE May 1954	FLOW CHART	MODEL

NORMAL OPERATION

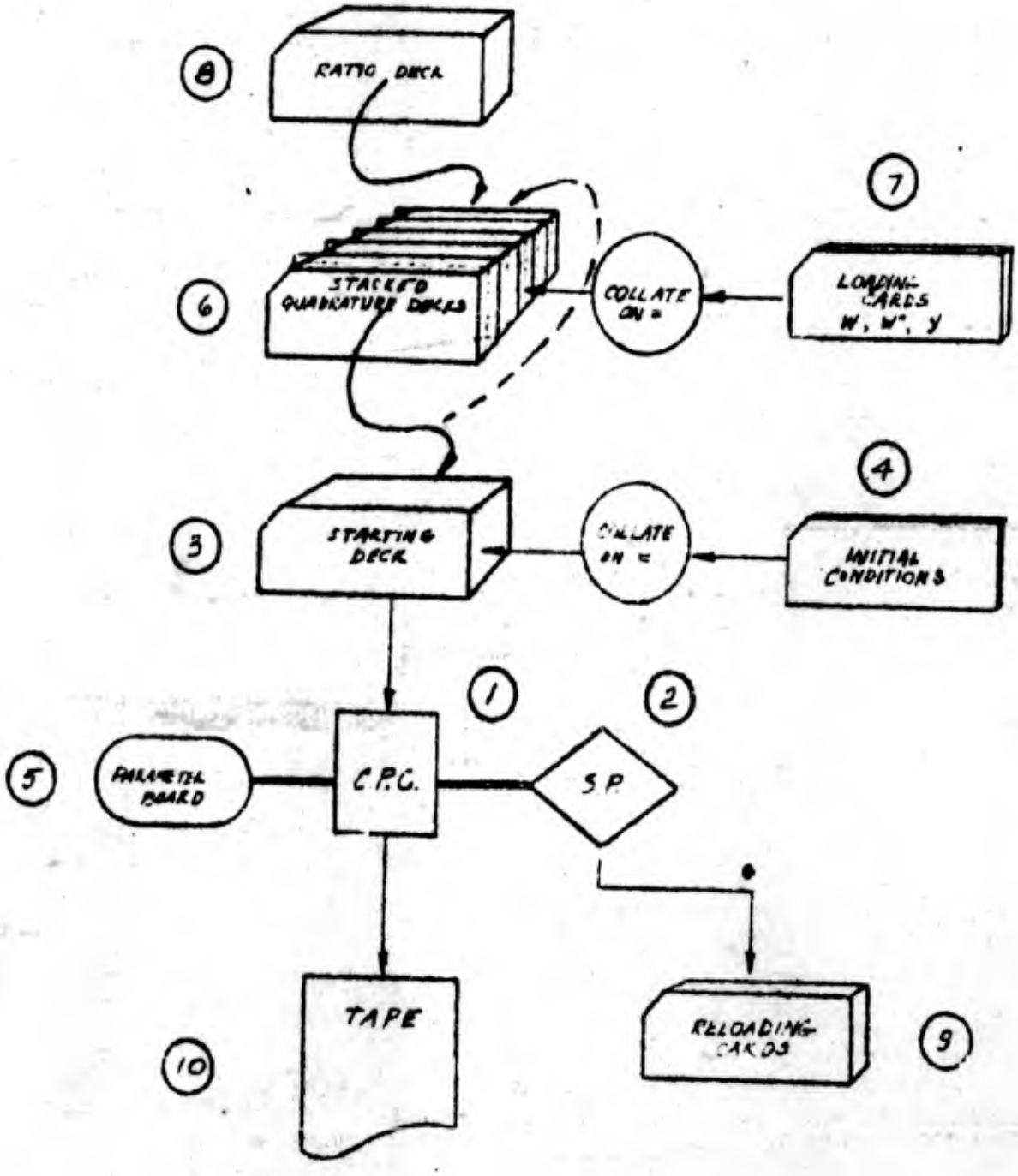

CONFIDENTIAL

NORTHROP AIRCRAFT, INC.

HAWTHORNE, CALIFORNIA

REPORT NO. BLC-42

EFFECT ON WAVINESS AND STRESS

OF DRAPING FLAT SKINS OVER WING SPARS

May 1954

PREPARED BY

S. Dexter

W. R. Slagg

APPROVED BY

W. Pfenninger

S. Detzer
May 1954

I. PURPOSE

It is the purpose of this test to determine the smoothness of a .250 and a .188 plate draped over simulated spars and to determine loads necessary to bring the plates into contact with the spars. It is also the purpose of the test to determine waviness both before and after draping the sheets. Draping can be defined as bringing a flat sheet in contact with spars by attachment devices on the spars.

II. PROCEDURE

The sheets from the mill were cleaned and points located and marked. Care was taken to burnish marks on the sheets with an eraser so that the original surface was not disturbed.

Readings were taken with a .0001" dial gage from a surface plate on which the sheets had been placed. Waviness readings were taken with the same dial indicator with the waviness indicator points set two inches apart. (Figure XI.)

The sheets were then placed in the jig and clamped at spars 8 and 9. The sheets were then loaded with shot bags and lead pigs in the vicinity of spar number 1.

A pair of straight edges was set up on the jig, one on each side of

the plate (Figure I) from which contour readings were obtained. A slight error might have been introduced by this method due to the deflection of the straight edges under their own weight and that of the dial gage fixture. The maximum calculated value of this deflection at the center of the straight edges is in the order of .0015 inches. (Figure V - Figure IX.) Waviness was read with the waviness indicator with the points set two inches apart and again with the points set six inches apart.

III. ANALYSIS

In order to determine the stresses in the sheets after cold bending and the loads to be imposed upon the spar structure by such bending, the theoretical values of such loads and stresses will be determined, based upon the radius of curvature of the sheets.

The radius of curvature was determined in three ways. First, an approximation of this value was obtained from Figure X and Table II. Second, closer approximations were obtained by the use of the waviness indicator with legs set two inches and six inches apart respectively. The radius of curvature used is an average of two values determined as follows:

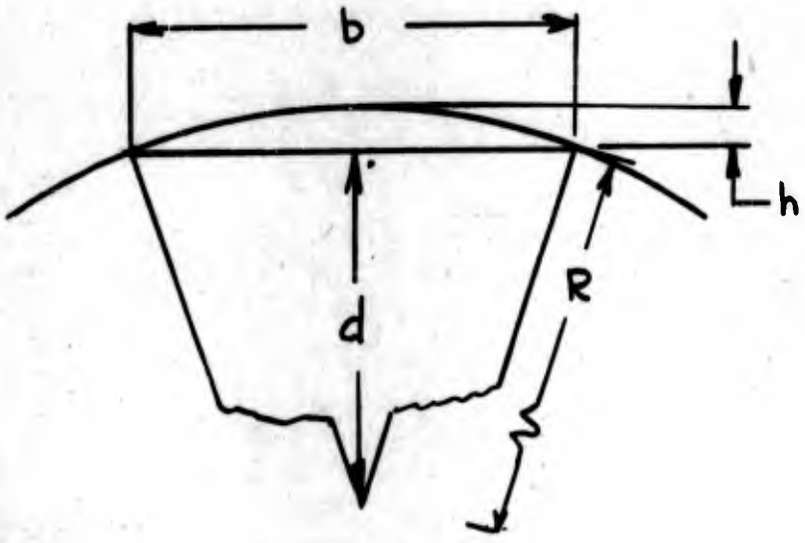

$$d = R - h$$

$$d^2 = R^2 - 2Rh + h^2$$

From geometry, $d^2 = 1/4\ (4R^2 - b^2)$

combining, $R^2 - 2Rh + h^2 = R^2 - \frac{b^2}{4}$

$$-2Rh + h^2 = -\frac{b^2}{4}$$

$$-2R + h = -\frac{b^2}{4h}$$

$$R = +\frac{h}{2} + \frac{b^2}{8h}$$

let $b = 2$

$$R = \frac{h}{2} + \frac{1}{2h}$$

let $b = 6$

$$R = \frac{h}{2} + \frac{4.5}{h}$$

From Figure IV and Figure VIII

$$h_{(max)} = .0940 - .0751 = .0198$$

$$R_6 = \frac{4.5}{.0198} + .0099 = 227 \quad (6'' \text{ spacing})$$

$$R_2 = \frac{1}{.0044} + .0022 = 220 \quad (2'' \text{ spacing})$$

These are minimum values of R.

Stress in formed plates may be determined from the two relationships,

$$M = \frac{EI}{R}$$

and

$$f = \frac{MC}{I} .$$

If d is the thickness of the plate,

$$c = \frac{d}{2}$$

combining these relationships,

$$f = \frac{Ed}{2R} .$$

By assigning a weighted average value

$$R = 225 \text{ in.},$$

the stress in the two plates is determined.

$$f_{(.250)} = \frac{10^7 \times .25}{450} = 5570 \text{ psi}$$

$$f_{(.188)} = \frac{10^7 \times .188}{450} = 4160 \text{ psi}$$

Loads required to bring the sheets in contact with a spar at any radius of curvature are determined from the geometry.

Assume the conditions as shown.

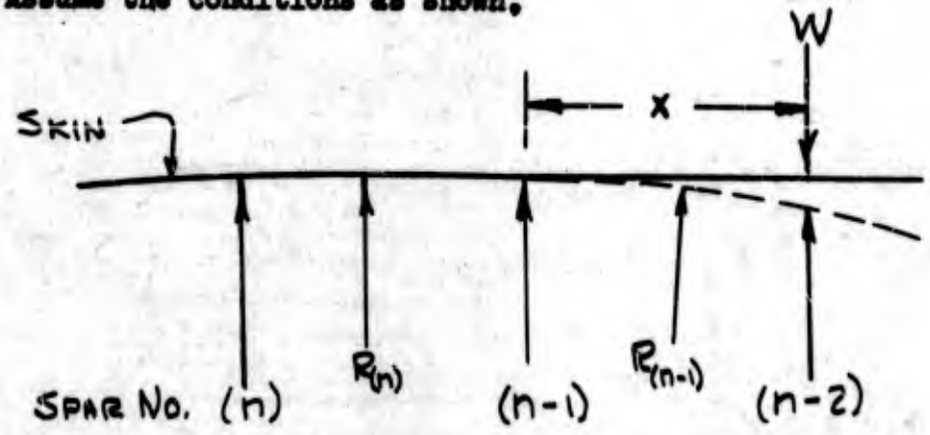

With the skin attached to spar n and (n - 1) the radius of curvature R_n over spar n has been draped into the skin. Since the sheet is flat between spar (n - 1) and (n - 2), $R_{(n-1)} \approx \infty$. The transition between the finite value of $R_{(n)}$ and the infinite value of $R_{(n-1)}$ occurs somewhere between spar (n) and spar (n - 1) and will appear as a flattening of the sheet. However, it is possible by means of a load (W) at spar (n - 1) to induce the radius $R_{(n-1)}$ over spar (n - 1).

Returning to the relationship of moment and curvature:

$$M = \frac{EI}{R},$$

and assuming that this required moment may be induced by the load W at the distance x, it follows that

$$W = \frac{EI}{Rx}.$$

Then

$$W = \frac{10^7 \times .0234}{225 \times 5.637} = 185\#$$

for the .250 sheet and

$$W = \frac{10^7 \times .010}{225 \times 5.637} = 79\#$$

for the .188 sheet, which are the theoretical loads to bring the sheet into contact with spar number 1 where the radius of curvature is a minimum.

IV. RESULTS

Plots have been made at an exaggerated scale of the flat sheets as they lay naturally on the surface plate. (Figure II, Fiugre VI.) These show a transverse (spanwise) crown as well as a considerable chordwise crown, waviness and twist in the .250 plate as received from the mill. The .188 sheet was in considerably better shape although there is a very slight crown in one end. There was no twist in this sheet.

Waviness of the two sheets has been plotted in both exaggerated scales and normal scales which show that, although wavy, the sheets are considerably smoother than comparable skins on airplanes measured by the Boundary Layer group at N.A.I. These curves also show the tendency toward flattening between spars #1 and #2 and between spars #8 and #9 which would be anticipated by analysis.

Loads were applied by means of lead pigs and shot bags over spar #1 to bring the sheets in contact with that spar. The moment arm was not measured due to inability to locate the center of gravity of the pigs, but was slightly less than the 5.637 inches assumed. The results of this loading are shown in Table I.

Sheet Gage	Loading	
	Calculated	Actual
.188	79	80
.250	185	224

TABLE I

A plot of the draped plate centerline readings was made with a vertical scale of .001 inch to 1 mm. and with a horizontal scale of 1 inch to 30 mm. This plot shows very little divergence from a smooth curve. It does show that there are low points over spars 1, 2, 3, 7, 8 and 9, with high points between these named spars. The curve from spar #4 to spar #6 is smooth and follows a splined curve within the accuracy attainable with usual drafting methods. The low points over the named spars might be attributable to the method of clamping the 18 inch wide sheet to the spars and to end effects of the plate. The plate also had a spanwise "crown" over spars 1 - 3 and 7 - 9 but not over spars 4 - 6. This "crown" was noticeable in the flat sheet as delivered from the mill.

In order to give a graphic picture in a size which can be handled, (Figure V and Figure IX) each ordinate was multiplied by 5 and the first and second differences plotted in the five times scale, together with a plot of the actual contour. This plot was made for the center line contour only.

V. CONCLUSIONS

There appears to be no way of comparing waviness from absolute values, but relative values may be obtained by comparing waviness curves plotted to the same scale. (Figure IV vs. Figure VIII.)

The structure of simulated spars can be considered infinitely stiff, compared to the sheets tested. Therefore in attaching a skin to a more flexible wing structure, the skin should be formed. This forming should be incomplete to allow a certain amount of splining action and a tensile stress level not more than 2% to 3% of the working stress level of the completed structure. Forming will also relieve the flattening noted over spars at each end of the sheet by eliminating "end effects".

FORM 30-7A (R. 9-51)

ENGINEER	NORTHROP AIRCRAFT, INC.	PAGE 9
CHECKER		REPORT NO. BIC-42
DATE 10 May 54	ARRANGEMENT OF DRAPED PLATE	MODEL

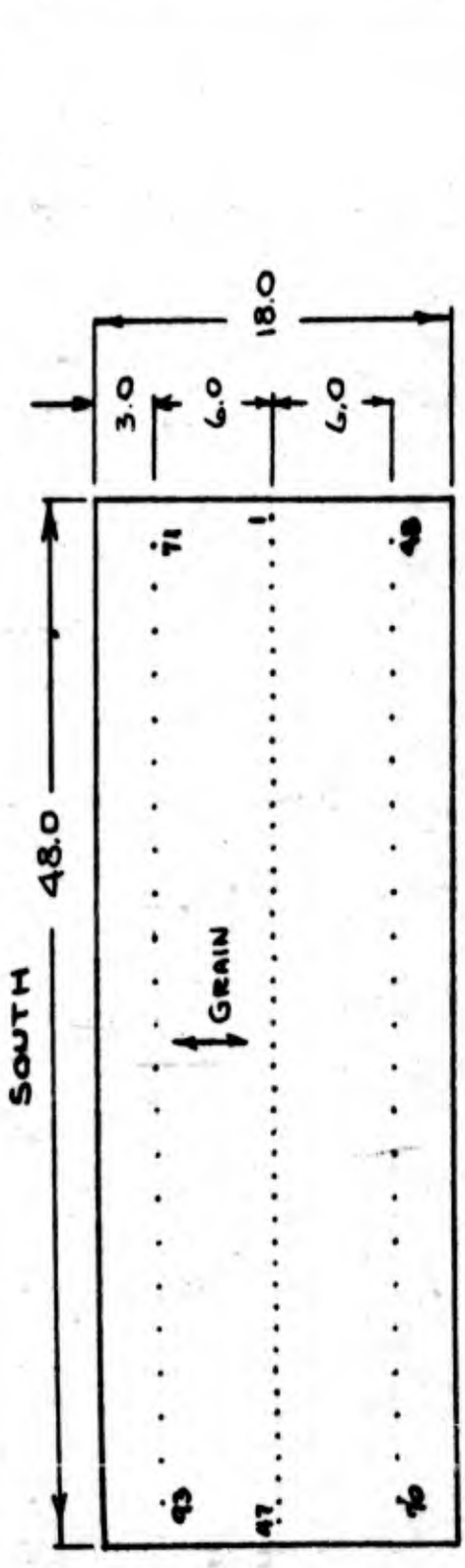

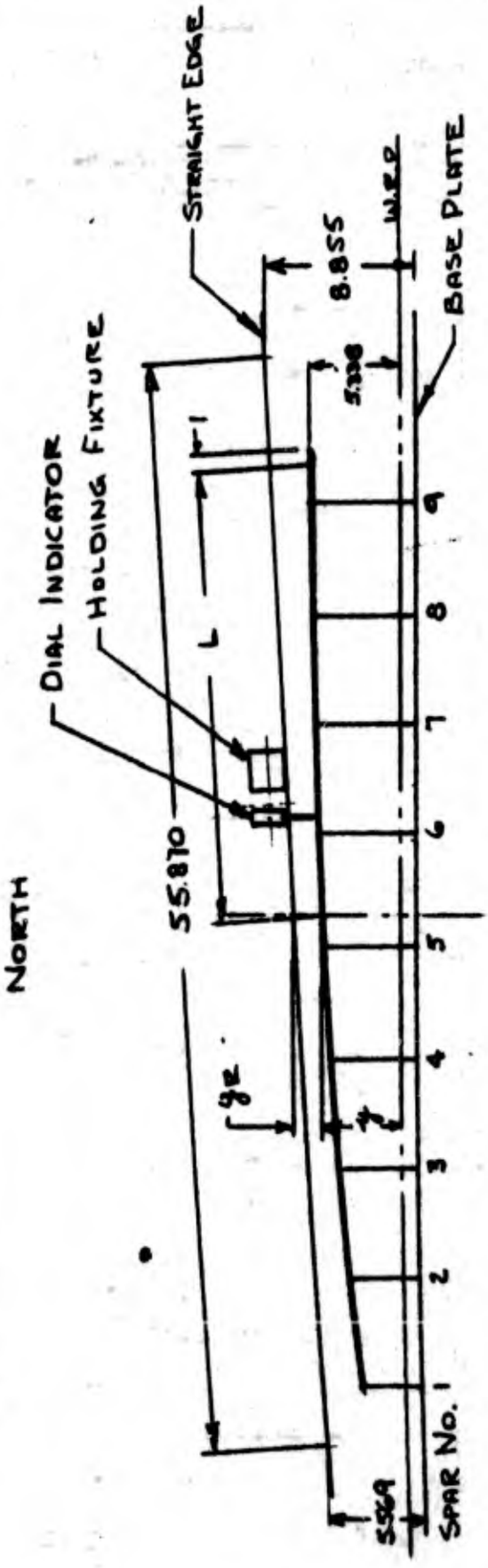

FIG. I

CONFIDENTIAL

ENGINEER	NORTHROP AIRCRAFT INC.	PAGE 10
CHECKER		REPORT NO. BLC-42
DATE 10 May 54	CONTOUR OF .250 75ST-6 FLAT SHEET	MODEL

FORM 20-118 (R. 6-51)

ABSOLUTE VALUES

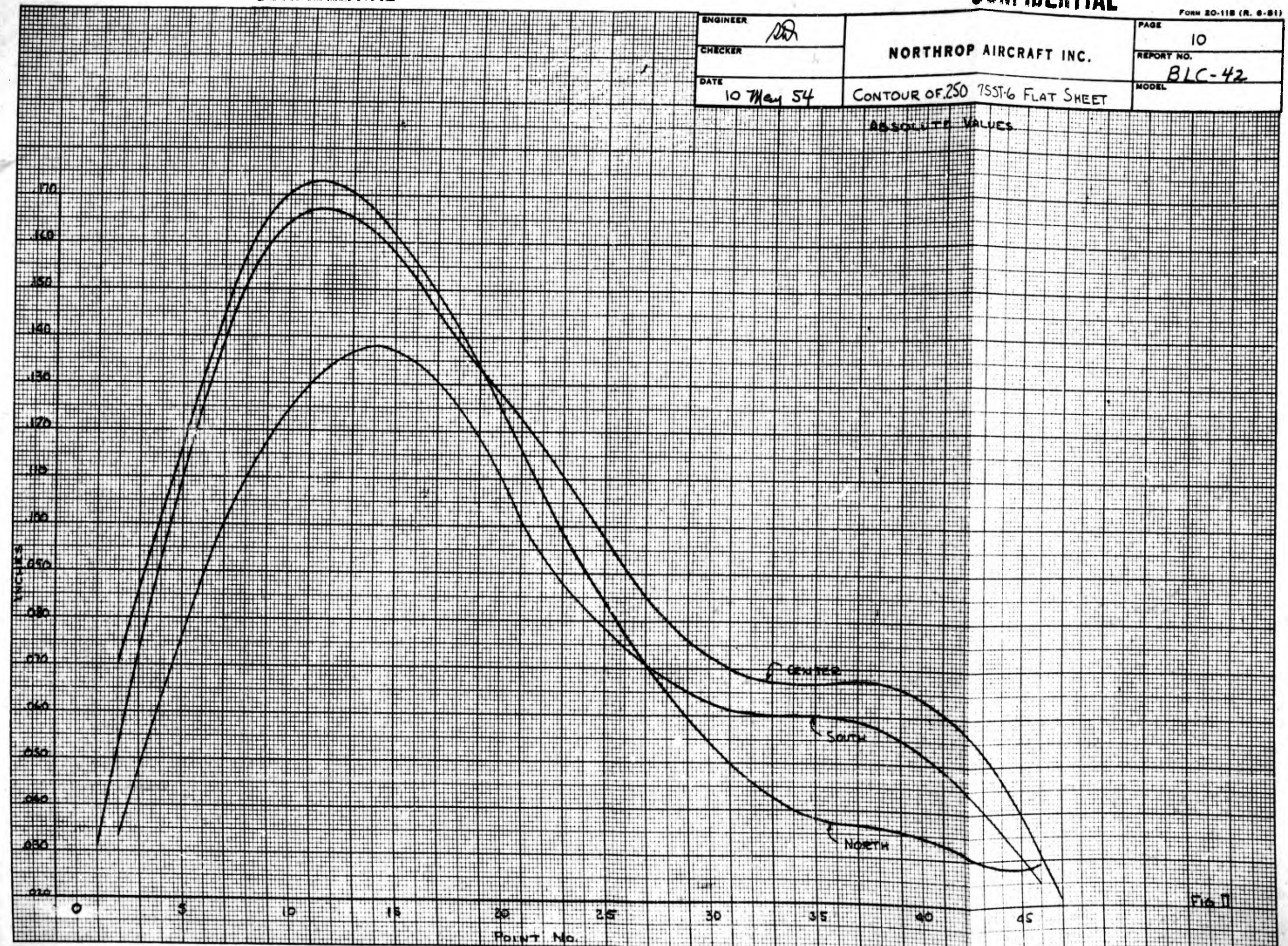

Fig 11

CONFIDENTIAL

CONFIDENTIAL

FORM 20-11B (R. 6-51)

ENGINEER sb	NORTHROP AIRCRAFT INC.	PAGE 11
CHECKER		REPORT NO. BLC-42
DATE 10 May 54	WAVINESS OF .250 75ST-6 FLAT PLATE	MODEL

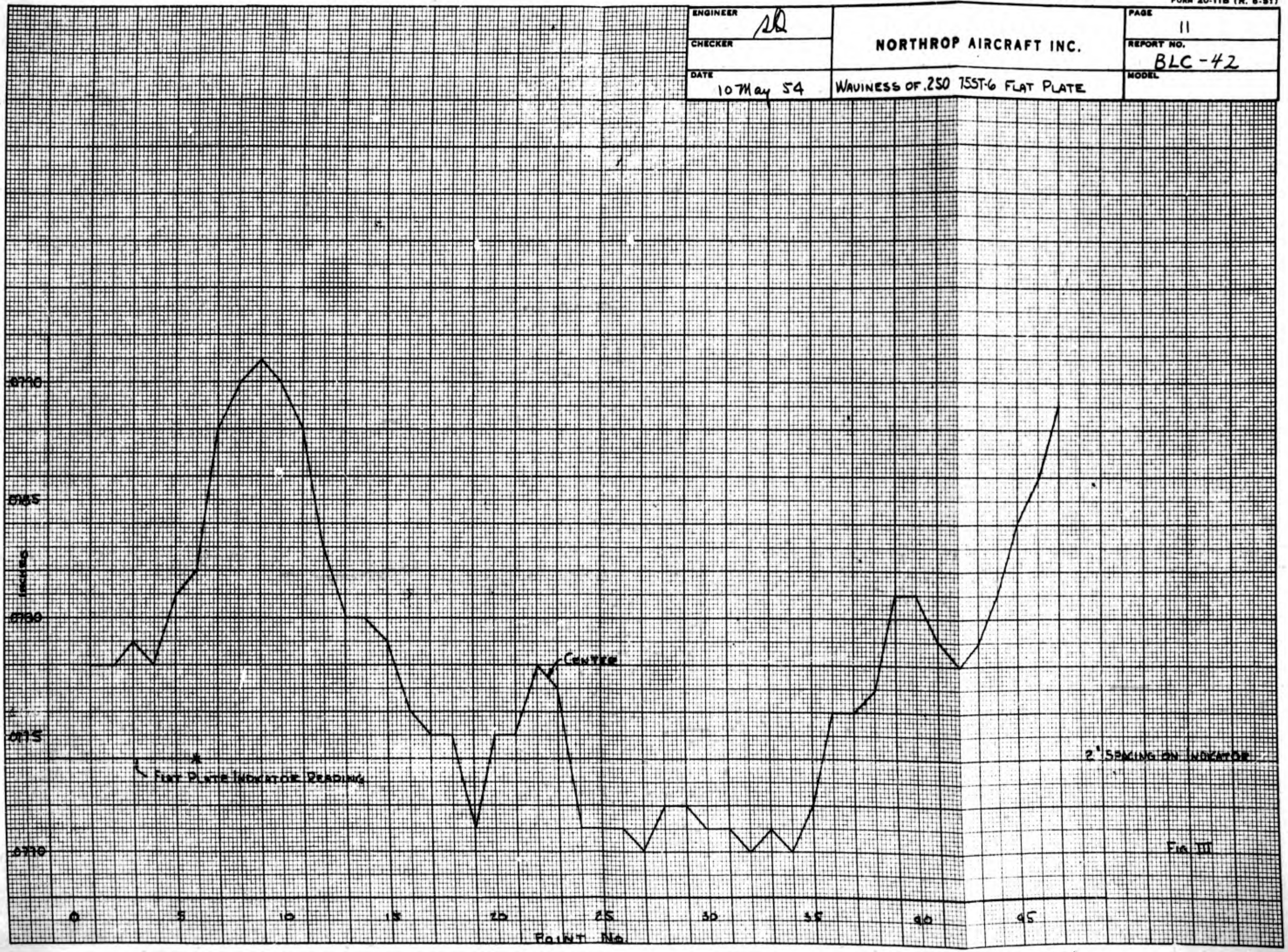

CONFIDENTIAL

CONFIDENTIAL

CONFIDENTIAL

ENGINEER	NORTHROP AIRCRAFT INC.	PAGE 12
CHECKER		REPORT NO. BLC-42
DATE 6 May 54	Waviness .250 Plate 75ST-6	MODEL

FORM 20-118 (R. 6-51)

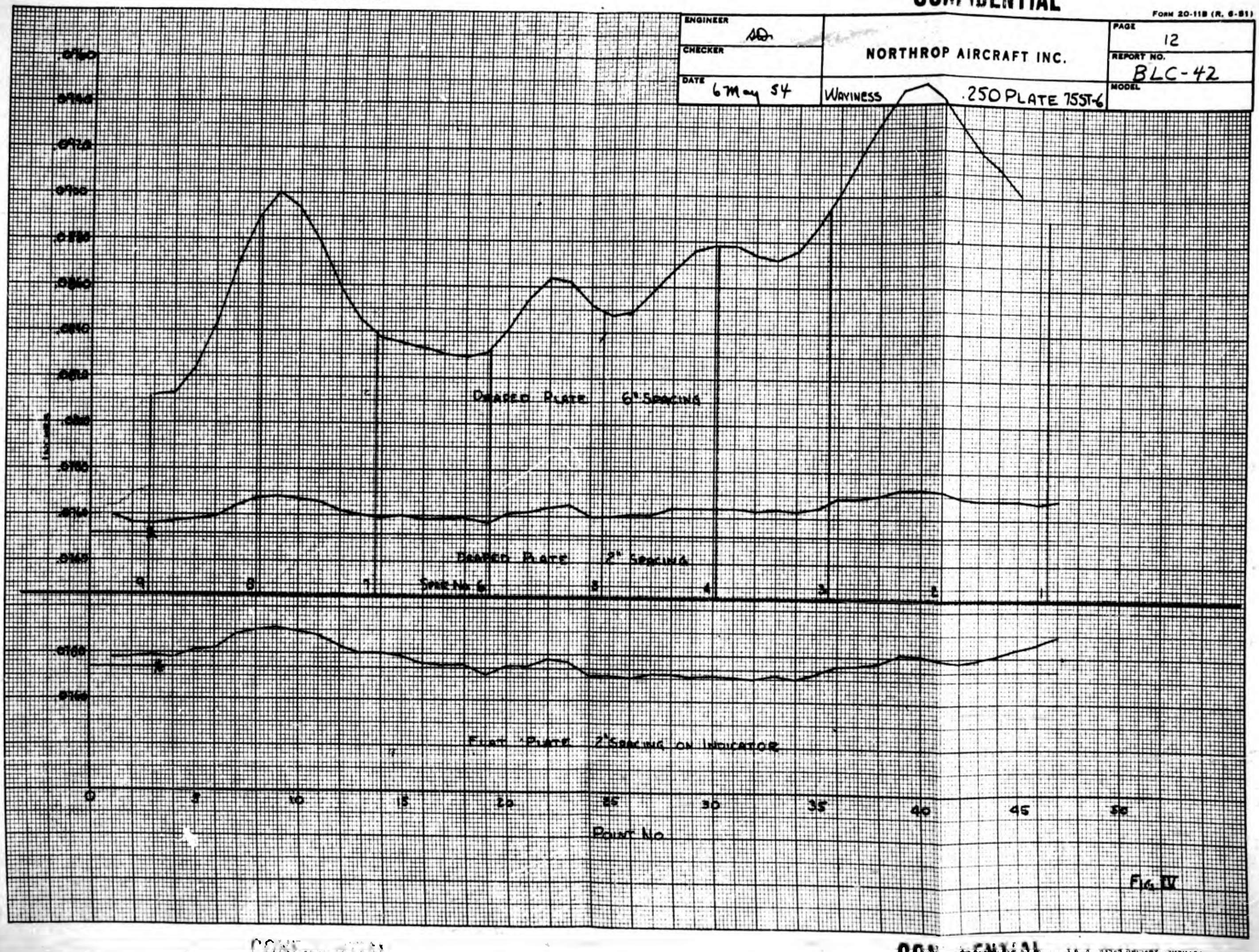

Fig. IV

CONFIDENTIAL

CONFIDENTIAL

ENGINEER		NORTHROP AIRCRAFT INC.	PAGE 13
CHECKER	10 May 54		REPORT NO. BLC-42
DATE		.250 DRAPE PLATE 75ST-6	MODEL

FORM 20-11B (R. 6-51)

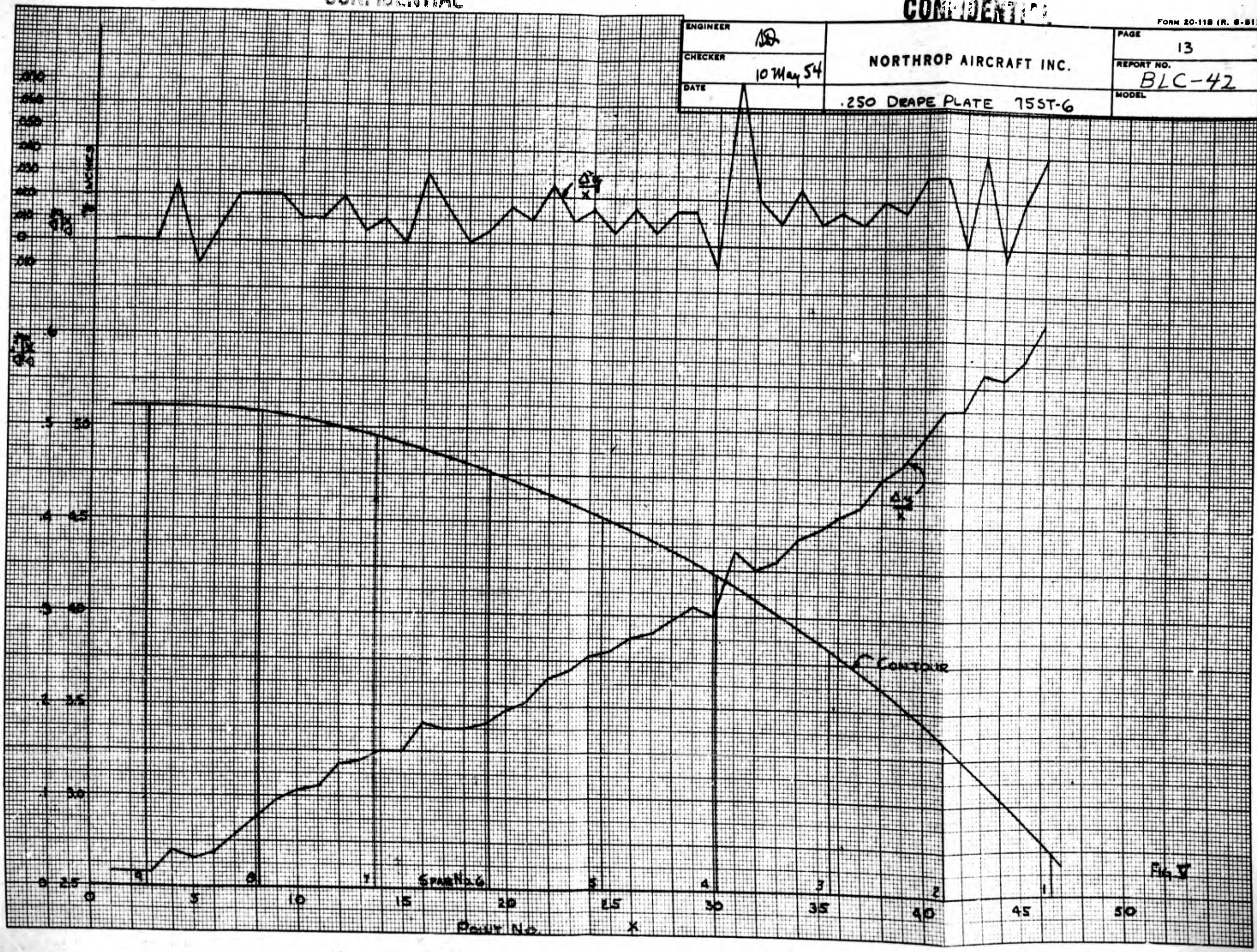

CONFIDENTIAL

Form 20-11B (R. 6-51)

ENGINEER	NORTHROP AIRCRAFT INC.	PAGE 14
CHECKER		REPORT NO. BLC-42
DATE 12 May 54	CONTOUR OF .188 75ST-6AL FLAT SHEET	MODEL

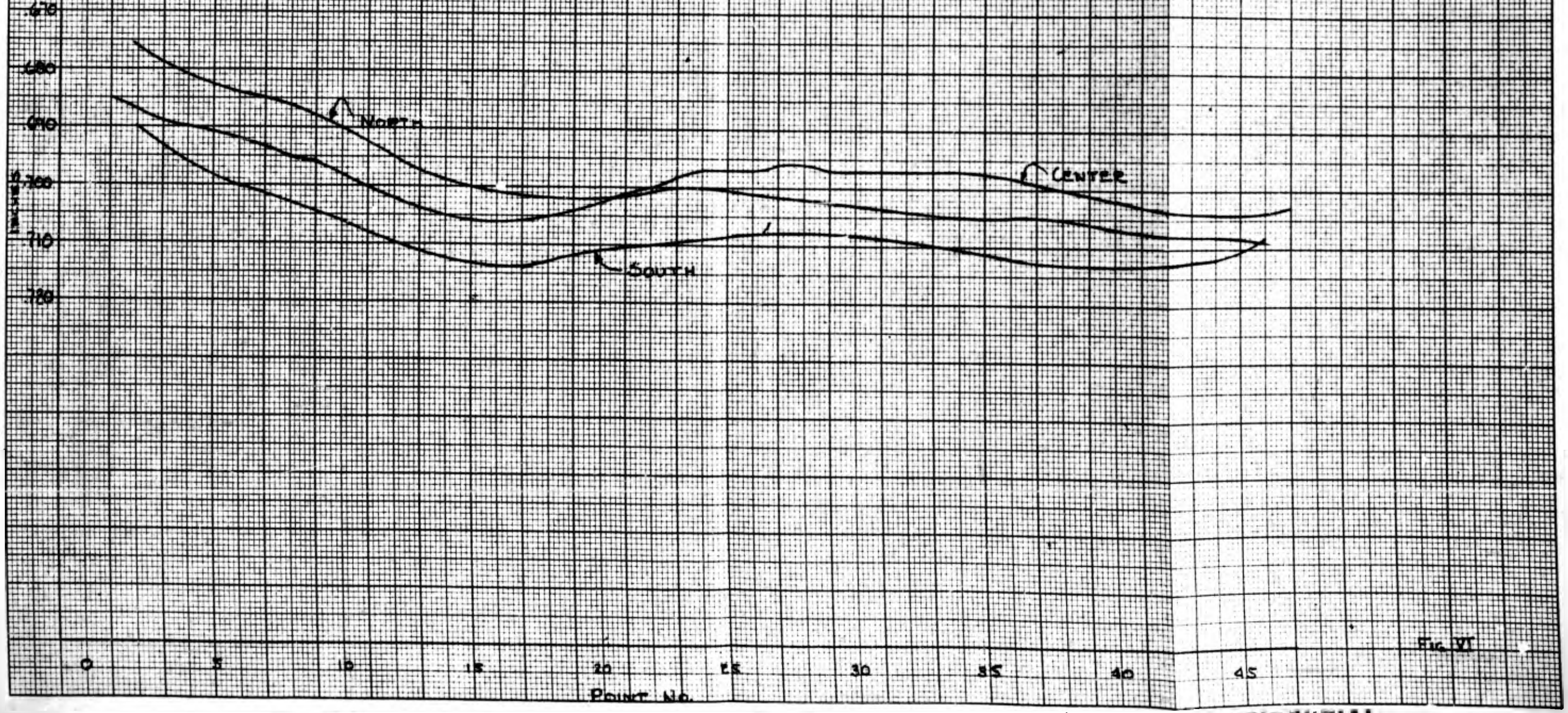

FIG. VI

CONFIDENTIAL

CONFIDENTIAL

CONFIDENTIAL

FORM 20-11B (R. 6-51)

ENGINEER SD	NORTHROP AIRCRAFT INC.	PAGE 15
CHECKER		REPORT NO. BLC-42
DATE 12 May 54	WAVINESS OF .188 75ST-6AL FLAT PLATE	MODEL

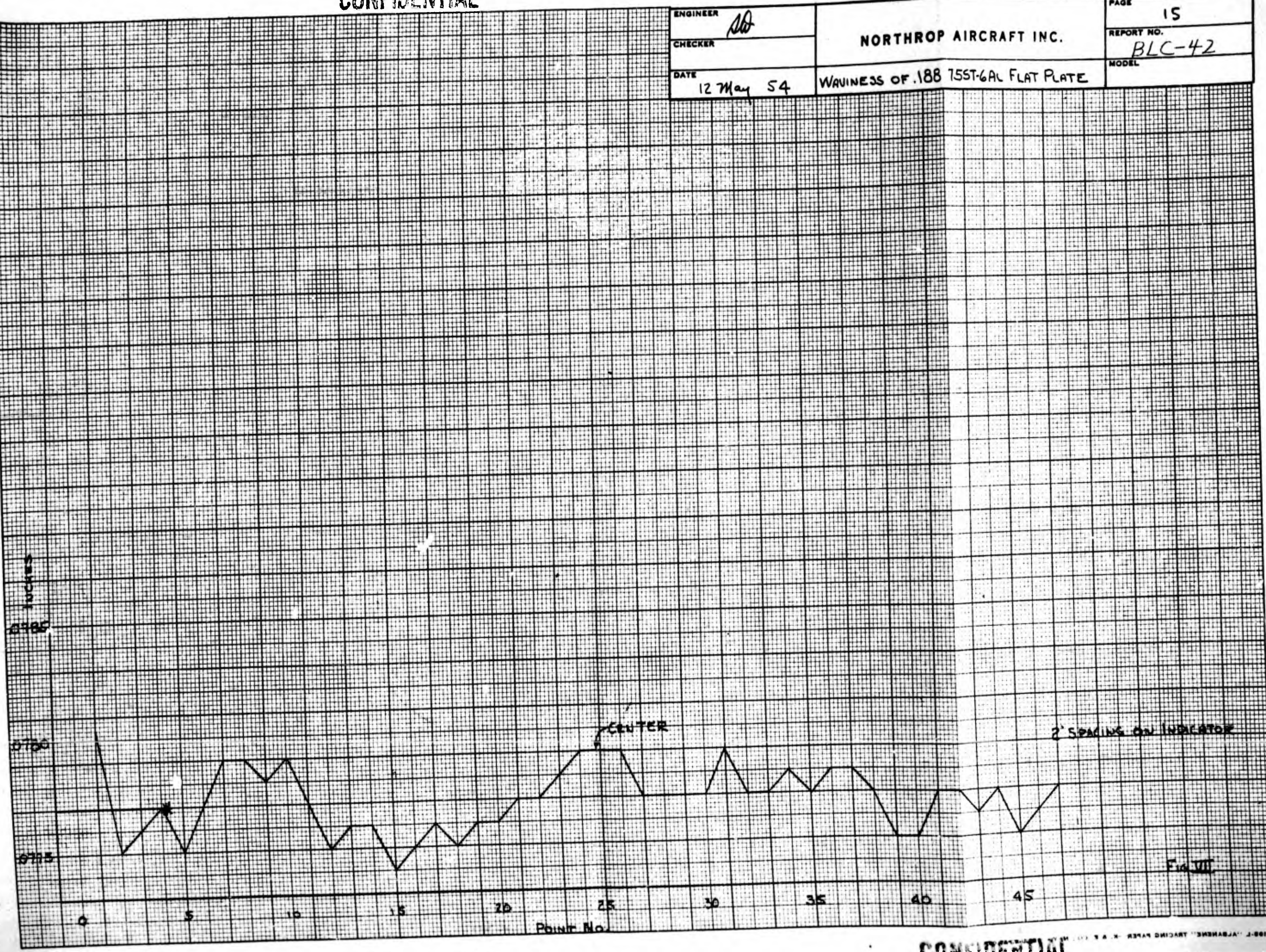

FIG VII

CONFIDENTIAL

CONFIDENTIAL

FORM 20-11B (R. 6-51)

ENGINEER	[signature]	NORTHROP AIRCRAFT INC.	PAGE 16
CHECKER			REPORT NO. BLC-42
DATE	12 May 54	WAVINESS .188 75ST-6AL SHEET	MODEL "

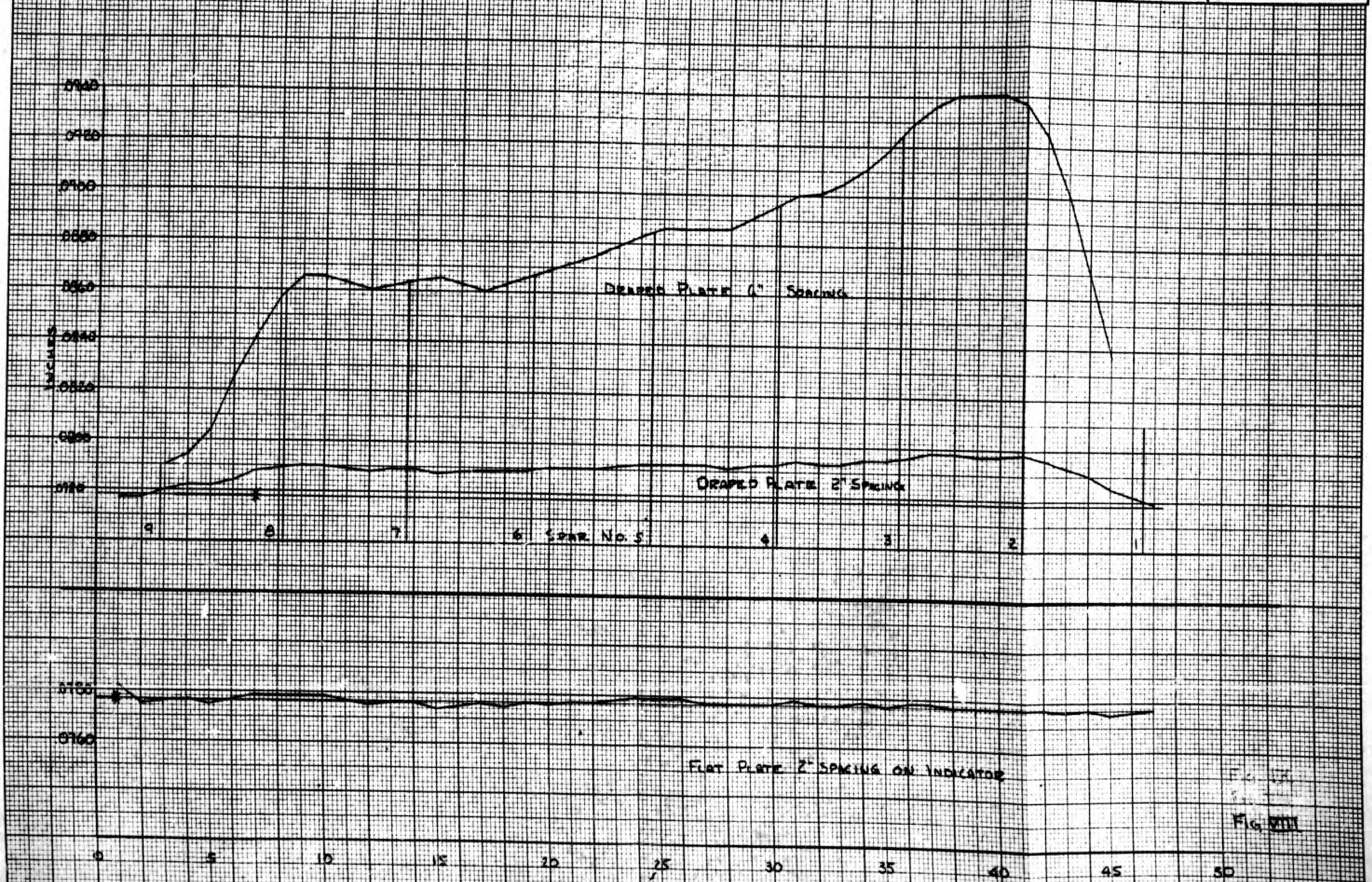

FIG. VIII

CONFIDENTIAL

CONFIDENTIAL

ENGINEER RD	NORTHROP AIRCRAFT INC.	PAGE 17
CHECKER		REPORT NO. BLC-42
DATE 13 May 54	CONTOUR OF .188 75ST-6AL SHEET	MODEL

FORM 20-118 (R. 6-51)

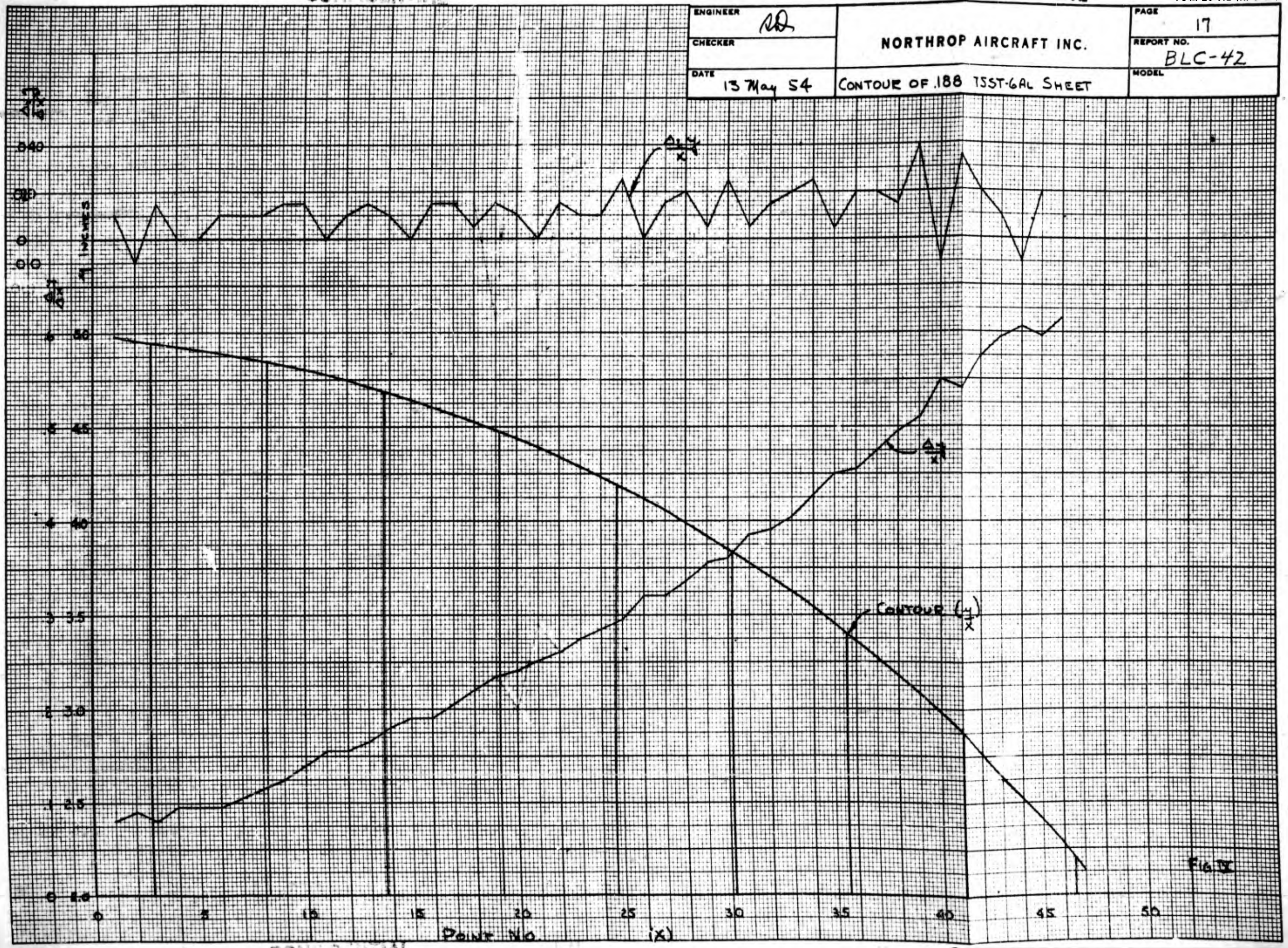

FIG IX

TABLE II

(1) SPAR	(2) ORD	(3) DIFF	(4) (3)/5.637	(5) ANGLE tan⁻¹ (4)	(6) α DIFF (5)	(7) α/2 = (6)/2	(8) SIN (7)	(9) R = 5.637/2 x (8)
1	2.671							
		.693	.1229595	7.0093				
2	3.364				1.5162	.7581	.0132309	213
		.542	.0961675	5.4931				
3	3.906				1.0897	.5448	.0095084	296
		.434	.0770050	4.4034				
4	4.340				0.9309	.4655	.0081244	347
		.342	.0606813	3.4725				
5	4.682				0.7602	.3801	.0066339	425
		.267	.0473740	2.7123				
6	4.949				.7307	.3653	.0063791	442
		.195	.0345990	1.9816				
7	5.144				.6806	.3403	.0059391	474
		.128	.0227111	1.3010				
8	5.272				.6300	.3150	.0054978	513
		.066	.0117104	0.6710				
9	5.338				.6710	.3355	.0058555	481
		.00	0	0				
10	5.338				.6505	.3253	.0056775	496
		.064	.0113556	0.6505				
11	5.274				.7115	.3558	.0062099	454
		.134	.0237757	1.3620				
12	5.140							

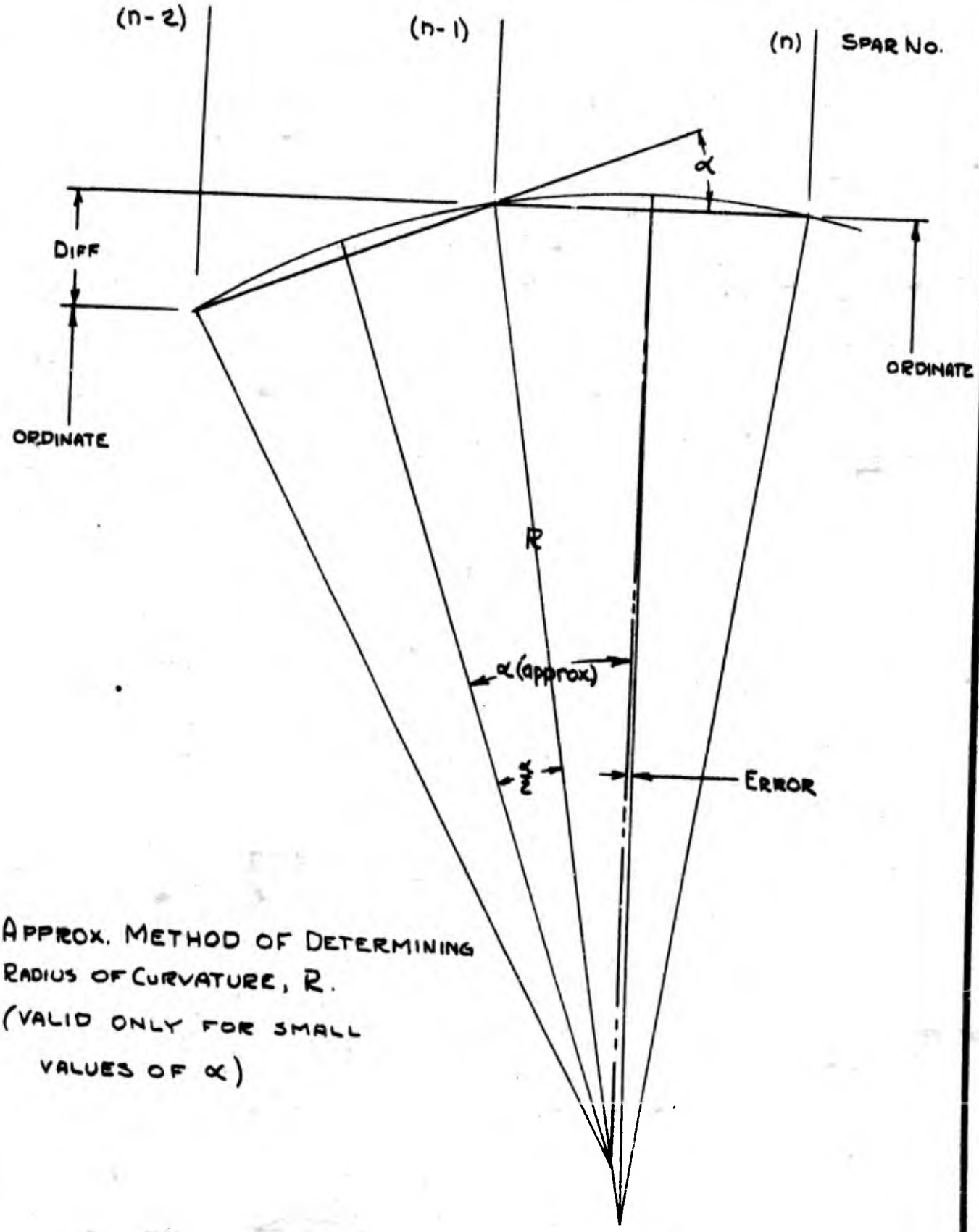

APPROX. METHOD OF DETERMINING RADIUS OF CURVATURE, R.
(VALID ONLY FOR SMALL VALUES OF α)

FIG. X

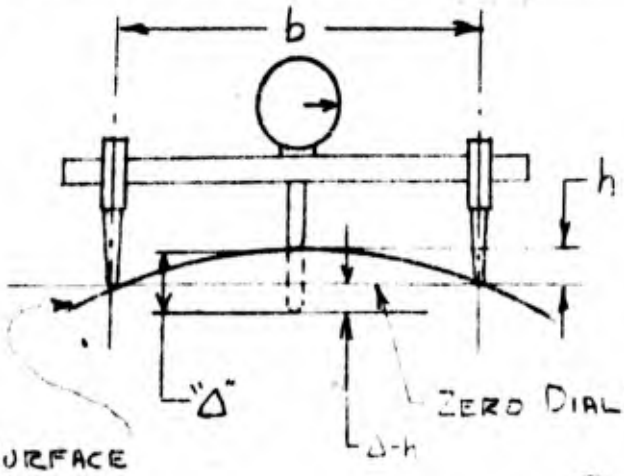

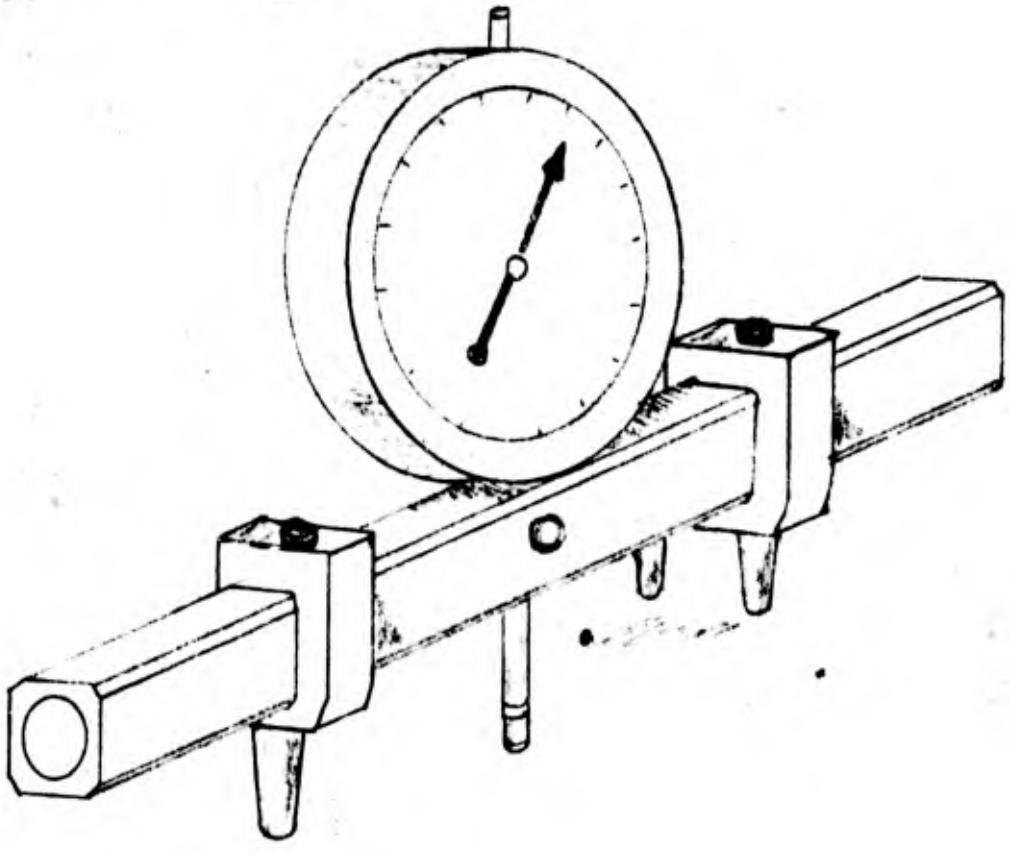

WAVINESS INDICATOR

FIG. XI

CONFIDENTIAL

NORTHROP AIRCRAFT, INC.

HAWTHORNE, CALIFORNIA

REPORT NO. BLC-39

DEFLECTION INDUCED LOADS ACTING ON A CONTINUOUSLY HINGED UNLOADED AILERON

April
1954

PREPARED BY

H. C. Schjelderup

APPROVED BY

W. Pfenninger

REVISIONS

CHG. NO.	DATE	ENGR.	PAGES AFFECTED	REMARKS

CONFIDENTIAL

CONTENTS

LIST OF ILLUSTRATIONS

I. INTRODUCTION

If an aileron is attached to the wing by a continuous connection, one would expect the aileron to assume the same deflected contour as the wing. However, in order to satisfy this condition, at or near the end of the aileron, large intensities of load must act through the connection. These loads are necessary in order to induce into the aileron, a curvature compatible with the wing. Any mathematical attempt to evaluate these end loads will yield undefinable intensities.

The reason for this difficulty is the assumption that the wing and aileron assume the same contour. A more real assumption is to assume that the wing and aileron are connected by an elastic medium such that the wing and aileron may have a relative deflection .

Figure 1 shows a system by which the elastic medium might be represented. The wing and aileron are connected by a continuous spring of spring constant K lbs/in^2 . Then Δ , the relative deflection, is related to the load intensity g acting between the wing and aileron by the equation

$$\Delta = \frac{g}{K} = z_2 - z_1 \qquad (1)$$

where z_1 and z_2 are the deflection curves for the wing and aileron respectively. If the spring constant K can be evaluated, then equation (1) will be a sufficient addition from which determinate values for g can be obtained.

II. ANALYSIS OF AN UNLOADED, UNDEFLECTED AILERON

As a basic assumption, assume the deflection of the wing and aileron may be computed from simple beam deflection formulae. Then, if X_W and X_A are the bending stiffness of the wing and aileron respectively, the simple beam deflection equations may be written

$$X_W \frac{d^4 z_1}{dy^4} = g \tag{2}$$

and

$$X_A \frac{d^4 z_2}{dy^4} = -g \tag{3}$$

Coordinates and sign convention are given in Figure 1.

A solution of equations (1), (2) and (3) will yield for g

$$g = A \cosh \beta y \cos \beta y + B \sinh \beta y \cos \beta y + C \cosh \beta y \sin \beta y + D \sinh \beta y \sin \beta y \tag{4}$$

where

$$\beta^4 = \frac{X_W + X_A}{4 X_W X_A} K$$

The solution of equation (4) for the constants A , B , C , and D is most simply obtained by dividing the solution into two parts:

(a) The load on the wing is symmetric about the midpoint of the aileron, and

(b) The load on the wing is antisymmetric about the midpoint of the aileron.

A general loading of the wing is then obtained by an appropriate summation of parts (a) and (b).

(a) Symmetric Loading

From the assumed symmetry, B and C are zero. Symmetric boundary conditions on equations (1), (2) and (3) are

at $y = \pm b/2$

$$z_1 = 0 \qquad z_2 = g/k \tag{5}$$

$$\frac{d^2z_1}{dy^2} = \frac{1}{R_s} \qquad \frac{d^2z_2}{dy^2} = 0 \tag{6}$$

$$\frac{d^3z_1}{dy^3} = 0 \qquad \frac{d^3z_2}{dy^3} = 0 \tag{7}$$

where $\frac{1}{R_s}$ is the symmetric radius of curvature in the wing and b is the length of the aileron.

These boundary conditions yield from equation (1)

$$\frac{d^3g}{dy^3}(y = b/2) = 0 \tag{8}$$

and

$$\frac{d^2g}{dy^2}(y = b/2) = -\frac{K}{R_s} \tag{9}$$

or substituting equation (4)

$$A(\text{Cosh}\,\alpha\,\text{Sin}\,\alpha + \text{Sinh}\,\alpha\,\text{Cos}\,\alpha) + D(\text{Sinh}\,\alpha\,\text{Cos}\,\alpha - \text{Cosh}\,\alpha\,\text{Sin}\,\alpha) = 0 \tag{10}$$

and

$$A\,\text{Sinh}\,\alpha\,\text{Sin}\,\alpha - D\,\text{Cosh}\,\alpha\,\text{Cos}\,\alpha = \frac{K}{2\beta^2 R_s} \tag{11}$$

where $\alpha = \beta\, b/2$

Equations (10) and (11) define the constants A and D .

$$A = \frac{+K}{2\beta^2 R_s} \frac{\cosh\alpha \sin\alpha - \sinh\alpha \cos\alpha}{\sinh\alpha \cosh\alpha + \sin\alpha \cos\alpha} \tag{12}$$

and

$$D = \frac{-K}{2\beta^2 R_s} \frac{\cosh\alpha \sin\alpha + \sinh\alpha \cos\alpha}{\sinh\alpha \cosh\alpha + \sin\alpha \cos\alpha} \tag{13}$$

Now since g is defined explicitly by equations (4), (12), and (13), equations (2) and (3) may be solved for z_1 and z_2 . The result is

$$4\beta^4 X_w z_1 = -g + C_1 \alpha^2 \left(\frac{2y}{b}\right)^2 + C_2 \tag{14}$$

and

$$4\beta^4 X_A z_2 = g + D_1 \alpha^2 \left(\frac{2y}{b}\right)^2 + D_2 \tag{15}$$

where C_1 , C_2 , D_1 , and D_2 are determined by equations (5), (6) and (7).

In general, the only function of interest is g , as g is the load intensity acting on the hinge as well as being proportional to the shape of the step Δ between the wing deflection and aileron deflection. The maximum value of Δ will occur where g is a maximum. This point of maximum relative deflection occurs where $y = \pm b/2$ and is given by the equation

$$\Delta_{max} = \frac{g_{max}}{K} \frac{-1}{2\beta^2 R_s} \left[\frac{\cosh\alpha \sinh\alpha - \sin\alpha \cos\alpha}{\cosh\alpha \sinh\alpha + \sin\alpha \cos\alpha}\right] \tag{16}$$

The term within the brackets is plotted in Figure 2 which shows that for $\alpha \geqslant \pi$ this expression may be approximated by unity. Then equation (16) may be approximated

$$\Delta_{max} = \frac{-1}{2\beta^2 R_s} \tag{17}$$

or from equation (1)

$$g_{max} = \frac{-K}{2\beta^2 R_s} \tag{18}$$

A study of the general symmetric solution will show that for α large, g will very quickly approach zero as y varies from a value $\pm$ b/2 to zero. This rapid dissipation of g , the interaction, indicates that for symmetric loading, the forces necessary to force the aileron into curvature exist only at or near the ends of the aileron. In fact, these forces form a couple of intensity sufficient to cause a curvature $\frac{1}{R_s}\frac{X_w}{X_w + X_A}$ in the aileron. The magnitude of one of the forces developing the couple is identical to the integral of g from $y = b/2$ to $y = y_g = 0$.

It can be shown that for α greater than $\frac{3\pi}{4}$, the point of zero load ($g = 0$) will occur at $1 - \frac{2y}{b}$ equal to $\frac{\pi}{4\alpha}$ and the magnitude of the force is given by equation (19)

$$V_{max} = \frac{0.1624\ K}{\beta^3 R_s} \tag{19}$$

For instances when α is less than $\frac{3\pi}{4}$, V_{max} must be obtained by integration of the general equation. In order to show the origin of the value α equal to $\frac{3\pi}{4}$, a plot of values of y vs α is shown in Figure 3. y is the absissae at which g equals zero.

(b) Antisymmetric Loading

From the assumed symmetry, A and D of equation (4) are zero. Antisymmetric boundary conditions on equations (1), (2), and (3) are

At $y = \pm b/2$

$$z_1 = 0 \qquad z_2 = g/K \tag{20}$$

$$\frac{d^2z_1}{dy^2} = \mp\frac{1}{R_s} \qquad \frac{d^2z_2}{dy^2} = 0 \tag{21}$$

$$\frac{d^3z_1}{dy^3} = -\frac{V}{K_w} = -\frac{2}{bR_s} \qquad \frac{d^3z_2}{dy^3} = 0 \tag{22}$$

where $1/R_s$ is the curvature of the wing at $y = \pm b/2$.

These boundary conditions yield at $y = b/2$

$$\frac{d^3g}{dy^3} = \frac{2K}{bR_s} \tag{23}$$

and

$$\frac{d^2g}{dy^2} = \frac{K}{R_s} \tag{24}$$

A substitution of equation (4) in equations (23) and (24) will give

$$(\text{Sinh}\,\alpha\,\text{Sin}\,\alpha + \text{Cosh}\,\alpha\,\text{Cos}\,\alpha)B + (\text{Sinh}\,\alpha\,\text{Sin}\,\alpha - \text{Cosh}\,\alpha\,\text{Cos}\,\alpha)C = \frac{-K}{b\beta^3R_s} \tag{25}$$

and

$$\text{Cosh}\,\alpha\,\text{Sin}\,\alpha\,B - \text{Sinh}\,\alpha\,\text{Cos}\,\alpha\,C = \frac{K}{2\beta^2R_s} \tag{26}$$

or solving for B and C

$$B = \frac{K}{2\beta^2R_s}\cdot\frac{\frac{1}{\alpha}(\text{Sinh}\,\alpha\,\text{Cos}\,\alpha) + (\text{Sinh}\,\alpha\,\text{Sin}\,\alpha - \text{Cosh}\,\alpha\,\text{Cos}\,\alpha)}{\text{Sin}\,\alpha\,\text{Cos}\,\alpha - \text{Sinh}\,\alpha\,\text{Cosh}\,\alpha} \tag{27}$$

$$C = \frac{K}{2\beta^2 R_s} \cdot \frac{\frac{1}{\alpha}(\text{Cosh}\,\alpha\,\text{Sin}\,\alpha) + (\text{Sinh}\,\alpha\,\text{Sin}\,\alpha + \text{Cosh}\,\alpha\,\text{Cos}\,\alpha)}{\text{Sin}\,\alpha\,\text{Cos}\,\alpha - \text{Sinh}\,\alpha\,\text{Cosh}\,\alpha} \qquad (28)$$

Again g is a maximum at the ends $y = \pm b/2$. A study of the equation for g will show that if α is greater than π, g may be approximated

$$g_{max} = \frac{-K}{2\beta^2 \alpha R_s} + \frac{K}{2\beta^2 R_s} \qquad (29)$$

A comparison of equation (29) with equation (18) shows that the intensity of loading required to force the symmetric beam into curvature, is greater than those required to force the same beam into antisymmetrical curvature. This conclusion would be expected as in the case of the antisymmetrical loading, curvature of the wing is decreasing away from the ends.

III. ANALYSIS OF AN UNLOADED, DEFLECTED AILERON

Again, as a basic assumption, assume the deflection of the wing and aileron may be handled by simple beam deflection equations. However, as an additional assumption, assume the hinge infinitely rigid against bending about on axis perpendicular to its plane. Deformation of the hinge will then be restricted to displacement perpendicular to the plane of the hinge.

Now if X_w, X_A, Z_A are the bending stiffness of the wing about the X axis, and the aileron about the X_2 and Z_2 axis respectively, for the configuration of Figure 4,

$$z_1^{iv} = \frac{g_1}{X_w} \tag{30}$$

$$z_2^{iv} = \frac{g_2}{X_A} \tag{31}$$

and $$x_2^{iv} = \frac{p_2}{Z_A} \tag{32}$$

where $$z_1^{i} = \frac{dz_1}{dy}$$

A consideration of statics will yield the equations

$$p_1 = -p_2\text{Cos}\theta - g_2\text{Sin}\theta \tag{33}$$

$$g_1 = p_2\text{Sin}\theta - g_2\text{Cos}\theta \tag{34}$$

and a consideration of deformation will yield

$$z_1 - z_2\text{Cos}\theta + x_2\text{Sin}\theta = -\frac{g_1}{K_1} + \frac{g_2}{K_2}\text{Cos}\theta \tag{35}$$

and $$z_2\text{Sin}\theta + x_2\text{cos}\theta = -\frac{g_2}{K_2}\text{Sin}\theta \tag{36}$$

where θ is the deflection of the aileron.

Equations (31), (32) and (36) will give

$$p_2 = -\frac{\text{Tan}\theta Z_A}{K_2} g_2^{iv} - \frac{Z_A}{X_A} g_2\text{Tan}\theta \tag{37}$$

Equation (37) substituted in equation (34) gives

$$g_1 = -\frac{Z_A \mathrm{Tan}\theta \mathrm{Sin}\theta}{K_2} g_2^{iv} - \left(\frac{Z_A \mathrm{Tan}\theta \mathrm{Sin}\theta}{X_A} + \mathrm{Cos}\theta\right) g_2 \tag{38}$$

Finally, equations (30), (31), (32), (37) and (38) substituted in equation (35) will give

$$a g_2^{viii} + b g_2^{iv} + c g_2 = 0 \tag{39}$$

where

$$a = \frac{Z_A \mathrm{Tan}\theta \mathrm{Sin}\theta}{K_2 K_1}$$

$$b = \frac{1}{K_1}\left(\mathrm{Cos}\theta + Z_A \frac{\mathrm{Tan}\theta \mathrm{Sin}\theta}{X_A}\right) + \frac{1}{K_2}\left(\frac{Z_A \mathrm{Tan}\theta \mathrm{Sin}\theta}{X_w} + \frac{1}{\mathrm{Cos}\theta}\right)$$

and

$$c = \frac{1}{X_w X_A}\left(X_A \mathrm{Cos}\theta + \frac{X_w}{\mathrm{Cos}\theta} + Z_A \mathrm{Tan}\theta \mathrm{Sin}\theta\right)$$

Equation (39) is an eighth order homogeneous differential equation with constant coefficients, the solution of which may be obtained by various methods.

Before discussing this solution further, consider the condition where the rear hinge is attached directly to the aileron. For this condition, $K_2 \longrightarrow \infty$ and equation (39) becomes

$$g_2^{iv} + 4\gamma^4 g_2 = 0 \tag{40}$$

where

$$\gamma^4 = \frac{K_1\left(1 + \frac{Z_A \mathrm{Tan}^2\theta}{X_A} + \frac{X_w}{X_A \mathrm{Cos}^2\theta}\right)}{4\left(X_w + \frac{X_w Z_A \mathrm{Tan}^2\theta}{X_A}\right)}$$

The general solution of equation (40) will be identical to equation (4) where $\beta = \gamma$. However, the boundary conditions will be modified.

a. Symmetric Solution $K_2 \longrightarrow \infty$

Symmetric boundary conditions for the system are as follows:

At $y = \pm b/2$

$$z_1 = 0 \qquad z_2 = + \frac{g_1}{K_1}\mathrm{Cos}\theta \qquad x_2 = - \frac{g_1}{K_1}\mathrm{Sin}\theta \tag{41}$$

$$z_1^{ii} = \frac{1}{R_s} \qquad z_2^{ii} = 0 \qquad x_2^{ii} = 0 \tag{42}$$

$$z_1^{iii} = 0 \qquad z_2^{iii} = 0 \qquad x_2^{iii} = 0 \tag{43}$$

Now for the condition $K_2 \longrightarrow \infty$, boundary condition (43), will give from equations (35), (36), and (38)

$$g_2^{iii} = 0 \tag{44}$$

and boundary conditon (42) will give from equations (35), (36), and (38)

$$g_2^{ii} = \frac{K_1}{R_s}\left(\frac{X_A}{X_A\mathrm{Cos}\theta + Z_A\mathrm{Tan}\theta\mathrm{Sin}\theta}\right) \tag{45}$$

Now similarily to the treatment of equation (4)

$$g_{2_{max}} = \frac{K_1}{2\gamma^2 R_s}\,\frac{X_A}{X_A\mathrm{Cos}\theta + Z_A\mathrm{Tan}\theta\mathrm{Sin}\theta} \tag{46}$$

and from equations (33), (37), and (38)

$$p_{2_{max}} = \frac{K_1}{2\gamma^2 R_s} \frac{Z_A \mathrm{Tan}\theta}{X_A \mathrm{Cos}\theta + Z_A \mathrm{Tan}\theta \mathrm{Sin}\theta} \tag{47}$$

$$g_{1_{max}} = \frac{-K_1}{2\gamma^2 R_s} \tag{48}$$

and

$$p_{1_{max}} = \frac{K_1}{2\gamma^2 R_s}\left(\frac{Z_A - X_A}{X_A \mathrm{Cos}\theta + Z_A \mathrm{Tan}\theta \mathrm{Sin}\theta}\right)\mathrm{Sin}\theta \tag{49}$$

Since the solution here is identical in form to equation (4), conclusions made for the undeflected aileron are also valid for the deflected aileron.

b. Antisymmetric Solution $K_2 \longrightarrow \infty$

Antisymmetric boundary conditions for the system are as follows:

At $y = \pm b/2$

$$z_1^{ii} = \mp 1/R_s \qquad z_2^{ii} = 0 \qquad x_2^{ii} = 0 \tag{50}$$

$$z_1^{iii} = -\frac{2}{bR_s} \qquad z_2^{iii} = 0 \qquad x_2^{iii} = 0 \tag{51}$$

These boundary conditions applied to equations (35), (36), and (38) yield at

$y = \pm b/2$

$$g_2^{ii} = \mp \frac{K_1}{R_s}\left(\frac{X_A}{X_A \mathrm{Cos}\theta + Z_A \mathrm{Tan}\theta \mathrm{Sin}\theta}\right) \tag{52}$$

$$g_2^{iii} = -\frac{2K_1}{bR_s}\left(\frac{X_A}{X_A\text{Cos}\theta + Z_A\text{Tan}\theta\text{Sin}\theta}\right) \tag{53}$$

Now similarily to the treatment of equation (4),

at $y = b/2$

$$g2_{max} = \frac{X_A}{X_A\text{Cos}\theta + Z_A\text{Tan}\theta\text{Sin}\theta}\left(\frac{K_1}{b\,\gamma^3 R_s} - \frac{K_1}{2\,\gamma^2 R_s}\right) \tag{54}$$

and from equation (38)

$$g_{1_{max}} = \frac{K_1}{2\,\gamma^2 R_s} - \frac{K_1}{b\,\gamma^3 R_s} \tag{55}$$

Thus, equations (46) to (55) give the various hinge loadings for the deflected aileron under the condition that K_2 the elastic constraint hinge to aileron is very much greater than K_1 the elastic constraint, hinge to wing.

For the condition that K_2 is not large, the general equation will be the solution of equation (39). This solution is

$$\begin{aligned} g_2 = {} & A\,\text{Cosh}\,\gamma y\,\text{Cos}\,\gamma y + B\,\text{Sinh}\,\gamma y\,\text{Sin}\,\gamma y \\ & + C\,\text{Cosh}\,\delta y\,\text{Cos}\,\delta y + D\,\text{Sinh}\,\delta y\,\text{Sin}\,\delta y \\ & + E\,\text{Cosh}\,\gamma y\,\text{Sin}\,\gamma y + F\,\text{Sinh}\,\gamma y\,\text{Cos}\,\gamma y \\ & + G\,\text{Cosh}\,\delta y\,\text{Sin}\,\delta y + H\,\text{Sinh}\,\delta y\,\text{Cos}\,\delta y \end{aligned}$$

where $\gamma = \dfrac{|m_1|^{1/4}}{\sqrt{2}}$ and $\delta = \dfrac{|m_2|^{1/4}}{\sqrt{2}}$

and m_1 and m_2 are the roots of the equation

$$am^2 + bm + c = 0 \tag{57}$$

where a , b , and c , are the coefficients of equation (39).

Boundary conditions on the system are those of equations (41), (42), and (43) for the symmetric case and (50) and (51) for the antisymmetric case.

For the symmetric case, the coefficients, E , F , G , and H of equation (56) are zero. Equations (41), (42), and (43) will give

for $y = \pm b/2$

$$g_2^{ii} = 0 \tag{58}$$

$$g_2^{iii} = 0 \tag{59}$$

$$g_2^{vi} = \frac{K_1 K_2}{R_s} \frac{1}{Z_A \mathrm{Tan}\theta \mathrm{Sin}\theta} \tag{60}$$

$$g_2^{vii} = 0 \tag{61}$$

For the antisymmetrical case, the coefficients A , B , C , and D of equation (56) are zero. Equations (50) and (51) will give

for $y = b/2$

$$g_2^{ii} = 0 \tag{62}$$

$$g_2^{iii} = 0 \tag{63}$$

$$g_2^{vi} = -\frac{K_1 K_2}{R_s} \frac{1}{Z_A \mathrm{Tan}\theta \mathrm{Sin}\theta} \tag{64}$$

$$g_2^{vii} = \frac{-2K_1 K_2}{bR_s} \frac{1}{Z_A \mathrm{Tan}\theta \mathrm{Sin}\theta} \tag{65}$$

These boundary conditions and equations (58) to (65) provide the necessary equations to solve for the constants A , B , C , etc. The load g_2 may then be evaluated for any y .

IV. CONCLUSIONS

The above show that much complication of analysis may be avoided if the hinge is designed such that the elastic constant K_2 is large compared to K_1 . In design, this condition is not difficult to meet, as a direct attachment hinge to aileron will fulfill the requirement. The problem of design is then to choose hinge dimensions such that the load g does not become sufficiently large to cause bending stresses in the hinge that will exceed the material design stresses.

In order to clarify results, and in order to illustrate the evaluation of the spring constants, etc., a short example calculation is presented in Appendix I.

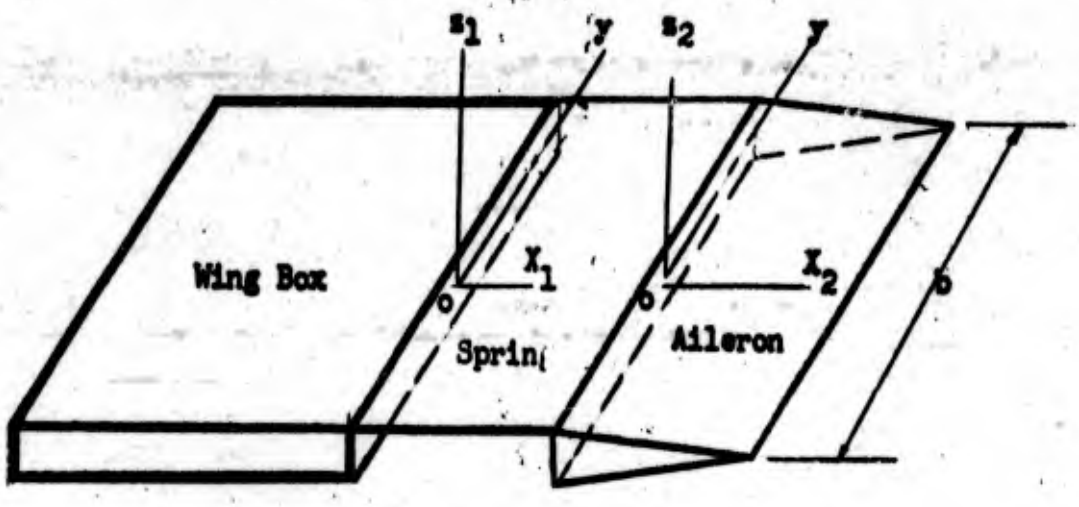

(a)

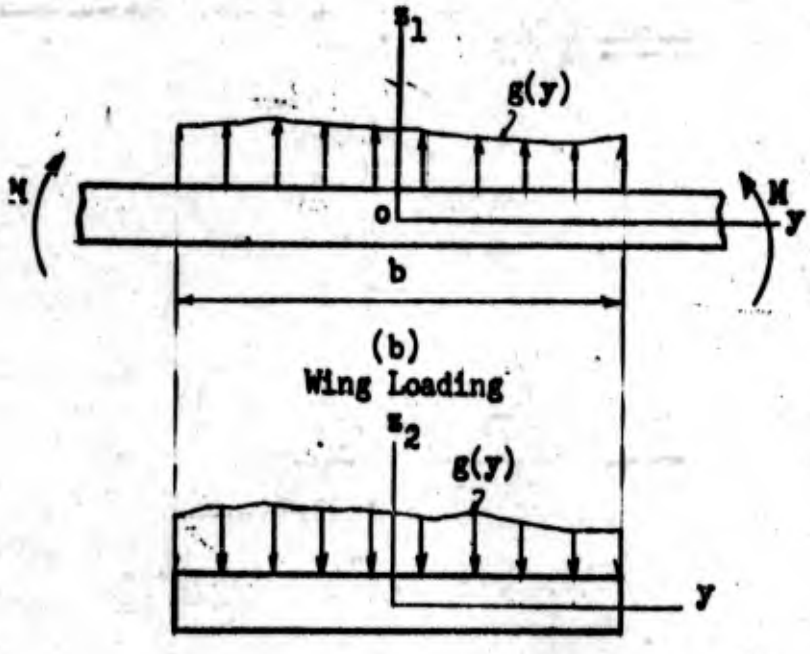

(b)
Wing Loading

(c)
Aileron Loading

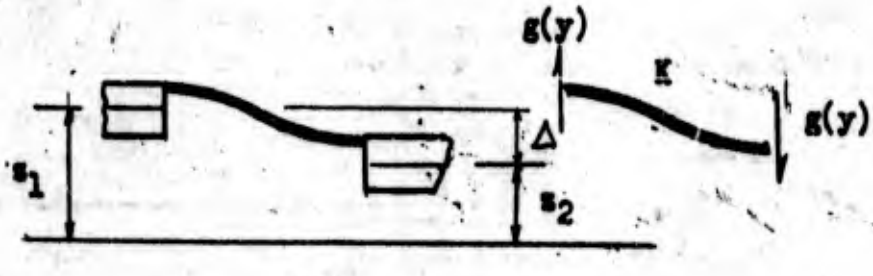

(d)
Spring Deformation

Figure I

Curve showing the magnitude of

$$\frac{\text{Cosh}\alpha\,\text{Sinh}\alpha - \text{Cos}\alpha\,\text{Sin}\alpha}{\text{Cosh}\alpha\,\text{Sinh}\alpha + \text{Cos}\alpha\,\text{Sin}\alpha}$$

as α varies from 0.2 to π

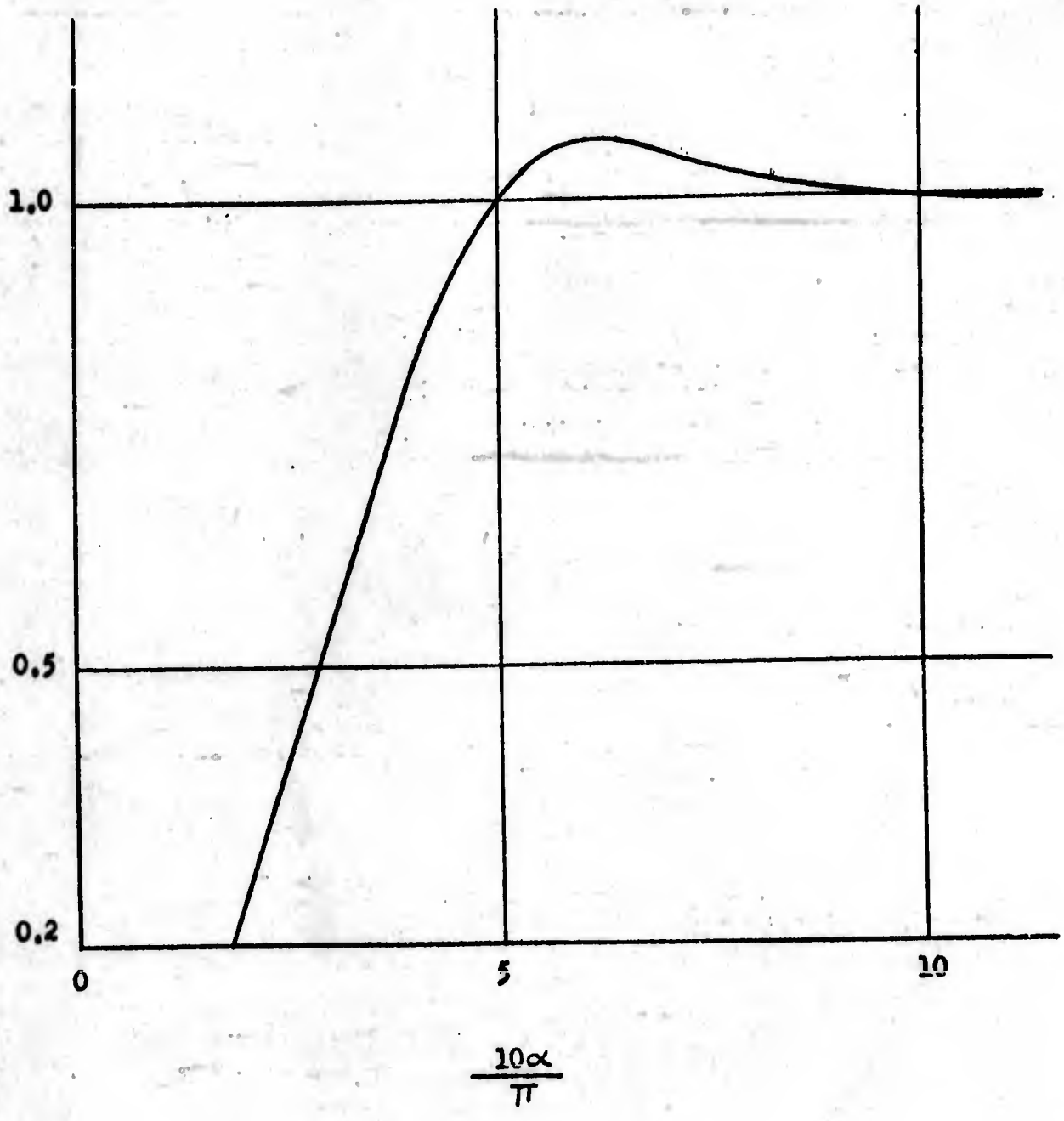

Figure 2

Curve showing the coordinate of
zero hinge load for various values of α.

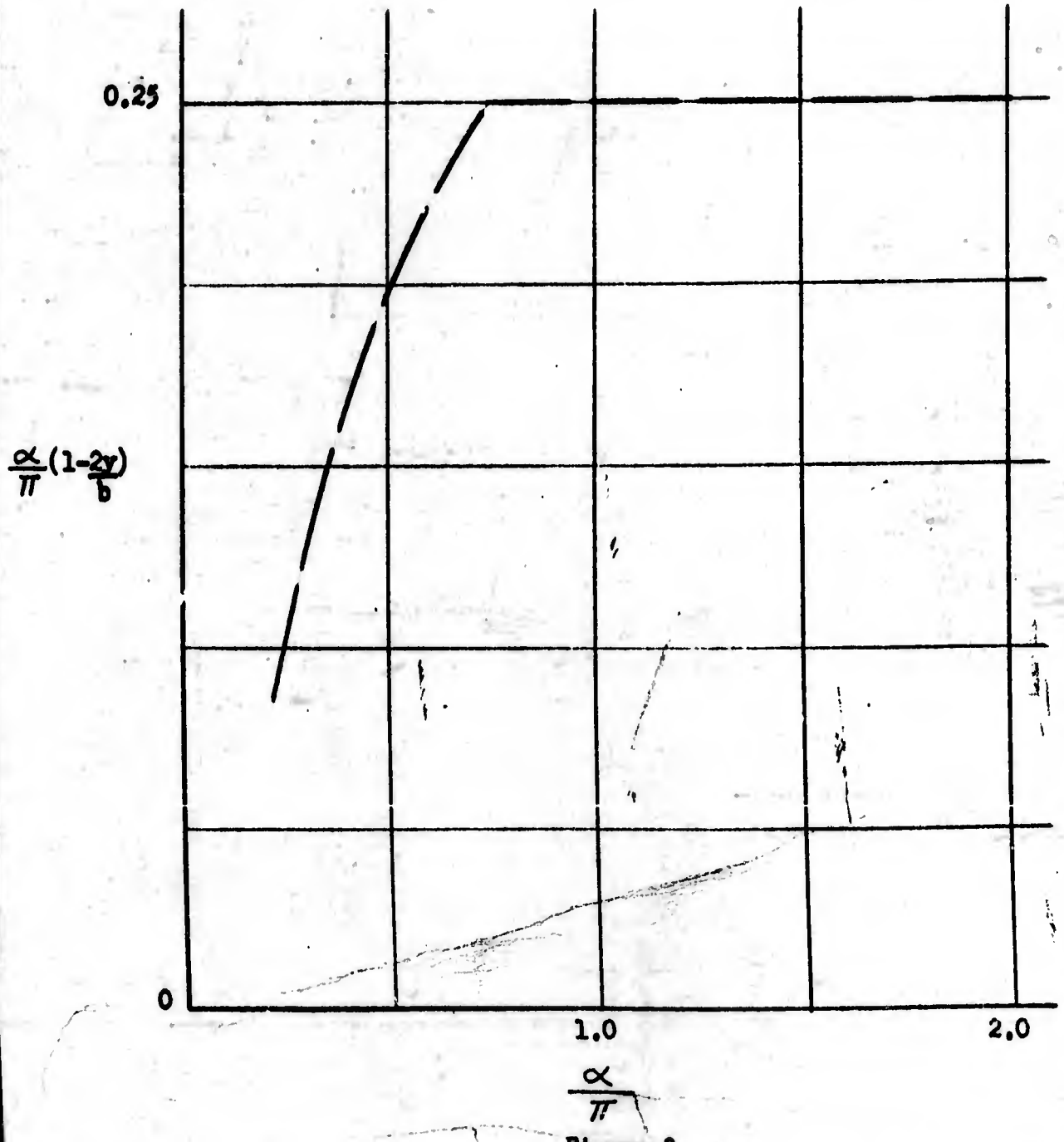

Figure 3

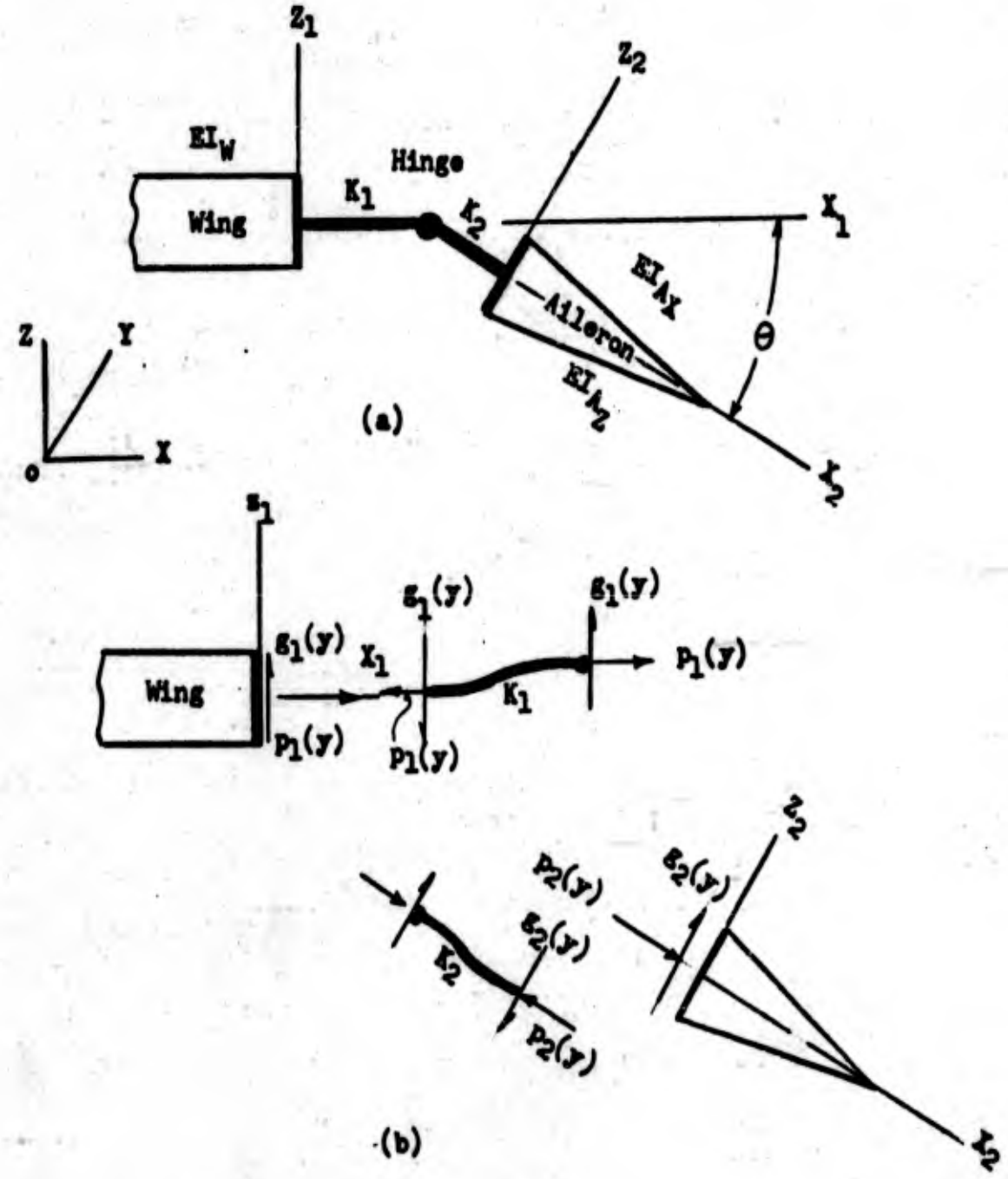

Schematic Sketch of Deflected Aileron

Figure 4

APPENDIX I

EXAMPLE CALCULATION OF AILERON HINGE LOADS

For an example calculation assume a symmetric loading and various dimensions as follows:

b	length of aileron	= 60 inches
K_1	spring constant hinge to wing	= 5714 lbs/in^2
K_2	spring constant hinge to aileron	= 66225 lbs/in^2
X_w	bending rigidity of the wing	= 3.5 E lbs in^2
X_A	bending rigidity of the aileron	= 0.39 E lbs in^2
Z_A	bending rigidity of the aileron	= 7.0 E lbs in^2
R_s	bending curvature of the wing	= 2290 inches
θ	deflection of the aileron	= 20 degrees
E	modulus of elasticity	= 10^7 lbs/in^2

(a) The Undeflected Aileron

(i) Neglect K_2

$$\beta = \left(\frac{3.5 + 0.39}{4(3.5)(0.39)} \cdot \frac{5715}{E}\right)^{1/4} = 0.142$$

Then from equation (18) since $\alpha = 4.26$

$$g_{max} = \frac{-5714}{2(0.142)^2\ 2290} = -61.7 \text{ lbs/in}$$

(ii) Include K_2

$$\frac{1}{K} = \frac{1}{K_1} + \frac{1}{K_2} \qquad K = 5550$$

then $\beta = 0.141$.

Again from equation (18) since $\alpha = 4.23$

$$g_{max} = \frac{-5550}{2(0.141)^2\ 2290} = 60.75 \text{ lbs/in}$$

For the undeflected aileron, the inclusion of K_2 changes the load g_2 by a small amount

(b) The Deflected Aileron

(i) Neglect K_2

$$\gamma^4 = \frac{1 + \frac{7.0}{0.39}\text{Tan}^2\theta + \frac{3.5}{0.39\ \text{Cos}^2\theta}}{4\left(3.5 + \frac{(3.5)7(\text{Tan}^2\theta)}{0.39}\right)} \cdot \frac{5714}{E} = 0.0001638$$

$$\gamma = 0.113$$

Now from equation (46), (47), (48), and (49) since $\alpha = 3.39$,

$$g_1 = \frac{-5714}{2(0.113)^2\ 2290} = -97.5 \text{ lbs/in}$$

$$P_1 = 97.5\left(\frac{7.0 - 0.39}{0.39\ \text{Cos}\theta + 7.0\ \text{Tan}\theta\text{Sin}\theta}\right)\text{Sin}\theta = 178.2 \text{ lbs/in}$$

$$g_2 = 97.5\left(\frac{0.29}{1.237}\right) = 30.8 \text{ lbs/in}$$

$$P_2 = -97.5\left(\frac{7.0\ \text{Tan}\theta}{1.237}\right) = -201.0 \text{ lbs/in}$$

(ii) Including K_2

$$a = \frac{7(\text{Tan}\theta\text{Sin}\theta)E}{5714(66225)} = 0.023$$

$$b = \frac{1}{5714}\left(0.94 + \frac{7\ \text{Tan}\theta\text{Sin}\theta}{0.39}\right) + \frac{1}{66225}\left(\frac{7\ \text{Tan}\theta\text{Sin}\theta}{3.5} + \frac{1}{0.94}\right)$$

$$= 0.000555 + 0.00000472 = 0.0005597$$

$$c = \frac{10^{-7}}{3.5(0.39)}\left(0.39(0.94) + \frac{3.5}{0.94} + 7.0\ \text{Tan}\theta\text{Sin}\theta\right) = 3.63\times10^{-7}$$

Now equation (57) becomes

$$m^2 + 0.02433m + 0.00001578 = 0$$

The roots of this equation are

$$m_1 = -0.01216 - \sqrt{0.00013209} = -0.02365$$

$$m_2 = -0.00067$$

Now $\gamma = 0.277$ and $\delta = 0.113$

Boundary conditions on g_2 are at $y = 30$ inches

$$g_2^{ii} = 0$$

$$g_2^{iii} = 0$$

$$g_2^{vi} = \frac{5714(66225)}{(2290)10^7} \cdot \frac{1}{7(\text{Tan}\theta)\text{Sin}\theta} = 0.01895$$

and $$g_2^{vii} = 0$$

The various derivatives of g_2 are as follows if C , S , c , and s , represent the hyperbolic cosine, hyperbolic sine, cosine, and sine respectively.

$$g_2^{i} = -A\gamma\,(Cs - Sc)\,\gamma_y + B\gamma\,(Cs + Sc)\,\gamma_y$$

$$-C\delta\,(Cs - Sc)\zeta_y + D\delta\,(Cs + Sc)\zeta_y$$

$$g_2^{ii} = -2A\,\gamma^2(Ss)\,\gamma_y + 2B\,\gamma^2(Cc)\,\gamma_y$$

$$-2C\delta^2(Ss)\zeta_y + 2D\delta^2(Cc)\zeta_y$$

$$g_2^{iii} = -2A\,\gamma^3(Cs + Sc)\,\gamma_y + 2B\gamma^3(Sc - Cs)\,\gamma_y$$

$$-2C\delta^3(Cs + Sc)\zeta_y + 2D\delta^3(Sc - Cs)\zeta_y$$

$$g_2^{iv} = -4A\,\gamma^4(Cc)\gamma_y - 4B\,\gamma^4(Ss)\gamma_y$$

$$-4C\delta^4(Cc)\zeta_{\delta y} - 4D\delta^4(Ss)\zeta_{\delta y}$$

$$g_2^{vi} = 8A\,\gamma^6(Ss)\gamma_y - 8B\,\gamma^6(Cc)\gamma_y$$

$$+ 8C\delta^6(Ss)\zeta_{\delta y} - 8D\delta^6(Cc)\zeta_{\delta y}$$

$$g_2^{vii} = 8A\,\gamma^7(Cs + Sc)\gamma_y - 8B\,\gamma^7(Sc - Cs)\gamma_y$$

$$+ 8C\delta^7(Cs + Sc)\zeta_{\delta y} - 8D\delta^7(Sc - Cs)\zeta_{\delta y}$$

$$g_2^{viii} = 16A\,\gamma^8(Cc)\gamma_y + 16B\,\gamma^8(Ss)\gamma_y$$

$$+16C\delta^8(Cc)\zeta_{\delta y} + 16D\delta^8(Ss)\zeta_{\delta y}$$

A substitution of the above in equation (39) proves g_2 is a solution of this equation.

Now a substitution in the boundary conditions gives for A, B, C, and D

$$A = -0.004299 \qquad B = -0.016255$$

$$C = -1.5758 \qquad D = -2.6495$$

These constants substituted in equation (39) give for $y = b/2$

$$g_{2max} = 26.955 \text{ lbs/in}$$

and substituted into equation (38) give for $y = b/2$

$$g_{1max} = -99.415 \text{ lbs/in}$$

Then from equations (46) and (47)

$$P_{1max} = 194.38 \text{ lbs/in}$$

and

$$P_{2max} = -216.60 \text{ lbs/in}$$

The results of the above calculations show that the introduction of the constant K_2 into the deflected aileron calculation, increases the value of g_1 by a small amount. Then, since g_1 is the value of most interest as it is a record of the maximum transverse shear carried by the cantilevered hinge, the complicated analysis caused by including K_2 does not yield a sufficient change to merit the calculation, at least in the initial stages of design.

CONFIDENTIAL

NORTHROP AIRCRAFT, INC.

HAWTHORNE, CALIFORNIA

REPORT NO. BLC-44

THE STABILITY AND LINEAR DEFORMATION OF A FRAMEWORK FORMED BY A CANTILEVER, KNEE BRACE, AND JURY STRUT

MAY 1954

PREPARED BY

H. Sohjelderup

APPROVED BY

W. Pfenninger

TABLE OF CONTENTS

LIST OF FIGURES

TABLE OF CONTENTS (cont'd)

INTRODUCTION

On a high altitude long range laminar suction airplane the induced drag can be a large percentage of the total drag. A large wing span is therfore required. In order to reduce the weight of the wing and to increase its stiffness it is desirable to brace the wing with a strut, adding essentially a stiff inner wing panel to the cantilever part of the wing. (Figure 1 and References 1 and 2). A second or "jury strut" reduces the buckling length of the main strut (negative loads) and thus enables a considerably thinner strut. The bending moments and bending deformations of the inner wing panel can be further reduced when the main strut is slightly kinked at its juncture with the "jury strut" (Reference 3).

At positive loads the "jury strut" reduces the buckling length of the inner wing panel (compression loads) and thus enables thinner wing sections in this area.

In order to evaluate the effectiveness of this system, a study of deflections will be made.

This study may be broken down into three parts. First, the beam ABC will be isolated from the overall system of Figure 1. Loads and deformations will be forced on this beam such that these loads and deformations are compatible to the loads and deformations demanded by the configuration of Figure 1. This will be the theoretical analysis of the beam-column system. Second, equations will be derived which will define explicitly the parameters of Part 1. Finally, as a third part, the influence on the system of various parameters will be studied.

I. ANALYSIS OF THE BEAM COLUMN

The free body diagram of the isolated beam ABC, is shown in Figure 2. All loads M, V, P etc., may be expressed in terms of g, the air load; M_1, the statically indeterminate moment; and Δ, the total deflection of point B.

Assume these loads may be expressed in terms of g, M_1, and Δ as follows:

$$P_1 = aLg - i\frac{M_1}{L} \tag{1}$$

$$P_2 = bLg - j\frac{M_1}{L} \tag{2}$$

$$M = cL^2g \tag{3}$$

and $$V_1 = eLg - f\Delta g - k\frac{M_1}{L} - m\frac{M_1\Delta}{L^2} \tag{4}$$

where a, b, c, etc., are direct functions of the geometry of the system and L is the span of the strut.

(a) Consider the Beam Column AB.

The reaction V_A and the moment M_x are obtained from statics,

$$V_A = \frac{M}{L} - \frac{gl_1}{2} - \frac{V_1 l_2}{L} - \frac{M_1}{L} \tag{5}$$

and $$M_x = M_1 + V_A x + \frac{gx^2}{2} - P_1 y + P_1 \frac{\gamma\Delta}{L} x \tag{6}$$

Now for small deflections, the differential equation of a beam is

$$EI\frac{d^2y}{dx^2} = M_x \tag{7}$$

where EI is the flexural stiffness of the beam cross-section.

The solution of equation (7) if M_x is given by equation (6) is

$$y = A\,Cosk_1x + B\,Sin k_1x + \frac{M_1}{P_1} + \frac{V_a x}{P_1} + \frac{\gamma\Delta}{L}x + \frac{qx^2}{2P_1} - \frac{q}{P_1k_1^2} \tag{8}$$

where $k_1^2 = \frac{P_1}{EI_1}$

Boundary Conditions on equation (8) are

at $x=0$ $y=0$ and at $x=l_1$ $y=\Delta$

which give

$$A = -\frac{M_1}{P_1} + \frac{q}{P_1k_1^2} \tag{9}$$

and

$$B = \frac{\delta - \frac{V_a l_1}{P_1} - \frac{ql_1^2}{2P_1} + \left[\frac{ql_1^2}{P_1\mu_1^2} - \frac{M_1}{P_1}\right]\left[1 - Cos\mu_1\right]}{Sin\mu_1} \tag{10}$$

where $\mu_1 = k_1l_1$ and $\delta = \Delta - \frac{\gamma\Delta l_1}{L}$

(b) Consider the Beam Column BC

The reaction V_c and the moment M_{x_1} are obtained from statics

$$V_c = -\frac{M}{L} - \frac{V_1l_1}{L} - \frac{ql_2}{2} + \frac{M_1}{L} \tag{11}$$

and

$$M_{x_1} = M + V_c(l_2 - x_1) + \frac{q(l_2-x_1)^2}{2} - P_2\left(y + \frac{\gamma\Delta}{L}(l_2 - x_1)\right) \tag{12}$$

The solution of equation (7) if M_x is given by equation (12) is

$$y_1 = C\cos k_2 x_1 + D\sin k_2 x_1 + \frac{M}{P_2} + (l_2 - x_1)\frac{V_c}{P_2} \qquad (13)$$

$$-(l_2 - x_1)\frac{y\Delta}{L} + (l_2 - x_1)^2 \frac{q}{2P_2} - \frac{q}{P_2 k_2^2}$$

where $k_2^2 = \frac{P_2}{EI_2}$

Boundary conditions on equation (13) are at

$$x_1 = 0 \quad y_1 = (1-\gamma)\Delta \quad \text{and at} \quad x_1 = l_2 \quad y_1 = 0$$

which give

$$C = \delta - \frac{M}{P_2} - \frac{V_c l_2}{P_2} - \frac{q l_2^2}{2P_2} + \frac{q l_2^2}{P_2 \mu_2^2} \qquad (14)$$

and $$D = -C\cot\mu_2 - \frac{M}{P_2}\operatorname{Cosec}\mu_2 + \frac{q l_2^2}{P_2 \mu_2^2}\operatorname{Cosec}\mu_2 \qquad (15)$$

where $\mu_2 = k_2 l_2$

Equations (8) and (13) give the deflection curves for the beams AB and BC. However, these equations contain two unknowns, Δ and M_1. These unknowns are eliminated by the additional equations supplied by the slope at $X = 0$ and $X = l_1$. These equations are

$$\frac{dy}{dx} = 0 \quad \text{at} \quad X = 0 \qquad (16)$$

a condition of fixed support, and

$$\frac{dy}{dX}_{X=l_1} = \frac{dy_1}{dX_1}_{x_1=0} \qquad (17)$$

a condition of continuity between beam AB and BC.

Equation (16) gives

$$0 = Bk_1 + \frac{V_A}{P_1} + \frac{\gamma\Delta}{L} \tag{18}$$

or substituting equation (10)

$$0 = \frac{V_A}{P_1}\left[\frac{\sin\mu_1 - \mu_1}{\sin\mu_1}\right] + \left[\frac{q l_1}{P_1 \mu_1^2} - \frac{M_1}{P_1 l_1}\right]\left[\frac{1 - \cos\mu_1}{\sin\mu_1}\right]$$

$$- \frac{q l_1 \mu_1}{2 P_1 \sin\mu_1} + \frac{\delta \mu_1}{l_1 \sin\mu_1} + \frac{\gamma\Delta}{L} \tag{19}$$

and equation (17) gives

$$- \frac{A}{l_1}\mu_1 \sin\mu_1 + B\frac{\mu_1 \cos\mu_1}{l_1} + \frac{V_A}{P_1} + \frac{q l_1}{P_1} + \frac{\gamma\Delta}{L} \tag{20}$$

$$= \frac{D\mu_2}{l_2} - \frac{V_C}{P_2} + \frac{\gamma\Delta}{L} - \frac{q l_2}{P_2}$$

or substituting equations (9), (10), (14) and (15)

equation (20) becomes

$$\frac{V_A}{P_1}\left[1 - \mu_1 \cot\mu_1\right] + \frac{V_C}{P_2}\left[1 - \mu_2 \cot\mu_2\right] + \frac{M_1 \mu_1}{l_1 P_1}\left[\frac{1 - \cos\mu_1}{\sin\mu_1}\right] \tag{21}$$

$$+ \frac{M}{l_2 P_2}\left[\mu_2 \operatorname{cosec}\mu_2 - \mu_2 \cot\mu_2\right] - \frac{q l_1}{P_1}\left[\frac{1 - \cos\mu_1}{\mu_1 \sin\mu_1} + \frac{\mu_1 \cot\mu_1}{2} - 1\right]$$

$$+ \frac{q l_2}{P_2}\left[1 - \frac{\mu_2 \cot\mu_2}{2} - \frac{1 - \cos\mu_2}{\mu_2 \sin\mu_2}\right] + \frac{\delta}{l_1}\left[\mu_1 \cot\mu_1 + \frac{l_1}{l_2}\mu_2 \cot\mu_2\right]$$

$$= 0$$

Now substituting equations (5) and (11) equations (19) and (21) become

$$-\frac{V_1 l_2}{P_1 L}\left[\frac{\sin\mu_1 - \mu_1}{\sin\mu_1}\right] + \frac{M}{LP_1}\left[\frac{\sin\mu_1 - \mu_1}{\sin\mu_1}\right]$$

$$-\frac{g l_1}{2P_1}\left[1 - \frac{2\tan\mu_1/2}{\mu_1}\right] - \frac{M_1}{LP_1}\left[\frac{\sin\mu_1 - \mu_1}{\sin\mu_1} + \frac{L\mu_1}{l_1}\tan\mu_1/2\right]$$

$$+\frac{\Delta}{L}\left[\frac{\mu_1 L}{l_1 \sin\mu_1} + \frac{\sin\mu_1 - \mu_1}{\sin\mu_1}\gamma\right] = 0$$

and

$$-\frac{V_1 l_2}{LP_1}\left[1 - \mu_1 \cot\mu_1\right] - \frac{V_1 l_1}{LP_2}\left[1 - \mu_2 \cot\mu_2\right]$$

$$+\frac{M}{LP_1}\left[1 - \mu_1\cot\mu_1 - \frac{P_1}{P_2}\left(1 - \mu_2\cot\mu_2\right) + \frac{LP_1}{l_2 P_2}\left(\mu_2 \operatorname{Cosec}\mu_2 - \mu_2\cot\mu_2\right)\right]$$

$$+\frac{g l_1}{2P_1}\left[1 - \frac{2\tan\mu_1/2}{\mu_1}\right] + \frac{g l_2}{2P_2}\left[1 - \frac{2\tan\mu_2/2}{\mu_2}\right]$$

$$-\frac{M_1}{LP_1}\left[1 - \mu_1\cot\mu_1 - \frac{L\tan\mu_1/2}{l_1\mu_1} - \frac{P_1}{P_2}\left(1 - \mu_2\cot\mu_2\right)\right]$$

$$+\frac{\Delta}{\lambda_1}\left[1 - \frac{\gamma l_1}{L}\right]\left[\mu_1\cot\mu_1 + \frac{l_1}{l_2}\mu_2\cot\mu_2\right] = 0$$

Now, if P_1 , P_2 , M_1 and V_1 are given by equations (1), (2), (3) and (4) respectively, equations (22) and (23) may be written

$$\frac{\Delta}{L} = \left[-c + \frac{e l_2}{L} + \frac{l_1}{2L} \cdot \frac{1 - \frac{2 \operatorname{Tan} \mu_1/2}{\mu_1}}{\frac{\sin \mu_1 - \mu_1}{\sin \mu_1}} - \left(\frac{K l_2}{L} - 1 - \frac{\mu_1 L}{l_1} \cdot \frac{\operatorname{Tan} \mu_1/2}{\frac{\sin \mu_1 - \mu_1}{\mu_1}} \right) \frac{M_1}{g L^2} \right]$$

$$\times \left[\frac{f l_2}{L} + \gamma a + \frac{L a}{l_1} \cdot \frac{\mu_1}{\sin \mu_1 - \mu_1} + \left(\frac{m l_2}{L} - j\gamma - \frac{j L}{l_1} \frac{\mu_1}{\sin \mu_1 - \mu_1} \right) \frac{M_1}{g L^2} \right]^{-1} \quad (24)$$

and

$$\frac{\Delta}{L} = \left[\left[\frac{e l_2}{L} - c \right] \left[1 - \mu_1 \cot \mu_1 \right] - \frac{l_1}{2L} \left[1 - \frac{2 \operatorname{Tan} \mu_1/2}{\mu_1} \right] \right.$$

$$+ \left[\left(\frac{e l_1}{L} + c \right) \left(1 - \mu_2 \cot \mu_2 \right) - \frac{c L}{l_2} \left(\mu_2 \operatorname{Cosec} \mu_2 - \mu_2 \cot \mu_2 \right) \right.$$

$$\left. - \frac{l_2}{2L} \left(1 - \frac{2 \operatorname{Tan} \mu_2/2}{\mu_2} \right) \right] \frac{P_1}{P_2} - \left[\left(\frac{K l_2}{L} - 1 \right) \left(1 - \mu_1 \cot \mu_1 \right) \right. \quad (25)$$

$$\left. + \frac{L}{2 l_1} \cdot \frac{2 \operatorname{Tan} \mu_1/2}{\mu_1} + \frac{P_1}{P_2} \left(\frac{K l_1}{L} + 1 \right) \left(1 - \mu_2 \cot \mu_2 \right) \right] \frac{M_1}{g L^2} \Bigg]$$

$$\times \left[\frac{f l_2}{L} \left(1 - \mu_1 \cot \mu_1 \right) + \frac{a L}{l_1} \left(1 - \frac{\gamma l_1}{L} \right) \left(\mu_1 \cot \mu_1 + \frac{l_1}{l_2} \mu_2 \cot \mu_2 \right) \right.$$

$$+ \frac{f l_1}{L} \left(1 - \mu_2 \cot \mu_2 \right) \frac{P_1}{P_2} + \left[\frac{m l_2}{L} \left(1 - \mu_1 \cot \mu_1 \right) \right.$$

$$\left. \left. - \frac{j L}{l_1} \left(1 - \frac{\gamma l_1}{L} \right) \left(\mu_1 \cot \mu_1 + \frac{l_1}{l_2} \mu_2 \cot \mu_2 \right) + \frac{m l_1}{L} \left(1 - \mu_2 \cot \mu_2 \right) \frac{P_1}{P_2} \right] \frac{M_1}{g L^2} \right]^{-1}$$

where $$\frac{P_1}{P_2} = \frac{a - i\frac{M_1}{gL^2}}{b - j\frac{M_1}{gL^2}}$$

The solution of equations (24) and (25) for u_1 and u_2 constant will give the deflection $\frac{\Delta}{L}$ and the fixed end moment $\frac{M_1}{gL^2}$ for any particular combination of parameters a , b , c , etc.*

Equations (24) and (25) include the effects of axial load on the bending rigidity of the beam. However, these equations do not show the influence of the axial loads on Δ and M_1 . In order to show this, assume that P_1 and P_2 are negligible in equations (6) and (12) respectively. Then the integration of equation (7) will yield

$$EI_1 y = V_A\frac{x^3}{6} + \frac{gx^4}{24} + M_1\frac{x^2}{2} + Ax + B \qquad (2$$

and

$$EI_2 y_1 = V_c\frac{(l_2 - x_1)^3}{6} + \frac{g(l_2 - x_1)^4}{24} + M\frac{x_1^2}{2} + C(l_2 - x_1) + D \qquad (2$$

Boundary Conditions are as before.

Then

$$B = 0 \qquad (2$$

$$A = EI_1\frac{\Delta}{l_1} - \frac{V_a l_1^2}{6} - \frac{g l_1^3}{24} - \frac{M_1 l_1}{2} \qquad (2$$

---

* A considerable simplification of equations 24 and 25 can be obtained if parameters have values as derived in Part II.

$$D = -\frac{M l_2^2}{2} \tag{30}$$

$$C = EI_2(1-\gamma)\frac{\Delta}{l_2} + \frac{M l_2}{2} - \frac{V_0 l_2^2}{6} - \frac{g l_2^3}{24} \tag{31}$$

The condition of fixed support at A gives

$$EI_1 \frac{\Delta}{l_1} = V_A \frac{l_1^2}{6} + \frac{g l_1^3}{24} + \frac{M_1 l_1}{2} \tag{32}$$

and the condition of continuity gives

$$\frac{V_A l_1^2}{2} + \frac{g l_1^3}{6} + M_1 l_1 + A = \frac{EI_1}{EI_2}\left[-\frac{V_2 l_2^2}{2} - \frac{g l_2^3}{6} - C\right] \tag{33}$$

or substituting for V_A etc.

$$\frac{\Delta}{L} = \frac{g l_1^3}{6EI_1}\left[\frac{M}{gL^2} - \frac{l_1}{4L} - \frac{V_1 l_2}{gL^2} - \frac{M}{gL^2}\left(1 - \frac{3L}{l_1}\right)\right] \tag{34}$$

and

$$\left[\frac{6EI_1}{g l_1^3}\left(\frac{L}{l_1} + \frac{L}{l_2}(1-\gamma)\right)\right]\frac{\Delta}{L} = \frac{2V_1 l_2}{gL\, l_1}\left[1 + \frac{I_1 l_2}{I_2 l_1}\right] \tag{35}$$

$$-\frac{2ML}{gL^2 l_1}\left[1 - \frac{I_1 l_2^2}{I_2 l_1^2}\right] - \frac{3ML^2}{gL^2 l_1 l_2}\cdot\frac{I_1 l_2^2}{I_2 l_1^2}$$

$$+\frac{1}{4}\left[1 + \frac{I_1 l_2^2}{I_2 l_1^2}\right] + \frac{M_1 L}{gL^2 l_1}\left[\frac{L}{l_1}\left(\frac{2l_1}{L} - 3\right) - \frac{2I_1 l_2^2}{I_2 l_1^2}\right]$$

which gives in terms of parameters e , f , etc.

$$\frac{\Delta}{L} = \frac{\frac{l_1^3 \gamma}{6EI_1}\left[c - \frac{e l_2}{L} - \frac{l_1}{4L} - \left(1 - \frac{3L}{l_1} - \frac{k l_2}{L}\right)\frac{M_1}{gL^2}\right]}{1 - \frac{l_1^2 \gamma}{6EI_1}\frac{l_2}{L}\left(f + m\frac{M_1}{gL^2}\right)} \tag{3}$$

and

$$\frac{\Delta}{L} = \frac{l_1^3 \gamma}{6EI_1}\left[2e\frac{l_2}{l_1}\left(1+\frac{I_1 l_2}{I_2 l_1}\right) - 2c\frac{L}{l_1}\left(1-\frac{I_1 l_2^2}{I_2 l_1^2}\right) - 3c\frac{L^2}{l_1 l_2}\frac{I_1 l_2^2}{I_2 l_1^2} + \frac{1}{4}\left(1+\frac{I_1 l_2^3}{I_2 l_1^3}\right)\right.$$

$$\left. -\left[\frac{2k l_2}{l_1}\left(1+\frac{I_1 l_2}{I_2 l_1}\right) - \frac{L^2}{l_1^2}\left(2\frac{l_1}{L} - 3\right) + \frac{2L}{l_1}\frac{I_1 l_2^2}{I_2 l_1^2}\right]\frac{M_1}{gL^2}\right]^{-1}$$

$$\times\left[\frac{L}{l_1}\left(1+\frac{l_1}{l_2}(1-\gamma)\right) + \left[\frac{2\gamma l_1^3}{6EI_1}\left(\frac{l_2}{l_1} + \frac{I_1 l_2^2}{I_2 l_1^2}\right)\right]\left[f + m\frac{M_1}{gL^2}\right]\right] \tag{3'}$$

Equations (35) and (36) may be solved similarily to equations (24) and (25) to give $\frac{\Delta}{L}$ and $\frac{M_1}{gL^2}$ *

---

* A considerable simplification of equations (35) and (36) can be obtained if parameters have values as derived in Part II.

II. DERIVATION OF PARAMETERS

Equations (1), (2), (3) and (4) indicate that the various loads on the beam column of Figure 2, may be expressed in terms of g, the air load, Δ, the deflection at point B and M_1, the indeterminate moment. Figure 3 shows a free body diagram of the framework, whereas Figure 4 shows the change in geometry after a deflection Δ. Here, the axial extension of the various members is assumed small and may be neglected.

(a) Statics of the Undeformed System.

A statical consideration of the system of Figure 1 will yield

$$P_1 = \frac{\lambda^2 L^2 g}{2d}(1+\eta) - \frac{M_1}{d} \tag{38}$$

$$V_A = P_1 \operatorname{Tan}\alpha_5 - \lambda L q\left(1+\frac{\lambda\eta}{2}\right) \tag{39}$$

and $$M = \frac{L^2(\lambda-1)^2 g}{2} \tag{40}$$

or $$a = \frac{\lambda^2 L}{2d}(1+\eta) \tag{41}$$

$$i = \frac{L}{d} = \frac{2}{\lambda^2(1+\eta)}a \tag{42}$$

$$c = \frac{(\lambda-1)^2}{2} \tag{43}$$

A statical consideration of the system of Figure 3 will yield

$$V_1 = \frac{M}{l_2} - \frac{l_1 L g}{2 l_2} - \frac{V_A L_1}{l_2} - \frac{M_1}{l_2} \tag{44}$$

and $$P_2 = P_1 + \left(V_1 - \frac{2L}{2}\right) Cot\,\alpha_4 \tag{45}$$

or $$e = \frac{\lambda^2 L}{2 l_2}(1+\eta)\left(1 - \frac{L}{d} Tan\,\alpha_5\right) + 0.5 \tag{46}$$

$$k = \frac{L}{l_2} - \frac{L^2}{d\,l_2} Tan\,\alpha_5 \tag{47}$$

$$b = \frac{\lambda^2 L}{2d}(1+\eta)\left(1 + \frac{d}{l_2} Cot\,\alpha_4 - \frac{L}{l_2}\frac{Tan\,\alpha_5}{Tan\,\alpha_4}\right) \tag{48}$$

and $$j = \frac{L}{d} - \frac{L}{l_2}\left(\frac{L}{d} Tan\,\alpha_5 - 1\right) Cot\,\alpha_4 = \frac{2}{\lambda^2(1+\eta)}\, b \tag{49}$$

(b) Changes in Forces Caused by Deformation.

After a displacement Δ occurs in the system, all members will have moved to a new geometrical position by means of displacements and rotations. Since the members are assumed axially undeformable, triangle BCD of Figure 4 will be identical to triangle $B^1C^1D^1$. Then, all displacements may be defined in terms of Δ, the displacement of B. If we consider point A the fixed point, the displacement at C will be $\gamma\Delta$ where γ is defined by the geometry of the system.

Let us introduce a rotation $d\theta$ of the triangle BCD and a rotation $d\alpha_5$ of member DE. Then from Figure (4),

$$\gamma = 1 - \frac{l_2 d\theta}{\Delta} \tag{50}$$

and from triangle $D\,D^1\,D^{11}$

$$d\theta = \frac{\Delta}{l_4} \cdot \frac{Sin\,\alpha_5}{Sin(\alpha_4 - \alpha_5)} \tag{51}$$

$$\text{and} \quad d\alpha_5 = \frac{\Delta}{l_5} \cdot \frac{\sin\alpha_4}{\sin(\alpha_4-\alpha_5)}$$

$$\text{then} \quad \gamma = \frac{\sin\alpha_4 \sin(\alpha_3-\alpha_5)}{\sin\alpha_3 \sin(\alpha_4-\alpha_5)}$$

The change in forces caused by change in shape can be expressed in terms of $d\alpha_5$.

The change in V_A is given by the equation

$$-dV_A = P_1 \tan(\alpha_5+d\alpha_5) - P_1 \tan\alpha_5$$

or expanding and taking first order approximations:

$$dV_A = -P_1 d\alpha_5$$

and the change in V_1 becomes

$$dV_1 = \frac{L}{l_2} dV_A + \frac{P_1 \gamma \Delta}{l_2}$$

The axial load P_1 does not change with deformation. The axial load P_2 changes but by a small amount which will be neglected. Then the parameters f and m are obtained from equations (55) and (56)

$$f = \frac{\lambda^2 l_1}{2d}(1+\eta)\frac{L}{l_2}\left(\frac{L}{l_5}\frac{\sin\alpha_4}{\sin(\alpha_4-\alpha_5)} - \gamma\right)$$

$$\text{and} \quad m = \frac{L^2}{l_2 d}\left(\gamma - \frac{L}{l_5}\frac{\sin\alpha_4}{\sin(\alpha_4-\alpha_5)}\right) = -\frac{2f}{\lambda^2(1+\eta)}$$

The preceding equations define all parameters in terms of the geometry of the framework.

Equations (42) and (58) show a simple relationship between a and i and m and f .

This relationship may be used to improve the form and solution of equations (24) and (25). Note that the denominators of equations (24) and (25) may now be written

$$\left[\frac{fl_2}{L} + a\gamma + \frac{La}{l_1}\frac{\mu_1}{\sin\mu_1 - \mu_1}\right]\left[1 - \frac{2}{\lambda^2(1+\eta)}\cdot\frac{M_1}{gL^2}\right] \tag{5}$$

and

$$\left[\frac{fl_2}{L}(1-\mu_1\cot\mu_1) + \frac{aL}{l_1}\left(1-\frac{\gamma l_1}{L}\right)\left(\mu_1\cot\mu_1 + \frac{l_1}{l_2}\mu_2\cot\mu_2\right) + \frac{fl_1}{L}\left(1-\mu_2\cot\mu_2\right)\frac{P_1}{P_2}\right] \tag{6}$$

$$\times\left[1 - \frac{2}{\lambda^2(1+\eta)}\cdot\frac{M_1}{gL^2}\right]$$

Now, if we define ψ and χ as the first terms of equations (59) and (60) respectively, and from equations (24) and (25) define

$$A = -c + \frac{el_2}{L} + \frac{l_1}{2L}\cdot\frac{1 - \frac{2\tan\mu_1/2}{\mu_1}}{\frac{\sin\mu_1 - \mu_1}{\sin\mu_1}} \tag{6}$$

$$B = \frac{kl_2}{L} - 1 - \frac{\mu_1 L}{l_1}\,\frac{\tan\mu_1/2}{\frac{\sin\mu_1 - \mu_1}{\sin\mu_1}} \tag{6}$$

$$C = \left(\frac{el_2}{L} - c\right)\left(1-\mu_1\cot\mu_1\right) - \frac{l_1}{2L}\left(1 - \frac{2\tan\mu_1/2}{\mu_1}\right) \tag{6}$$

$$+\left[\left(\frac{el_1}{L}+c\right)\left(1-\mu_2\cot\mu_2\right) - \frac{cL}{l_2}\left(\mu_2\operatorname{cosec}\mu_2 - \mu_2\cot\mu_2\right) - \frac{l_2}{2L}\left(1-\frac{2\tan\mu_2/2}{\mu_2}\right)\right]$$

$$D = \left(\frac{kl_2}{L} - 1\right)\left(1-\mu_1\cot\mu_1\right) + \frac{L}{2l_1}\frac{2\tan\mu_1/2}{\mu_1} + \left[\left(\frac{kl_1}{L}+1\right)\left(1-\mu_2\cot\mu_2\right)\right]\frac{P_1}{P_2} \tag{6}$$

The solution of equations (24) and (25) takes the form

$$\frac{M_1}{qL^2} = \frac{\frac{C}{\chi} - \frac{A}{\psi}}{\frac{D}{\chi} - \frac{B}{\psi}} \tag{65}$$

and

$$\frac{\Delta}{L} = \frac{\frac{A}{\psi} - \frac{B}{\psi}\cdot\frac{M_1}{qL^2}}{1 - \frac{2}{\lambda^2(1+\eta)}\cdot\frac{M_1}{qL^2}} \tag{66}$$

Equations (36) and (37) may be simplified in a like manner if $\frac{ql_1^3}{6EI_1}$ is replaced by u_1. By definition

$$\mu_1^2 = \frac{Pl_1^2}{EI_1} = \frac{6aL}{l_1}\cdot\frac{ql_1^3}{6EI_1}\cdot\left(1 - \frac{2}{\lambda^2(1+\eta)}\frac{M_1}{qL^2}\right) \tag{67}$$

but $f = -\frac{\lambda^2(1+\eta)}{2}m$.

Now, from equations (36) and (37) noting $\frac{I_1 l_2^2}{I_2 l_1^2} = \frac{a\mu_2^2}{b\mu_1^2}$ define

$$\Theta = 1 - \frac{l_1 l_2}{6aL^2} f\mu_1^2 \tag{68}$$

$$\Phi = \frac{L}{I_1}\left(1 + \frac{l_1}{l_2}(1-\gamma)\right) + \frac{2l_2 f}{6La}\left(1 + \frac{l_1}{l_2}\cdot\frac{a\mu_2^2}{b\mu_1^2}\right)\mu_1^2 \tag{69}$$

$$\bar{A} = C - \frac{el_2}{L} - \frac{l_1}{4L} \tag{70}$$

$$\bar{B} = 1 - \frac{3L}{l_1} - \frac{kl_2}{L} \tag{71}$$

$$\bar{C} = \frac{2cl_2}{l_1}\left(1+\frac{l_1 a\mu_2^2}{l_2 b\mu_1^2}\right) - \frac{2cL}{l_1}\left(1-\frac{a\mu_2^2}{b\mu_1^2}\right) - \frac{3cL^2 a\mu_2^2}{l_1 l_2 b\mu_1^2} + \frac{1}{4}\left(1+\frac{l_1 a\mu_2^2}{l_2 b\mu_1^2}\right) \tag{72}$$

and $$D = \frac{2kl_2}{l_1}\left(1+\frac{l_1 a\mu_2^2}{l_2 b\mu_1^2}\right) - \frac{L^2}{l_1^2}\left(\frac{2l_1}{L}-3\right) + \frac{2La\mu_2^2}{l_1 b\mu_1^2} \tag{73}$$

then $$\frac{M_1}{qL^2} = \frac{\frac{\bar{C}}{\Phi} - \frac{\bar{A}}{\theta}}{\frac{D}{\Phi} - \frac{\bar{B}}{\theta}} \tag{74}$$

and $$\frac{\Delta}{L} = \frac{\frac{\bar{A}}{\theta} - \frac{\bar{B}}{\theta}\frac{M_1}{qL^2}}{1 - \frac{2}{\lambda^2(1+\eta)}\frac{M_1}{qL^2}} \cdot \frac{\mu_1^2 l_1}{6aL} \tag{75}$$

III. A STUDY OF A PARTICULAR FRAMEWORK

In order to design an efficient framework, the change in deflections and fixed-end moments with changes in various parameters should be studied. Then, the configuration that will yield the most favorable values of the above may be determined.

As a typical configuration assume:

$$\frac{L}{l_1} = 2.03704 \qquad \frac{L}{l_2} = 1.96429 \qquad \frac{L}{d} = 3.27381$$

$$\mu_1 = \mu_2 \qquad \alpha_4 = 107^\circ \qquad \lambda = 1.962 \qquad \eta = -0.108$$

The remaining parameter which will define the system is the angle of kink $\alpha_{35} = \alpha_3 - \alpha_5$

Figures 5 to 13 inclusive show the deflection $\frac{\Delta}{L}$, the fixed end moment $\frac{M_1}{qL^2}$, the tip moment $\frac{M}{qL^2}$ and the interior moment $\frac{M_B}{qL^2}$ for various values of the kink angle α_{35}. Plots are shown for the variation of axial loads P_1 and the variation of total distributed load $q\lambda L$. These two plots are shown since the axial load P_1 is not a true representation of the total distributed load carried by the beam.

These figures indicate that for a particular loading, there exists an "optimum" configuration for which either deflections or moments are a minimum. These figures also show that the condition of instability occurs at axial loads less than simple Euler buckling. A stability analysis of the system for α_{35} equals zero shows that for these restricted conditions, there is an optimum angle of strut (90° to inclined strut) for which the Euler buckling value is attained. However, under the beam column loadings, this advantage is small. It was for this reason and the fact that other design criteria were better satisfied by the illustrated configuration that for the example problem the jury strut was not placed at the optimum angle.

Figures (8) and (9) show that as the load intensity increases, the relation $\frac{d\Delta}{d\alpha_{35}}$ becomes large. This means that a small change in α_{35} will yield a large change in deflection or the deflections at this point are very sensitive to the angle α_{35}. Then, even though an "optimum" configuration may be attempted, any small errors could contribute

to a premature collapse.

A design procedure is to establish a general configuration, compute curves similar to those of figures (6) and (7), and from these curves choose the best angle of kink for the strut. Once the configuration is chosen, the ultimate load may be computed either from stress calculations or a condition of excessive deformation.

REFERENCES

1 W. Pfenninger and J. W. Bacon: Design Considerations for Hypothetical Boundary Layer Control Airplane, Northrop Aircraft, Inc., Report No. BLC-1, 1951, 1953.

2 J. Bacon: An Aeroelastic Study of Configuration II of a Laminar Boundary Layer Control Airplane, Northrop Aircraft, Inc., Report No. BLC-2, May 1953.

3 W. Pfenninger: Ueber die Aerodynamische Durchbildung von Flügelstrebenanschlussen, Flugwehr und-Technik, Sept. 1942.

ENGINEER	NORTHROP AIRCRAFT, INC.	PAGE
H. Schjelderup		20
CHECKER		REPORT NO.
		BLC-44
DATE		MODEL
May 1954		

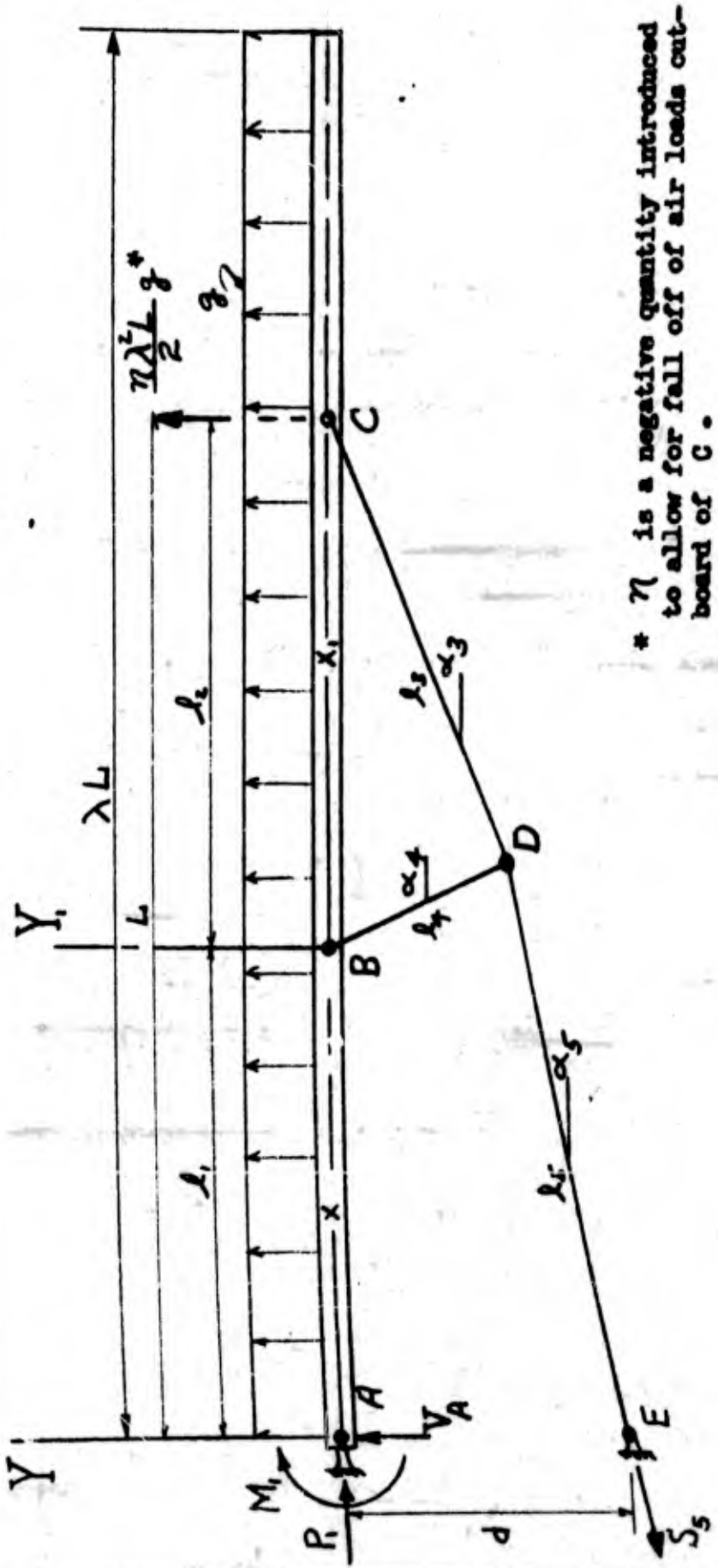

* η is a negative quantity introduced to allow for fall off of air loads outboard of C.

FIG. 1. Typical Strut System

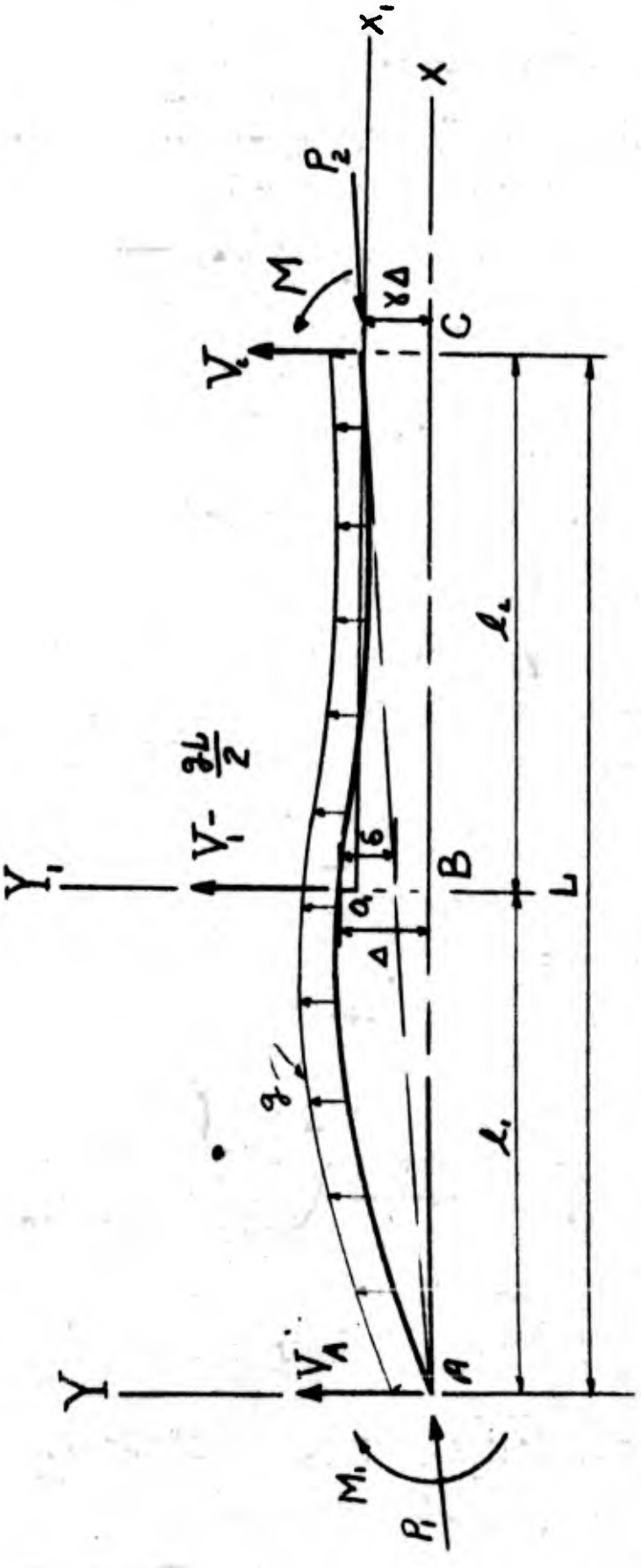

FIG. 2. Free Body Diagram of Beam Column ABC

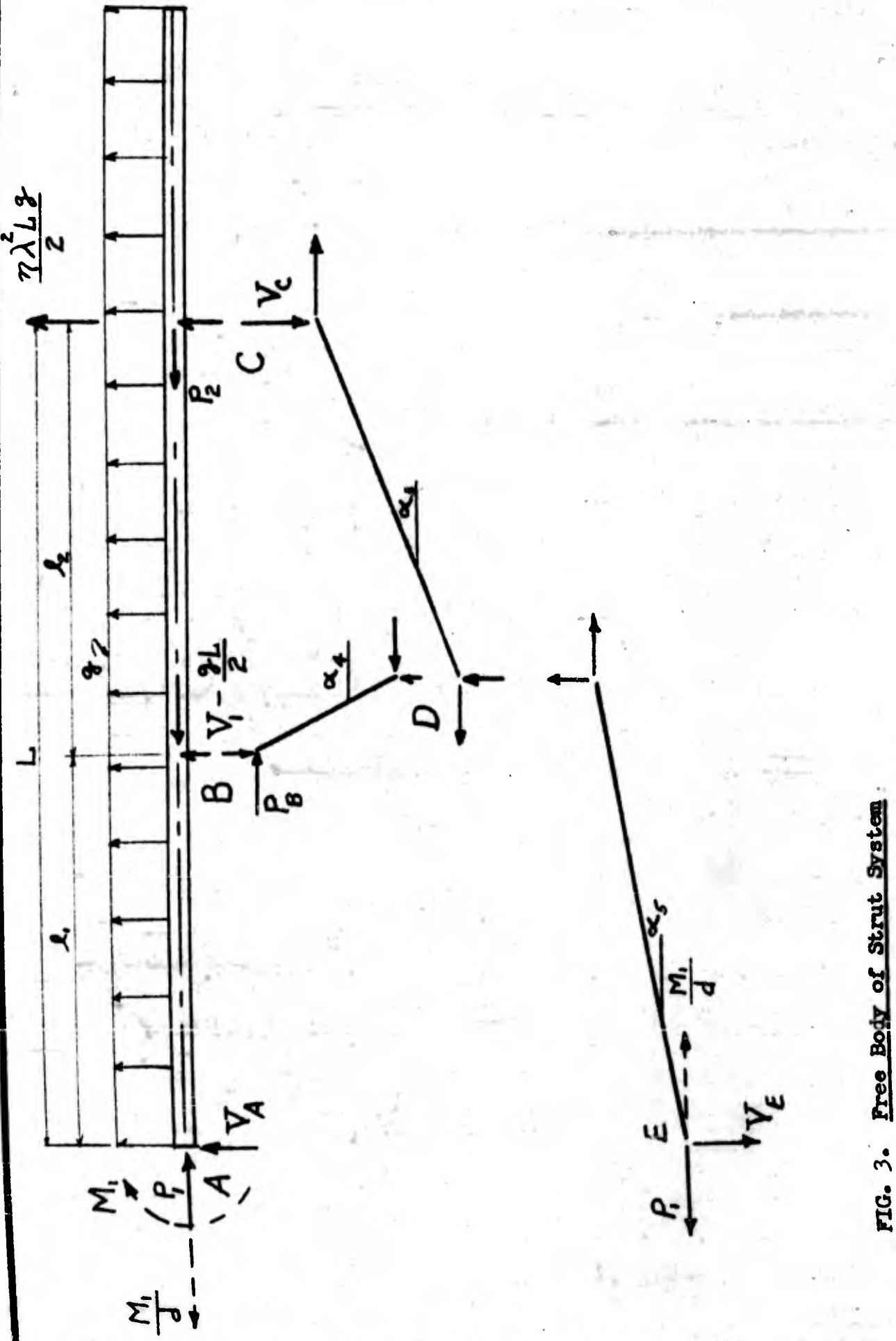

FIG. 3. Free Body of Strut System

ENGINEER	NORTHROP AIRCRAFT, INC.	PAGE 23
H. Schjelderup		REPORT NO. HLC-44
CHECKER		MODEL
DATE May 1954		

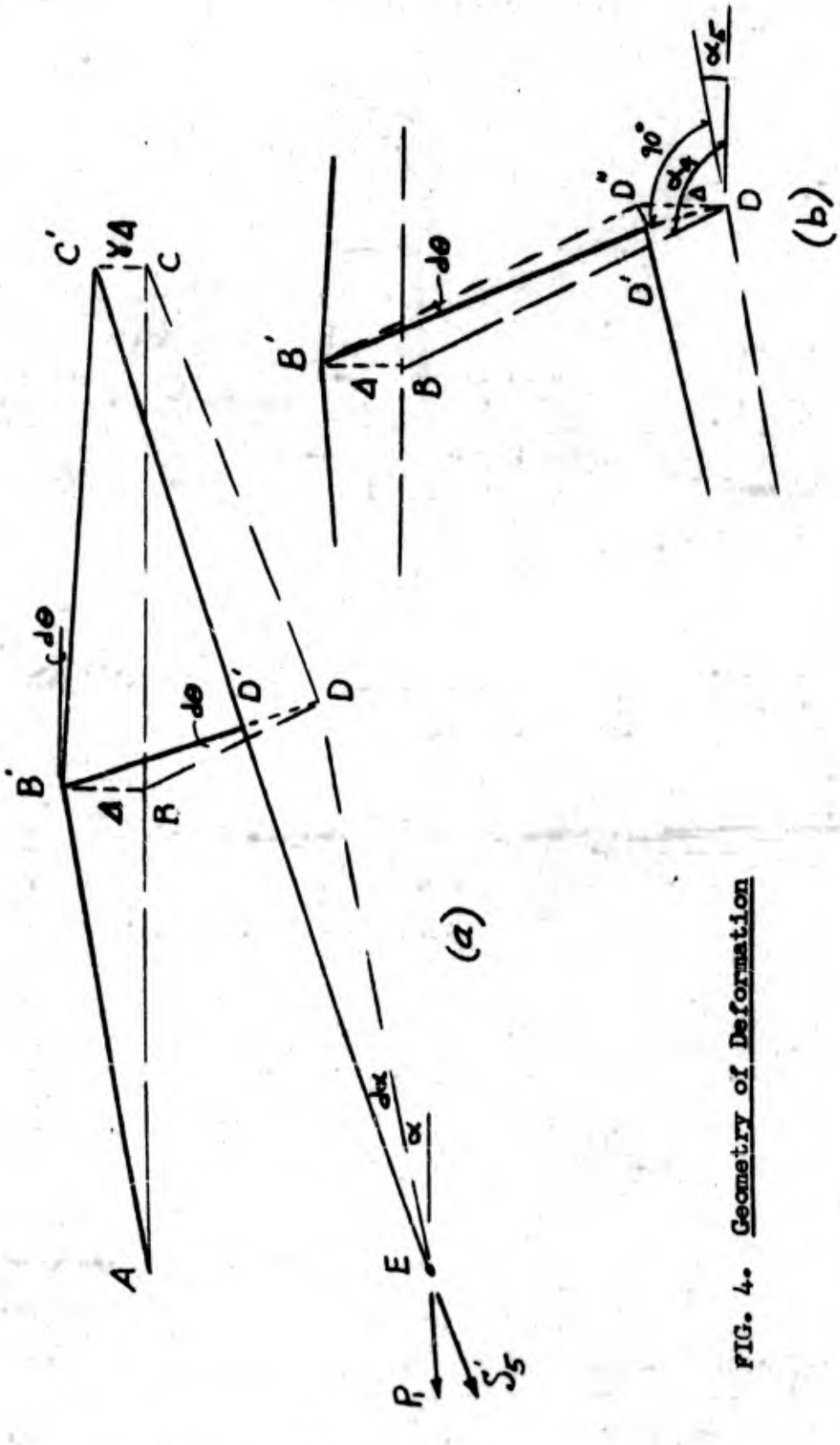

FIG. 4. Geometry of Deformation

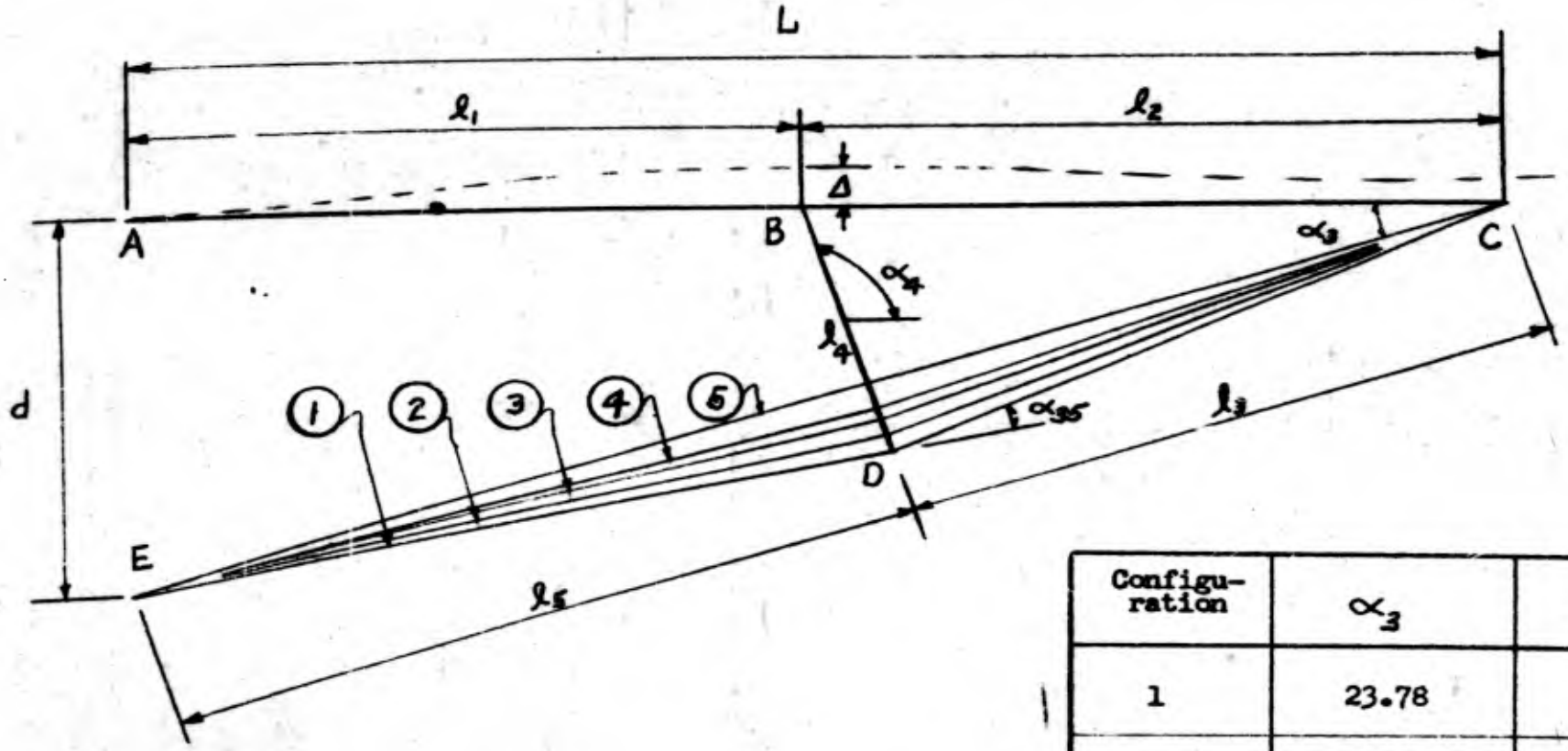

Configuration	α_3	α_{35}
1	23.78	12.68
2	22.32	10.0
3	20.825	7.183
4	19.683	5.05
5	17	0

FIG. 5. Various Strut Configurations

ENGINEER H. Schjelderup
CHECKER
DATE May 1954
NORTHROP AIRCRAFT, INC.
MODEL
REPORT NO. ELC-44
PAGE 24

Curves Showing Deflection $\frac{\Delta}{L}$ vs Axial Load μ_1 for Various Values of Kink Angle $\alpha_{3/4}$

$\mu_1 = \sqrt{\frac{P}{EI_1}}\, l_1$ $\qquad P_1 = \frac{\lambda^2 q L^2}{2d}(1+n)\left[1 - \frac{2}{\lambda^2(1+n)}\frac{M_1}{qL^2}\right]$ FIG. 6

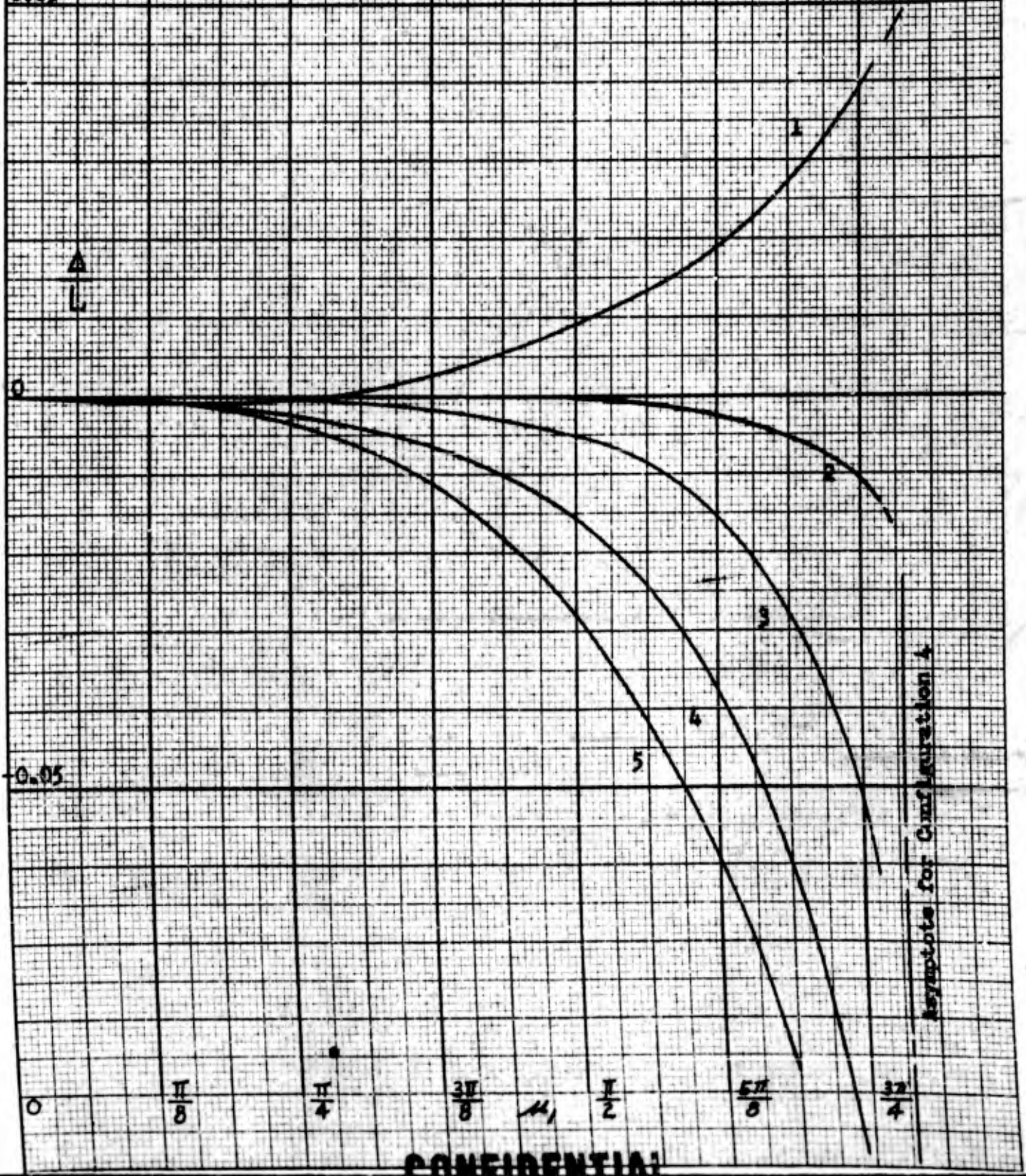

FIG. 7. Curves Showing Deflection $\frac{\Delta}{L}$ vs Total Distributed Load $\frac{f\lambda^2}{EI_1}$ * for Various Values of Kink Angle $\alpha_{.25}$

$$f = \frac{\lambda^2 q_L}{2} \cdot \left[\frac{z}{\lambda} + \eta\right]$$

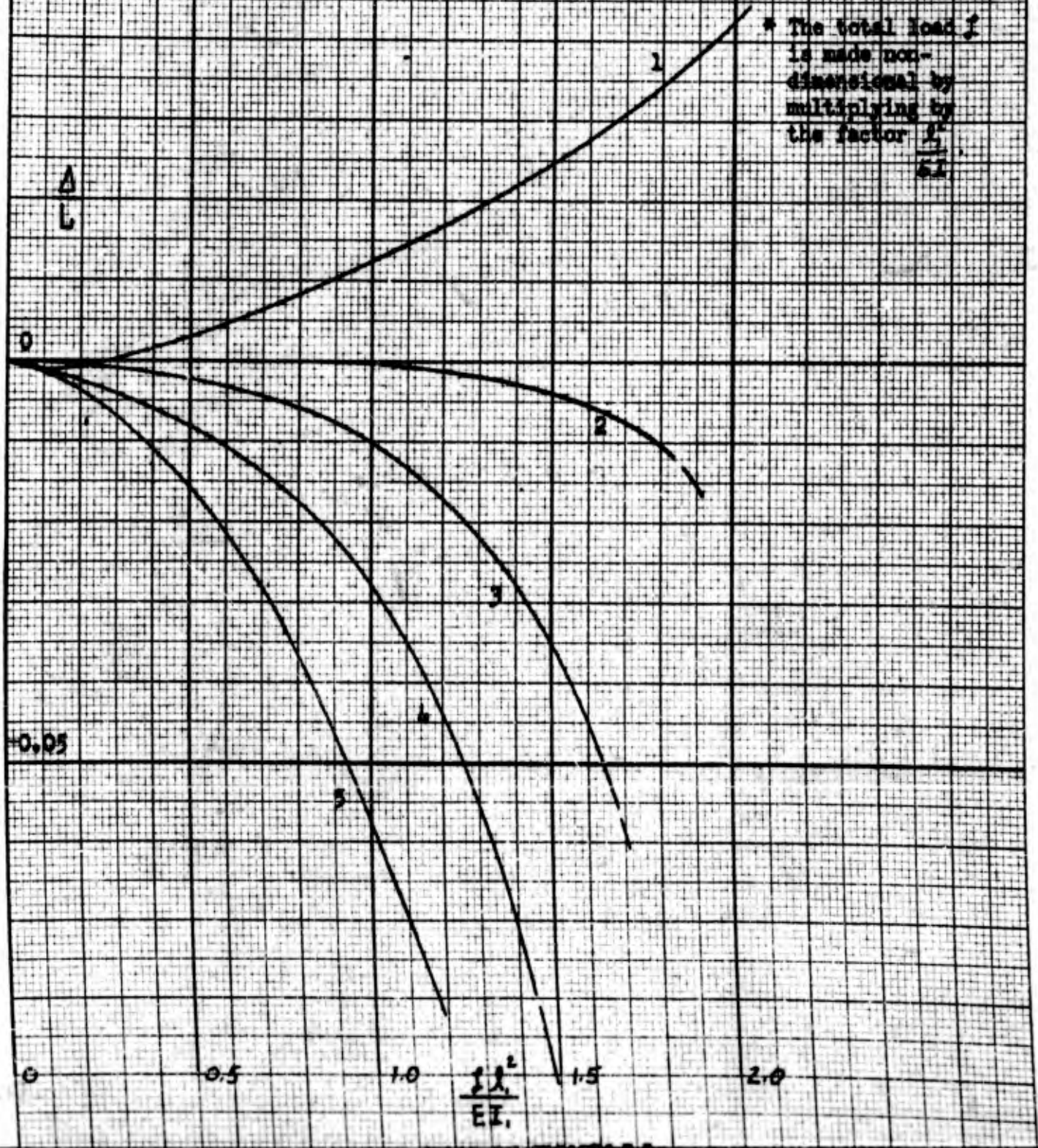

* The total load f is made non-dimensional by multiplying by the factor $\frac{\lambda^2}{EI_1}$.

CONFIDENTIAL

ENGINEER: H. Schjelderup	NORTHROP AIRCRAFT INC.	PAGE: 27
CHECKER:		REPORT NO.: NLC-44
DATE: May 1954		MODEL:

FIG. 8. Curves Showing Deflection $\frac{\Delta}{L}$ vs Angle of Kink α_{45} for Various Values of Axial Load μ.

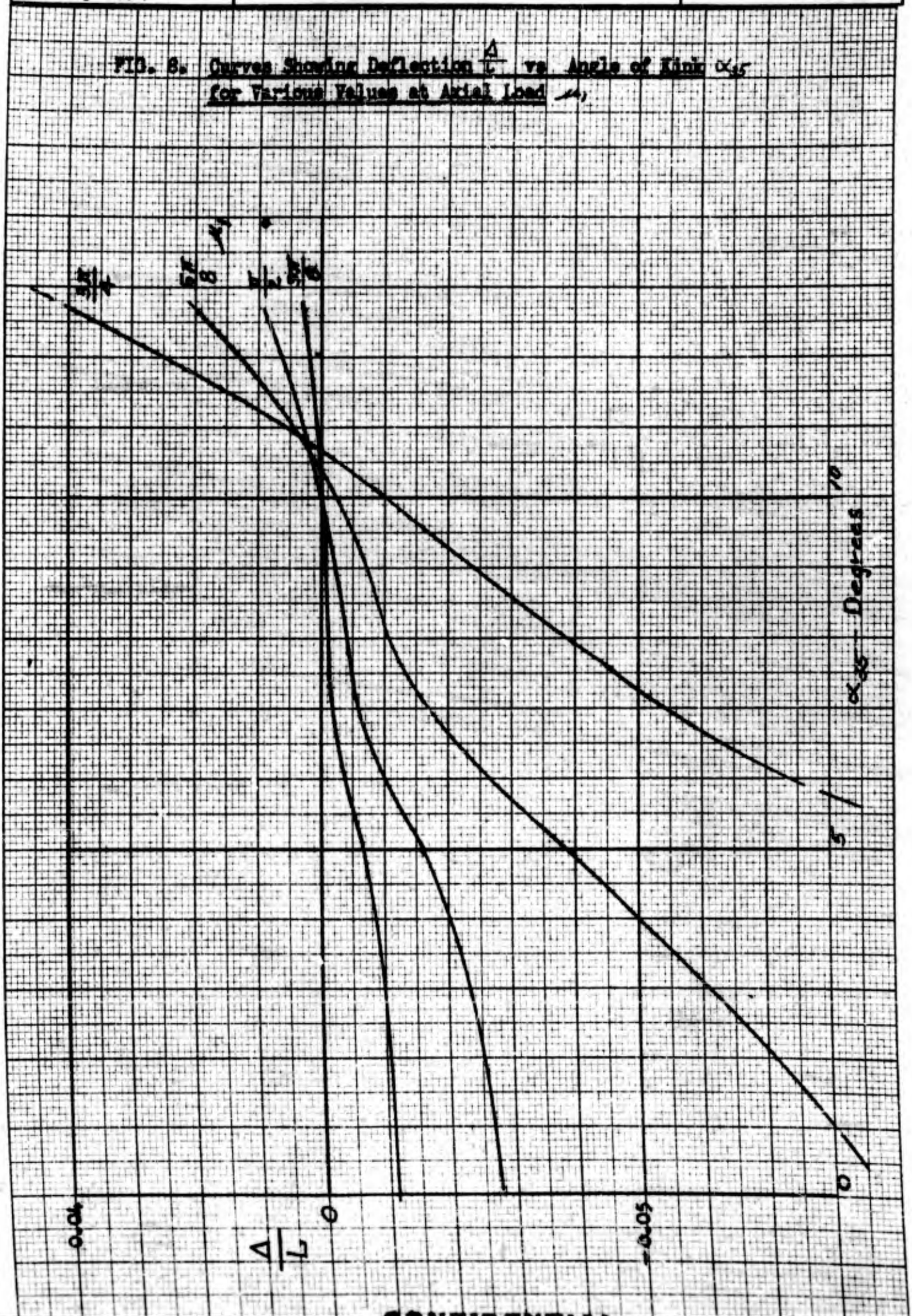

ENGINEER: H. Schjelderup	NORTHROP AIRCRAFT INC.	PAGE: 28
CHECKER:		REPORT NO.: HLC-44
DATE: May 1954		MODEL:

FIG. 9. Curve Showing Deflection $\frac{\Delta}{L}$ vs Angle of Kink α_{35} for Various Values of Total Distributed Load $\frac{WL^3}{EI}$

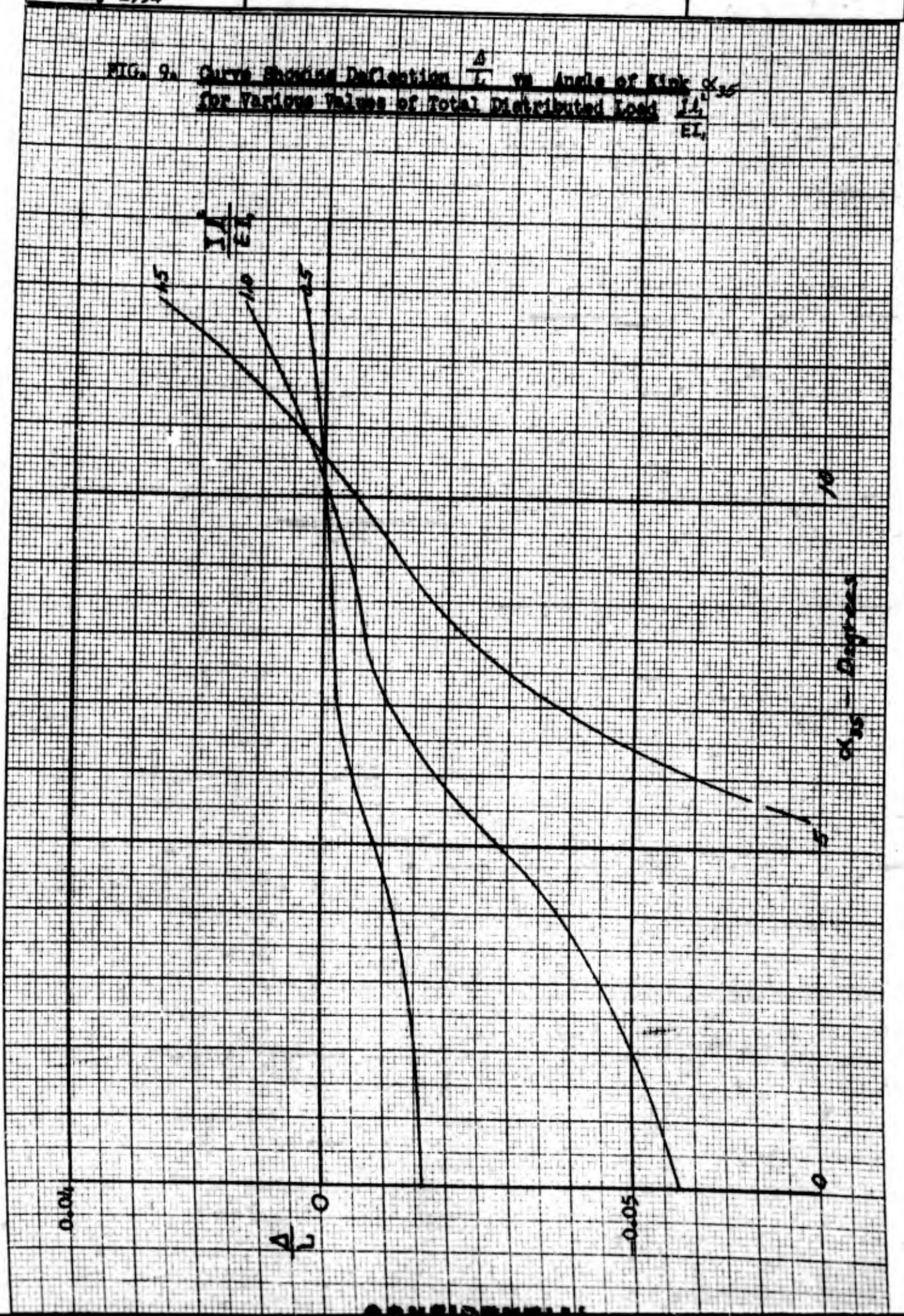

$\frac{M}{2L^2} = \frac{0.468}{2}$

FIG. 10. Curve Showing the Change in $\frac{M_1}{\rho U^2}$ with Axial Load μ_1 for Various Angles of Kink α_K

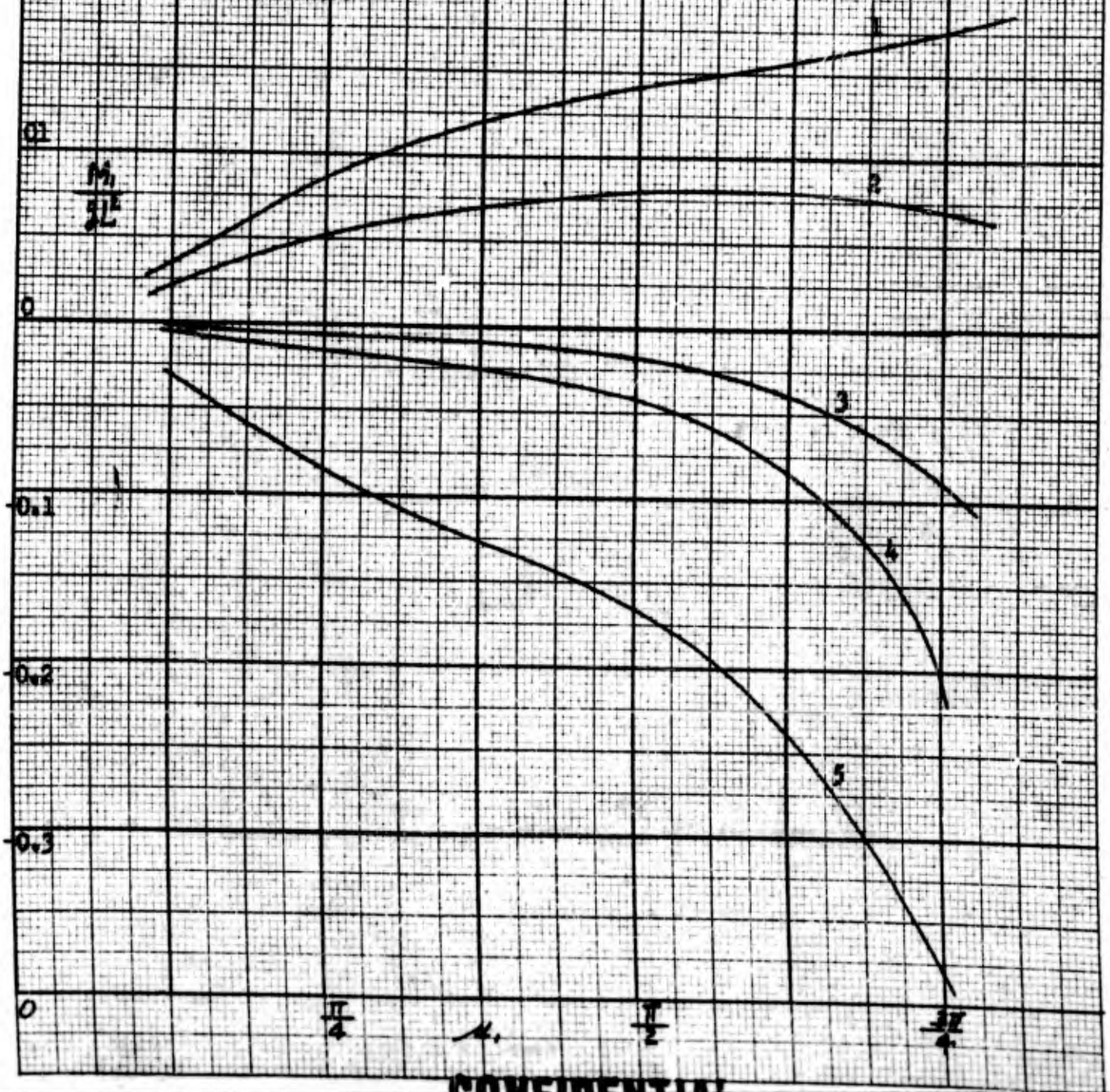

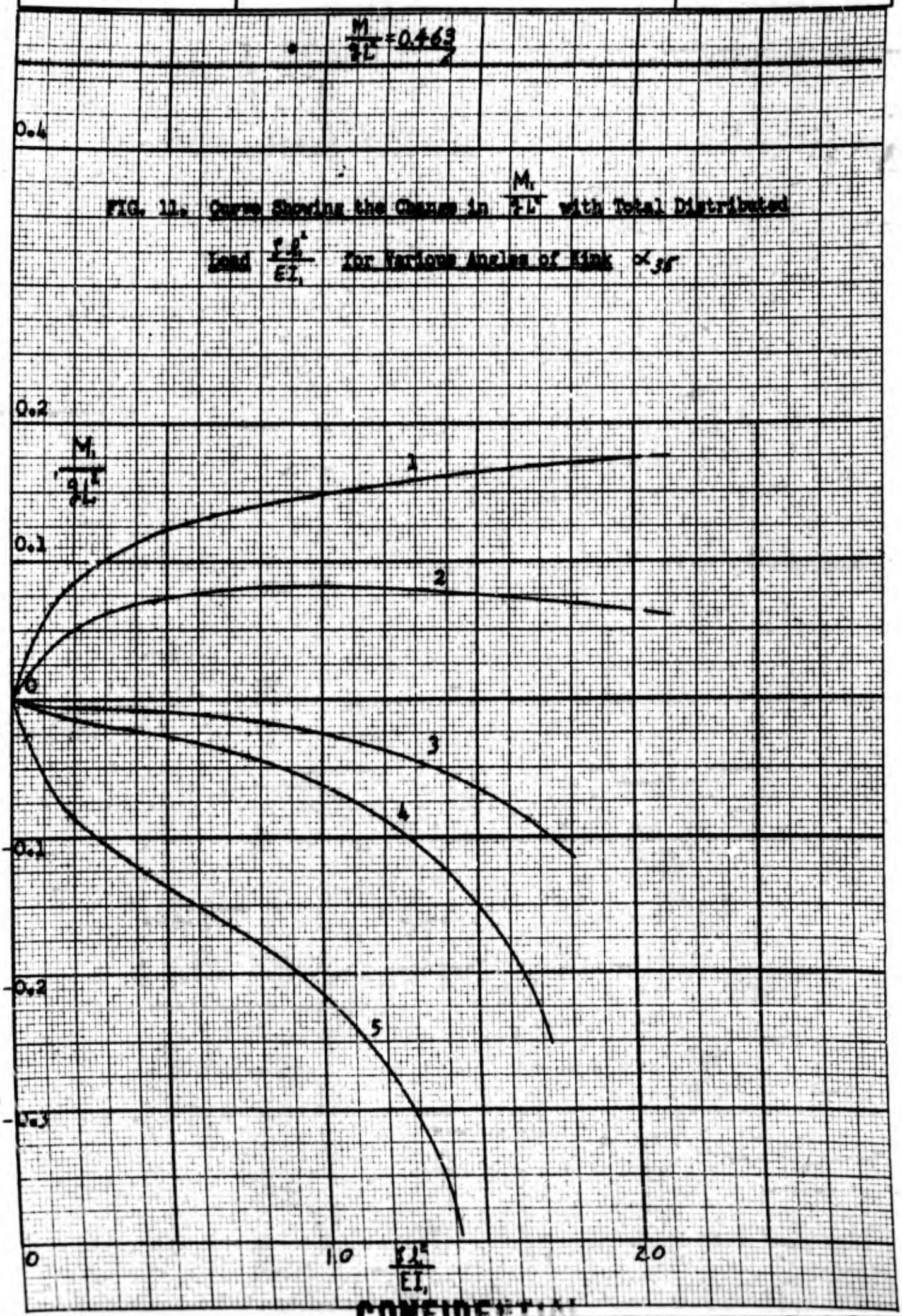

FIG. 11. Curve Showing the Change in $\frac{M_1}{qL^2}$ with Total Distributed Load $\frac{qL^2}{EI_1}$ for Various Angles of Kink α_{35}

FIG. 12. Curves Showing the Change in Moment $\frac{M_\theta}{\frac{1}{2}\rho V^2 L^2}$ with Axial Lead μ, for Various Angles of Kink $\alpha_{1/2}$

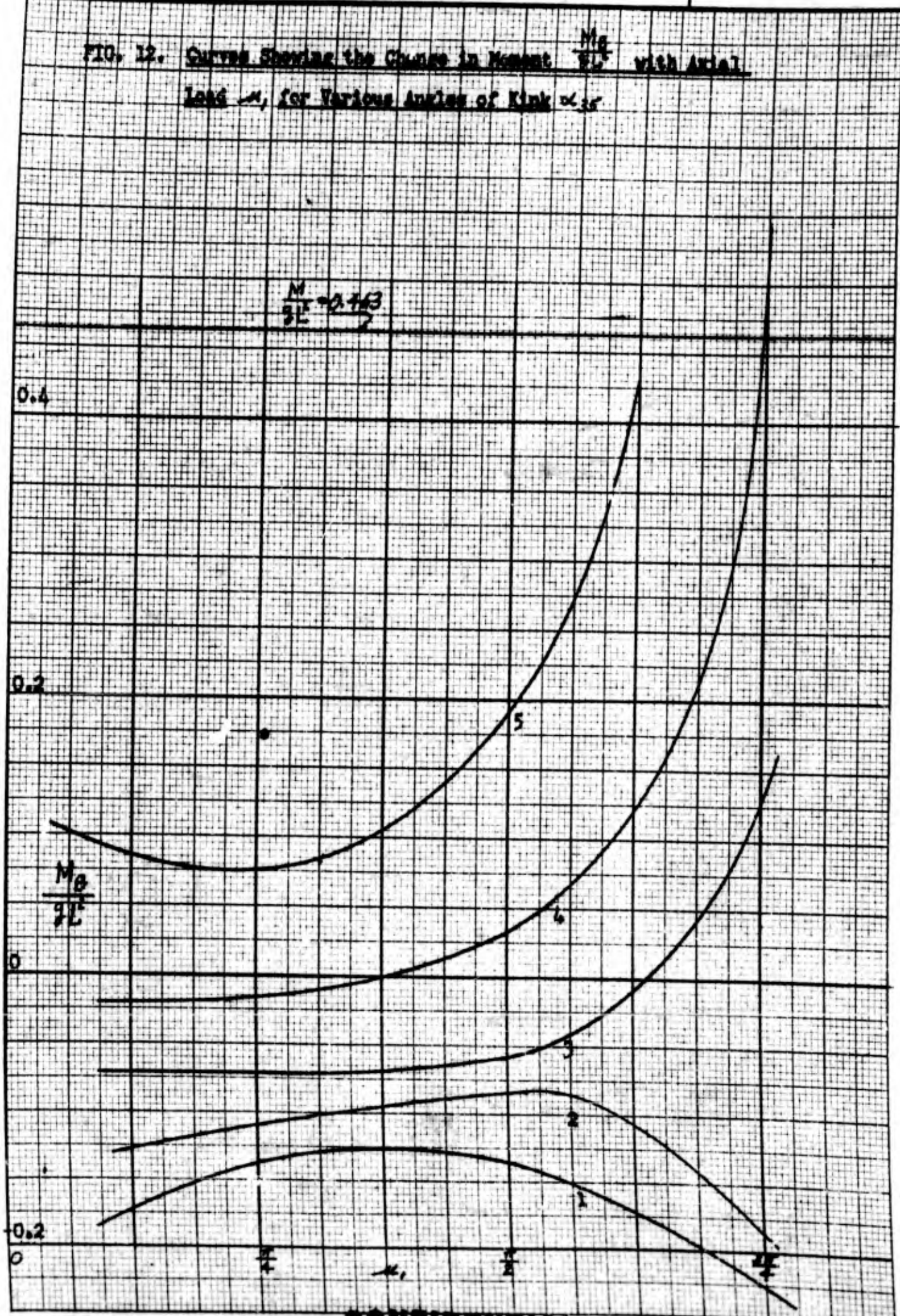

ENGINEER	NORTHROP AIRCRAFT INC.	PAGE
H. Schjelderup		32
CHECKER		REPORT NO. BLC-44
DATE May 1954		MODEL

FIG. 13. Curve Showing the Change in $\frac{M_B}{qL^2}$ with Total Distributed Load $\frac{qL^2}{EI_1}$ for Various Angles of Kink $\alpha_{3/4}$

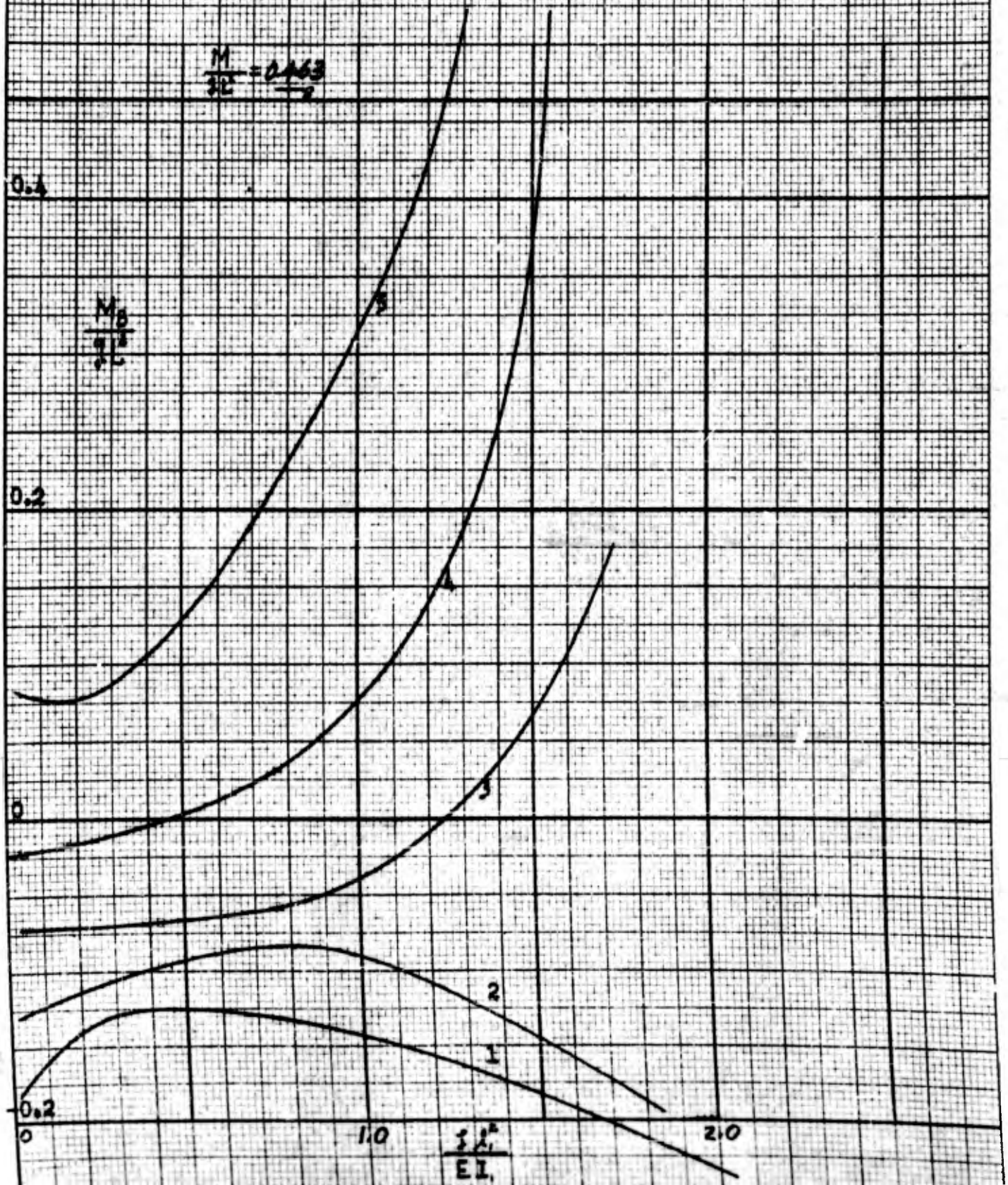

NORTHROP AIRCRAFT, INC.

HAWTHORNE, CALIFORNIA

REPORT NO. BLC-41

SHEAR AND COMPRESSION TESTS OF SANDWICH PANELS WITH BONDED OVERLAY STRIPS

May 1954

PREPARED BY

J. R. Clem

W. Dedon

APPROVED BY

W. Pfenninger

TABLE OF CONTENTS

SUMMARY

Panel Number 1 was tested by Engineering Test Group to obtain data for the shear strength of the bonding material and the honeycomb core. Both bonding material and core material developed shear stresses well above the minimum required stresses.

Panels 2, 3 and 4 were subjected to compression loads parallel to the overlay slots. The compression load produced no significant increase in the width of the overlay slots. All three panels developed ultimate stresses below the predicted stresses, varying from two to twelve percent.

No direct comparison (for repeated curing cycles) of the test results can be made since each panel was bonded with a variation of bonding material and processing method. Further tests and study are necessary in order to determine the effect of repeated curing cycles.

INTRODUCTION

Four panels were tested to obtain data for the following:

1. To determine bonding material shear strength.

2. To observe the effect of repeated curing of bonded joints, on the bonding strength.

3. To evaluate the core material shear strength.

4. To determine the effect of compression loads on the width of slots between the overlay strips.

PROCEDURE

The details for the four specimens were prepared as follows:

1. Alkaline cleaned with Turco aviation cleaner and washed in water.
2. Immerse the details in sodium dichromate-sulfuric acid solution for 5 minutes at 150°F. Wash in water and check details for "no water break". Air-dry thoroughly.

The specimens were then treated as follows:

Specimen No. 1 - The faying surfaces of the honeycomb sandwich details and the overlay strips were primed with 1/2 - 1 mil thickness of M3C primer and permitted to air-dry 15 minutes. Narmtape 102-45 adhesive was cut to size and fitted between the faying surfaces of the honeycomb sandwich and the overlay strips. The honeycomb sandwich and the overlay strips were placed in the alignment jig and a vacuum pressure was applied. The complete assembly was cured at 325°F for 1-1/2 hours in an air circulated oven, removed and cooled to room temperature.

Specimen No. 2 - The details of Specimen No. 2 were treated in the same manner as in the case of the details of Specimen No. 1 with these exceptions; the bonding was performed in two steps. The honeycomb sandwich was bonded first, then the overlay strips placed in position onto the honeycomb

sandwich and the complete assembly cured as mentioned above. This procedure subjected the honeycomb sandwich to a double cure cycle at 325°F.

Specimen No. 3 - The faying surfaces of the honeycomb sandwich details and the overlay strips were given four spray coats of plycozite adhesive. Each coat was permitted to dry for one hour. The details were pre-cured for 2 hours at 200°F. Then the details of the honeycomb sandwich and the overlay strips were placed in the alignment jig. The assembly was subjected to a vacuum pressure and cured at 325°F for 45 minutes in one step. At the end of the curing cycle the assembly was permitted to cool to room temperature.

Specimen No. 4 - The first step is to apply four coats of plycozite adhesive to the faying surfaces of the honeycomb sandwich details. Each coat was permitted to air-dry for one hour. The details were pre-cured for 2 hours at 200°F. They were then placed in the alignment jig, subjected to a vacuum pressure and cured for 45 minutes at 325°F. The assembly was removed from the oven and cooled to room temperature. The second step in the operation was to coat the faying surfaces of the honeycomb sandwich made in step one and the overlay strips with M3C primer, permit this to air-dry for 15 minutes. The Narmtape 102-45 adhesive was cut to dimension and placed between the faying surfaces of the overlay strips and honeycomb sandwich. The

assembly was placed in the alignment jig, a vacuum pressure applied and cured for 1½ hours at 325°F.

The adhesive entrapped in the venting system of the specimens was cleaned out in two stages: Specimens No. 1 and No. 3 were cleaned after complete assembly. Whereas Specimen No. 2 and No. 4 were cleaned prior to bonding the overlay strips to the honeycomb sandwich.

Sketch 1 shows positions at which measurements of the slots were made during the compression loading. The measurements were made at 1000 pound increments to the ultimate load. The changes in the slot widths under load conditions are recorded in Tables No. 1, No. 2 and No. 3.

FORM 30-7A (R. 8-51)

ENGINEER Noah Tielens	NORTHROP AIRCRAFT, INC.	PAGE 4
CHECKER		REPORT NO. BLC-41
DATE May 1954		MODEL General

Test Setup & Deflection Measurements
(Specimen #1)

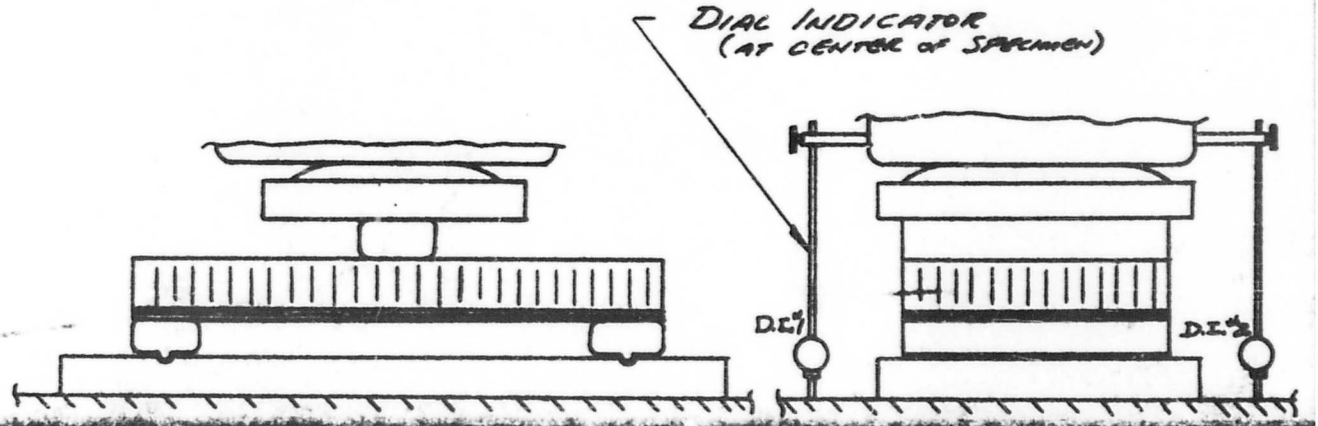

Load in Pounds	DI#1	DI#2	Load in Pounds	DI#1	DI#2
50	0	0	1200	0234	0210
100	.001	.001	1300	0259	0233
200	.0032	.0033	1400	0281	0255
300	0054	0053	1500	0308	0282
400	0076	0070	1600	0341	0315
500	0096	0088	1700	0380	0360
600	0118	0102	1800	0455	0435
700	0138	0120	1900	0580	0560
800	0156	0135	2000	0725	0710
900	0173	0152	2100	0890	0880
1000	0190	0170	2200	.1180	.1150
1100	0211	0190	2270	Failure	

FORM 20-10A
(R. 6-51)

ENGINEER	CONFIDENTIAL	PAGE
WIEDER	NORTHROP AIRCRAFT INC.	5
CHECKER		REPORT NO. BLC-41
DATE NOV. 5, 1953	OVERLAY HONEYCOMB PANEL - SHEAR TEST	MODEL General

LOAD - DEFORMATION CURVE

(REF DWG 5206002) (SPECIMEN #1)

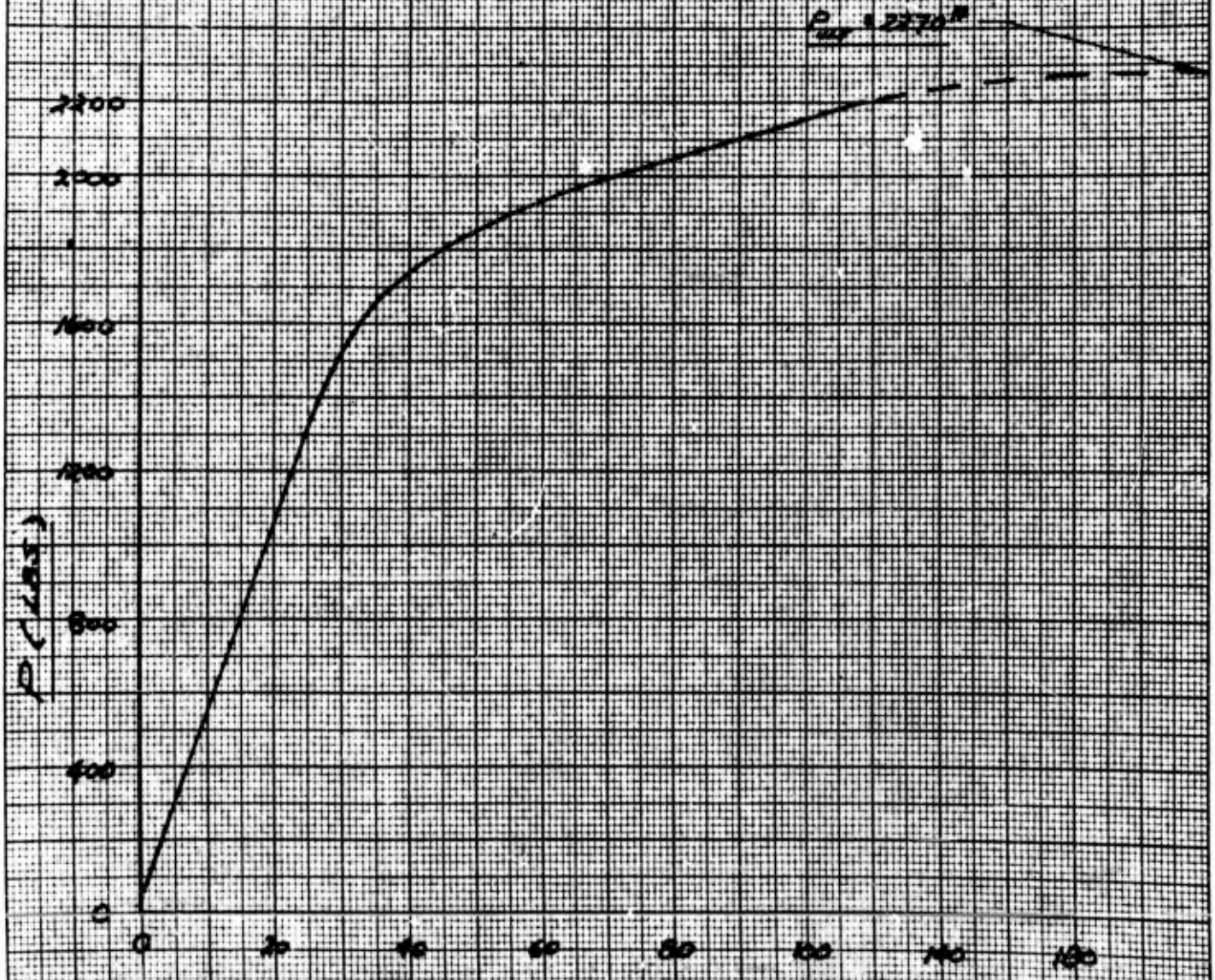

DEFORMATION x 10^{-3}

(INCHES)

BONDING SHEAR STRENGTH

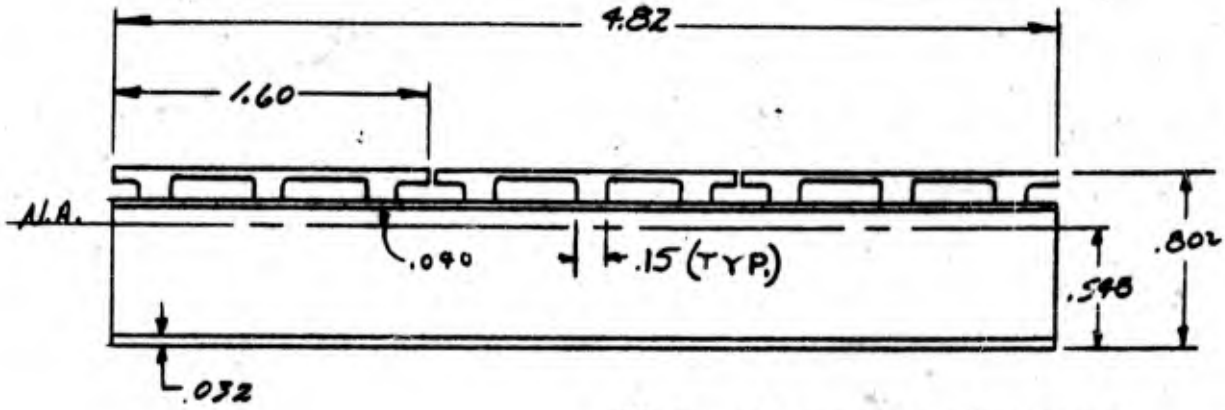

CORE MAT'L = AL. HONEYCOMB
.375 HEX-CELL, .004 THICKNESS
3 5 H

Overlay area = .297 sq. in.

Moment of Inertia = .059 in^4

$Q = A\bar{y} = .297\ (.209) = .062\ in^3$

Shear flow through bond

$$q = \frac{VQ}{I} = \frac{2270}{2} \times \frac{.062}{.059} = 1190\ \#/in.$$

length of bond = 9 x .15 = 1.35 inc.

$$f_s\ (bond) = \frac{1190}{1.35} = 880\ psi\ (no\ failure)$$

CORE SHEAR (Transverse)

Lower skin

$$f_s \text{ (core)} = \frac{VQ}{I_b}$$

V = 1135# (ult), 800# (yield)

Q = .154 (.532) = .082 in.^{3}

I = .059 in.^{4}

b = 4.82 in.

$$f_s \text{ ult} = \frac{1135}{4.82}\frac{(.082)}{(.059)} = 327 \text{ psi}$$

$$f_s, \text{yield} : \frac{800}{4.82}\frac{(.082)}{(.059)} = 231 \text{ psi}$$

F_s, all = 160 psi (Mil—C-7438, allowable)

F_s, all = 210 psi (Hexcell, allowable)

SKETCH 1

COMPRESSION TEST SETUP
(SPECIMEN #2, 3 & 4)

REF DRAWING NO. 5206007

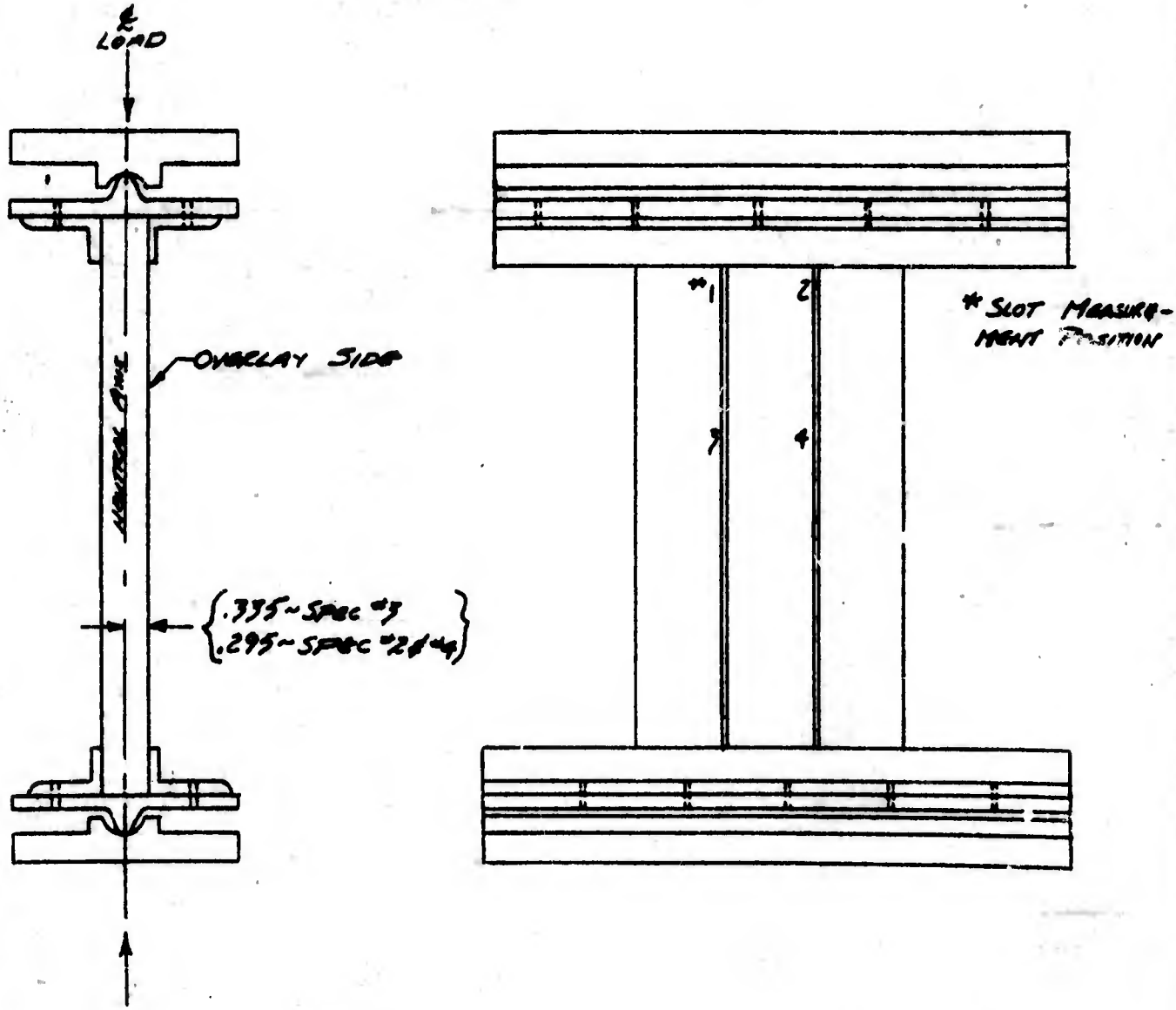

ENGINEER	NORTHROP AIRCRAFT. INC.	PAGE
Pease		9
REPORT DATE		REPORT NO. BLC-41
TEST DATE April 1954		MODEL General

SUBJECT

TEST PHASE

TABLE I (Panel No. 2)
SLOT WIDTH MEASUREMENTS

Load in Pound	POSITIONS AS INDICATED ON PANEL 1	2	3	4		Load in Pounds	1	2	3	4
0000	.008	.008	.0085	.0085						
1000	008	008	0085	0085		21000	0085	0085	009	009
2000	0085	0085	009	009		22000	0085	0085	009	009
3000	0085	0085	009	009		23000	0085	0085	009	009
4000	0085	0085	009	009		24000	0085	0085	009	009
5000	0085	0085	009	009		25000	0085	0085	009	009
6000	0085	0085	009	009		26000	0085	0085	009	009
7000	0085	0085	009	009		27000	0085	0085	009	009
8000	0085	0085	009	009		28000	0085	0085	009	009
9000	0085	0085	009	009		29000	0085	0085	009	009
10000	0085	0085	009	009		30000	0085	0085	0095	0095
11000	0085	0085	009	009		31000				
12000	0085	0085	009	009		32000				
13000	0085	0085	009	009		33000				
14000	0085	0085	009	009						
15000	0085	0085	009	009						
16000	0085	0085	009	009						
17000	0085	0085	009	009						
18000	0085	0085	009	009						
19000	0085	0085	009	009						
20000	0085	0085	009	009						

Ultimate 31000

ENGINEER	NORTHROP AIRCRAFT. INC.	PAGE
Pease		10
REPORT DATE		REPORT NO.
		BLC-41
TEST DATE		MODEL
April 1954		General

SUBJECT

TABLE 2 (Panel No. 3)

TEST PHASE

SLOT WIDTH MEASUREMENTS

Load in Pounds	POSITIONS AS INDICATED ON PANEL									
	1	2	3	4		Load in Pounds	1	2	3	4
0										
1000	0085	0085	0085	0085		21000	0085	0085	009	009
2000	0085	0085	0085	0085		22000	0085	0085	009	009
3000	0085	0085	009	0085		23000	0085	0085	009	009
4000	0085	0085	009	0085		24000	0085	0085	009	009
5000	0085	0085	009	0085		25000	0085	0085	009	009
6000	0085	0085	0085	0085		26000	0085	0085	009	009
7000	0085	0085	0085	0085		27000	0085	0085	009	009
8000	0085	0085	0085	0085		28000				
9000	0085	0085	0085	009		29000				
10000	0085	0085	009	009						
11000	0085	0085	009	009						
12000	0085	0085	009	009						
13000	0085	0085	009	009						
14000	0085	0085	009	009						
15000	0085	0085	009	009						
16000	0085	0085	009	009						
17000	0085	0085	009	009						
18000	0085	0085	009	009						
19000	0085	0085	009	009						
20000	0085	0085	009	009						

Ultimate 27550

DRM 20-138A (R.5-52)

ENGINEER: Pease	NORTHROP AIRCRAFT, INC.	PAGE: 11
REPORT DATE:		REPORT NO.: BLC-41
TEST DATE: April 1954		MODEL: General
SUBJECT:		
TEST PHASE:		

TABLE 3 (Panel No. 4)

SLOT WIDTH MEASUREMENTS

Load in Pounds	POSITIONS AS INDICATED ON PANEL				Load in Pounds				
	1	2	3	4		1	2	3	4
0									
1000	.008	.008	0075	0075	21000	008	0075	0075	0075
2000	.008	.008	0075	0075	22000	008	0075	0075	0075
3000	.008	0075	0075	0075	23000	008	0075	0075	0075
4000	.008	0075	0075	0075	24000	008	0075	0075	0075
5000	.008	0075	0075	0075	25000	008	0075	0075	0075
6000	.008	0075	0075	0075	26000	008	0075	0075	0075
7000	.008	0075	0075	0075	27000				
8000	.008	0075	0075	0075	28000				
9000	.008	0075	0075	0075	29000				
10000	.008	0075	0075	0075	30000				
11000	.008	0075	0075	0075					
12000	.008	0075	0075	0075					
13000	.008	0075	0075	0075					
14000	.008	0075	0075	0075					
15000	.008	0075	0075	0075					
16000	.008	0075	0075	0075					
17000	.008	0075	0075	0075					
18000	.008	0075	0075	0075					
19000	.008	0075	0075	0075					
20000	.008	0075	0075	0075					

Ultimate 26000

BASIC DATA (Specimen -2 & -4)

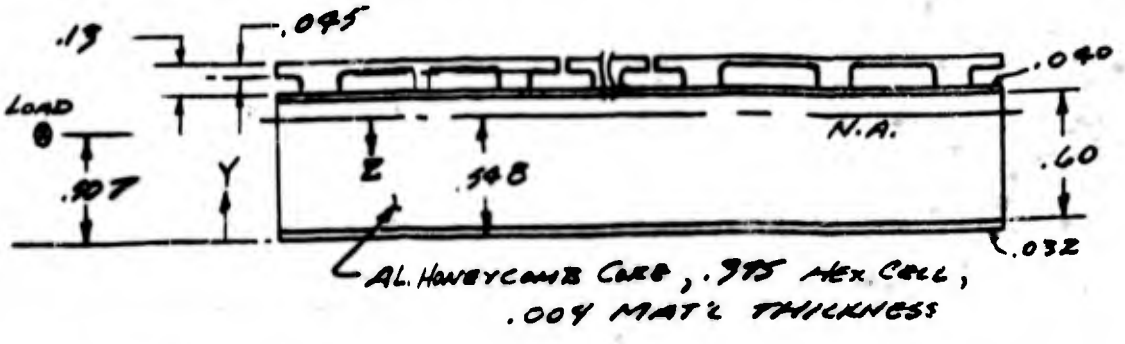

N.A. & Moment of Inertia

	Area	Y	Ay	Z	Az^2
Overlay	.297	.757	.225	.209	.013
Top Skin	.193	.652	.126	.104	.002
Lower Skin	.154	.016	.002	.532	.044
	.644		.353		.059

$$\bar{y} = \frac{.353}{.644} = .548$$

$$I = .059$$

OVERLAY

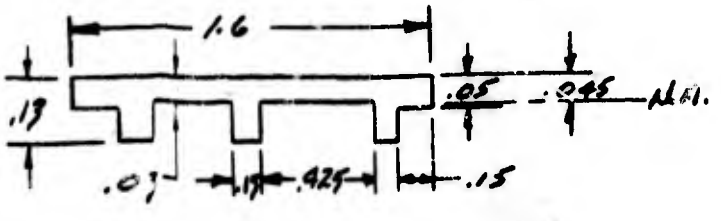

$$\text{Area} = .13 \times 1.6 - (.08)(.15)(2) - (.10)(.425)(2)$$

$$= .208 - .024 - .085 = .099$$

$$\bar{y} = \frac{\Sigma Ay}{A} = \frac{(.15)(.10)(3)(.065)}{.099} + .015$$

$$= \frac{.00293}{.099} + .015 = .045 \text{ in.}$$

BASIC DATA (Specimen -3)

N.A.

	A	y	Ay	Z	AZ^2
Overlay	.297	.757	.225	.244	.0117
Top skin	.154	.656	.101	.143	.0031
Lower skin	.193 / .644	.020	.004 / .330	.493	.0468 / .0616

$$\bar{y} = \frac{.330}{.644} = .513 \text{ in.}$$

$$I = .062 \text{ in.}^4$$

ULTIMATE STRESSES

(-2) $\frac{f_{max}}{\eta} = \frac{P}{A}\left[1 + \frac{ec}{\rho^2}\,\text{Sec}\,\frac{\pi}{2}\sqrt{\frac{P}{Pcr}}\right]$ (Ref. 1, page 309)

$\frac{f_{max}}{\eta} = 48{,}200\left[1 + (.245)\,(4.22)\right]$

$= 48{,}200\,(2.035) = 98{,}000$ psi

$f_{max} = 64{,}400$ psi

Pcr = 43,200 psi
e = .041
c = .548
P = 31,000 psi

(-3) $\frac{f_{max}}{\eta} = \frac{P}{A}\left[1 + \frac{ec}{\rho^2}\,\text{Sec}\,\frac{\pi}{2}\sqrt{\frac{P}{Pcr}}\right]$

$= 42{,}800\left[1 + (.245)\,(3.20)\right]$

$= 42{,}800\quad 1.784) = 76{,}400$ psi

$f_{max} = 59{,}200$ psi

Pcr = 43,200
P = 27,550
e = .046
c = .513
ρ^2 = .0963

(-4) $\frac{f_{max}}{\eta} = \frac{P}{A}\left[1 + \frac{ec}{\rho^2}\,\text{Sec}\,\frac{\pi}{2}\sqrt{\frac{P}{Pcr}}\right]$

$\frac{f_{max}}{\eta} = 40{,}300\left[1 + (.245)\,(2.90)\right]$

$= 40{,}300\,(1.71) = 69{,}000$ psi

$f_{max} = 57{,}000$ psi

Pcr^2 = 43,200
P = 26,000
e = .041
c = .548

ALLOWABLE LOADS & STRESSES

Allowable load (including shear effects)

$Pcr = \frac{Pe}{1 - \frac{Pe^1}{U}}$ (Ref 3, Section 3.15)

$Pe = \frac{\pi^2 D}{L^2} = \frac{(9.85)(.059 \times 10^7)}{10^2 \times .91} = 64{,}000\#$

Pe^1 (per inch) = 64,000 / 4.82 = 13,300 #/in.

$U = c\,G_{xz} = .6 \times 46{,}000 = 27{,}600$ #/in.

$\frac{Pe^1}{U} = \frac{13{,}300}{27{,}600} = .482$

$Pcr = \frac{64{,}000}{1.482} = 43{,}200\#$

Allowable load & stress for eccentric loading condition

(Ref. 1, page 309)

$$F_{max} = \frac{P}{A}\left[1 + \frac{ec}{\rho^2}\ \text{Sec}\ \frac{L}{2\rho}\sqrt{\frac{P}{EA}}\right]$$

$$= \frac{P}{A}\left[1 + \frac{ec}{\rho^2}\ \text{Sec}\ \frac{\pi}{2}\sqrt{\frac{P}{2EI/L^2}}\right]$$

$$= \frac{P}{A}\left[1 + \frac{ec}{\rho^2}\ \text{Sec}\ \frac{\pi}{2}\sqrt{\frac{P}{Pcr}}\right]$$

e = eccentricity

c = centroid to outer fiber dim.

$\rho = \sqrt{I/A}$

$$F_{max} = \frac{F_{cr}}{\eta} = \frac{P}{.644}\left[1 + \frac{(.04)(.548)}{.0916}\ \text{Sec}\ \frac{\pi}{2}\sqrt{\frac{P}{43{,}200}}\right]$$

Assume $\frac{F_{cr}}{\eta}$ = 102,000 psi & solve for P

$$\frac{F_{cr}}{\eta} A = 65{,}600 = P\left[1 + .235\ \text{Sec.}\ \frac{\pi}{2}\sqrt{\frac{P}{43{,}200}}\right]$$

For P = 31,700#

$$\frac{F_{cr}}{\eta} A = 31{,}700\left[1 + .235\ \text{Sec}\ \frac{\pi}{2}\sqrt{.733}\right]$$

$$= 31{,}700\left[1 + (.235)(4.45) \right. \quad = 31{,}000\ (2.045) = 64{,}800$$

$$F_{cr} = \frac{64{,}800}{.644} = 101{,}000\ \text{psi}$$

F_{max} = 65,000 psi (predicted allowable)

-2 Specimen

Predicted value is $\frac{64{,}400}{65{,}000} - 1 = 1\%$ unconservative

-3 Specimen

Predicted value is $\frac{59{,}200}{65{,}000} - 1 = 9\%$ unconservative

-4 Specimen

Predicted value is $\frac{57{,}000}{65{,}000} - 1 = 12.3\%$ unconservative

REFERENCES

1 Timoshenko, S. and MacCullough, G.H.: Elements of Strength of Materials, Third Edition. D. Van Nostrand Company, Inc. June 1949.

2 Northrop Aircraft, Inc. Drawing No. 5206002 & 5206007.

3 Sandwich Construction for Aircraft, Part II. ANC-23 Bulletin, May 1951.